AKADEMIA GÓRNICZO-HUTNICZA IM. STANISŁAWA STASZICA W KRAKOWIE

FIELD OF SCIENCE: Engineering and technology

SCIENTIFIC DISCIPLINE: Environmental Engineering, Mining and Energy

DOCTORAL DISSERTATION

Investigation of mercury capture effectiveness from process gases in various laboratory sorption reactor configurations

Badanie skuteczności wychwytu rtęci z gazów procesowych w różnych konfiguracjach laboratoryjnych reaktorów sorpcyjnych

Author: mgr inż. Yinyou Deng

First supervisor: dr hab. inż. Mariusz Macherzyński, associate professor

Completed at the AGH University of Krakow, Faculty of Energy and Fuels

Kraków, 2023

Abstract

Mercury is a naturally occurred element in Earth crust and like other heavy metals is toxic to organisms and people. It is also harmful to environment, especially the mankind's living environment. Therefore, study and understanding the mercury enter into environment and the capture mechanisms and methodologies is the only way to reduce the level of mercury in environment and its influence on environment and human health.

The main research aims of this study is to redesign the experimental set-up, adapt it to testing a capture of different pollutants present in a gaseous phase (laboratory simulated flue (process) gas) with particular emphasis on research on designing new reactors and testing sorbents for Hg(0) capture. The research focus on two topics: TOPIC (1): simultaneous, real time measurements of elemental mercury Hg(0) removal from streamline by using metal oxide and metal sulfide sorbents, TOPIC (2): application of different Hg(0) removal procedures from flue gas. Combination of both above topics are to study mercury capture processes in simulated process gas, mainly as from large pulverized coal-fired boilers. The goal of analyzing metal oxide and metal sulfur sorbents impact on Hg(0) capture in the experimental time (1-2 h on-line tests) was achieved. Also, the tests of other sorbents in different amounts, temperatures, sorption reactor and cell configurations and other variable conditions, were performed and described.

The selected metal oxide and metal sulfide sorbents were synthesized at laboratory. The other adsorbents, impregnated activated carbon was impregnated with transition metals (Fe, Cu), and rest of them were obtained from cooperation teams, like chemically modified synthetic zeolites or polymer based materials, were also tested to remove mercury Hg(0) from simulated flue gas. Measurements of Hg(0) capture efficiencies were performed in the redesigned set-up based on the laboratory system described by (Macherzynski, 2018) and (Macherzynski et al., 2015, 2020), at a certain flow rate of 54 dm^3/h and relatively low gas stream temperatures (110-140^oC). This temperature range is to simulate the case that an ESP system is set at downstream (cold-ESP) in the exhaust gas line in a real CFFPs. Also, the implementation of different kinds of reactor set-ups (fixed-bed type reactor and immobilized sorbent reactors) were applied. The change of flow rate, temperature, loading additional gases, applying WFGD system were also used to find the relation with the Hg(0) capture efficiency. Elemental Hg concentrations were measured online and

simultaneously in reference (empty reactor) and adsorbent reactor lines by two EPM-2 analyzers (NIC), equipped with flue gas treatment scrubbers (WLE-8). The difference in Hg(0) amounts in both lines shows the quantities of mercury captured by tested sorbents. The different way to study Hg(0) capture is to measure total mercury in sorbents before and after experiments with AAS cold vapors method - MA 3000 analyzer (NIC).
In my research project, a VFGR set-up, which was designed by my supervisor, was used to test materials of Hg(0) capture capability. Hg(0) capture results from VFGR were used as reference data to compare with data from newly designed reactors.

In cooperation with AGH employees, I designed two immobilized-sorbent reactors (MPR and MTLCR), they provided the long contact time and larger contact area than the VFGR. The MTLCR also had the slowest flue gas velocity, indicating causing that carbon base sorbents had a relative good Hg(0) capture efficiency in the MTLCR setting. The MPR and MTLCR were studied in terms to improve Hg(0) capture efficiency by comparing VFGR with the same mass of the same sorbent. The MPR and MTLCR are made of durable, relative cheap PTFE material and are easy to clean and reuse. The contact area, contact time and velocity are crucial factors for the sorbent passthrough high Hg(0) capture efficiency. Modifying these variables, one can improve Hg(0) capture efficiency, with contact area and time having a more significant impact.
Sulfur species: SO_2, SO_3, H_2S are commonly present in flue gas, and they highly influence the capture efficiency of mercury compounds. H_2S strongly influences the concentration of Hg(0) in a stream. It can react with Hg(0) in the gas phase without a catalyst or sorbent. SO_2, SO_3 react with mercury onto a gas/solid state interphase, when oxidation of Hg(0) to the Hg(II) is occurred. It is important to figure out which sulfur species have the highest impact on Hg(0) capture.

Finally, as expected, in the redesigned and modified laboratory system, one can regulate and control simulated flue gas conditions and composition as assumed in the research plan. The newly own designed reactors performed the good experimental results, which improved Hg(0) capture efficiency by comparing with the fixed-bed type reactor using the same amounts of selected sorbents. The Hg(0) capture efficiencies in different materials and set-ups were studied.

Table of Contents

Acknowledgement

I would like to express my special appreciation and thanks to my PhD thesis supervisor — Dr. Mariusz Macherzyński, associate professor of AGH University, who gave me the continuous help and support at every stage of making this thesis.

I also do appreciate Dr. Jerzy Górecki, associate professor of AGH University, who shared with me his precious time and experience.

Also thank to my collogue Wiktor Pacura MSc, who helped me in the daily work, as well as all the AGH stuffs somehow involved in my doctoral thesis.

I would also like to thank to my parents who unconditionally supported me throughout the duration of my doctoral program studies in Poland!

Abbreviations

ACs activated carbons
ACI activated carbons injection
ASGM Artisanal Small-scale Gold Mining
APCDs air pollutants control devices
BBA betweenness-based account
CBA consumption-based account
CDC centers for Disease Control and Prevention
CFPPs coal fired power plants
CVAAS cold-vapor atomic absorption spectrometry
CVAFS cold vapor atomic fluorescence spectrometry
ESP electrostatic precipitator
FDA Food and Drugs administration
FF fabric filter
FGD flue gas desulfurization
GMA global mercury assessment
GHSV gas hourly space velocity
Hg-TPD mercury-temperature-programmed decomposition
IGCC integrated gasification combined cycle
MOFs metal-organic frameworks
MPR multiple pipes reactor
MTLCR multiple thin layer cubic reactor
NZE Net Zero Emissions
OHM Ontario Hydro Method
PBA production-based account
SCE standard coal energy
SCR selected catalyst reduction
SI sorbent injection
SPC sorbent polymer composite
SRB sulfate-reducing bacteria
VFGR vertical flow glass reactor
WFGD wet flue gas desulfurization
WTO World Trade Organization

Introduction

Since the second industrial revolution, human society has achieved unprecedented development, such as technology, culture, economy, and science have been greatly improved compared with before. The living standards and population also were increased by comparing with two centuries ago.

Economic growth is by far the most important driver of energy trends. The link between energy demand, and economic output remains close, despite some signs of its loosening (Fig. 1.1). The world energy outlook predict the tendency of energy supply and GDP growth in 2000 (International Energy Agency, 2000). And this predict was proofed by the data from the world bank.

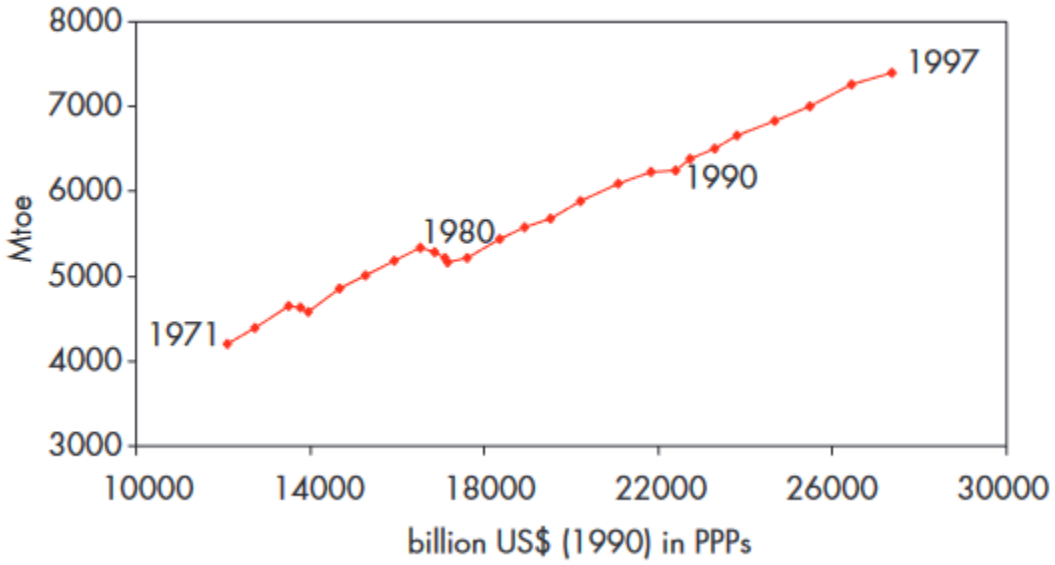

Figure 1.1: World TPES vs. GDP 1971-1997

Fig. 1.2 shows this relationship from 1971-2021 (world bank). However, the greatest achievements, what human obtained, companied a huge issue—environmental pollutions. The Fig. 1.2 Also showed the CO_2 emissions relate with the economic output. The CO_2 emissions was a sign relate

to other emissions, such as SO_2, NOx, pm, hydrocarbon, heavy metals, etc. (Kochel et al., 2012). The human living surroundings faced the significant challenging.

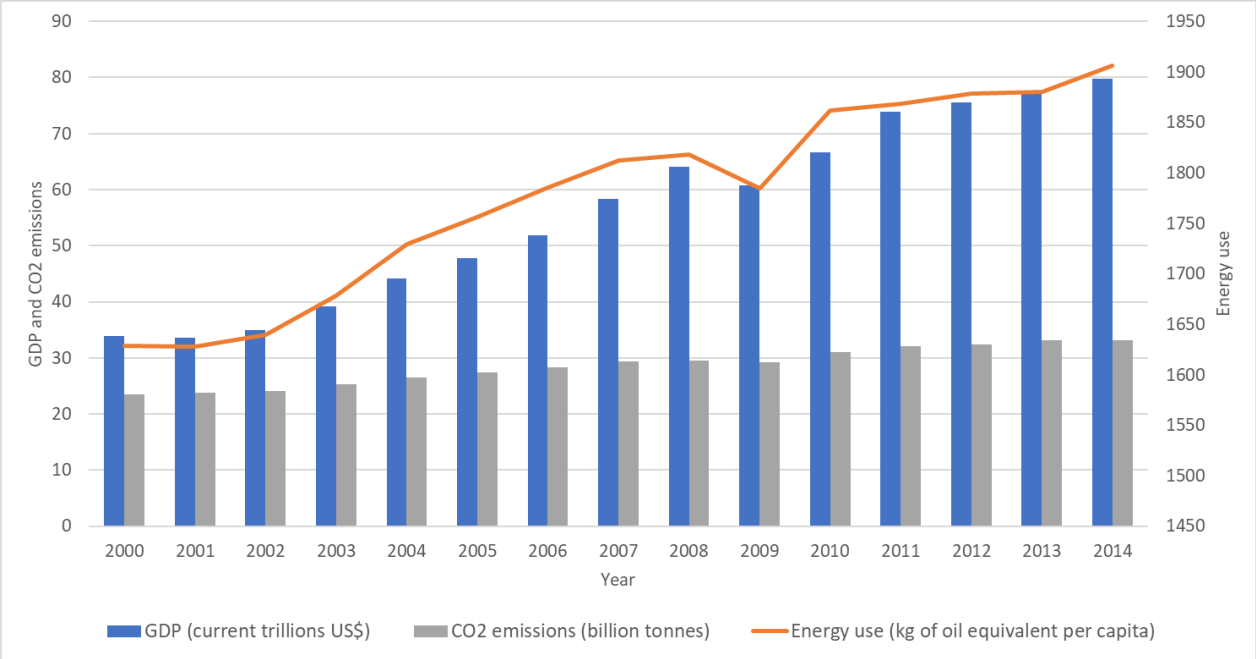

Figure 1.2: World TPES vs. GDP, CO_2 emissions 2000-2014

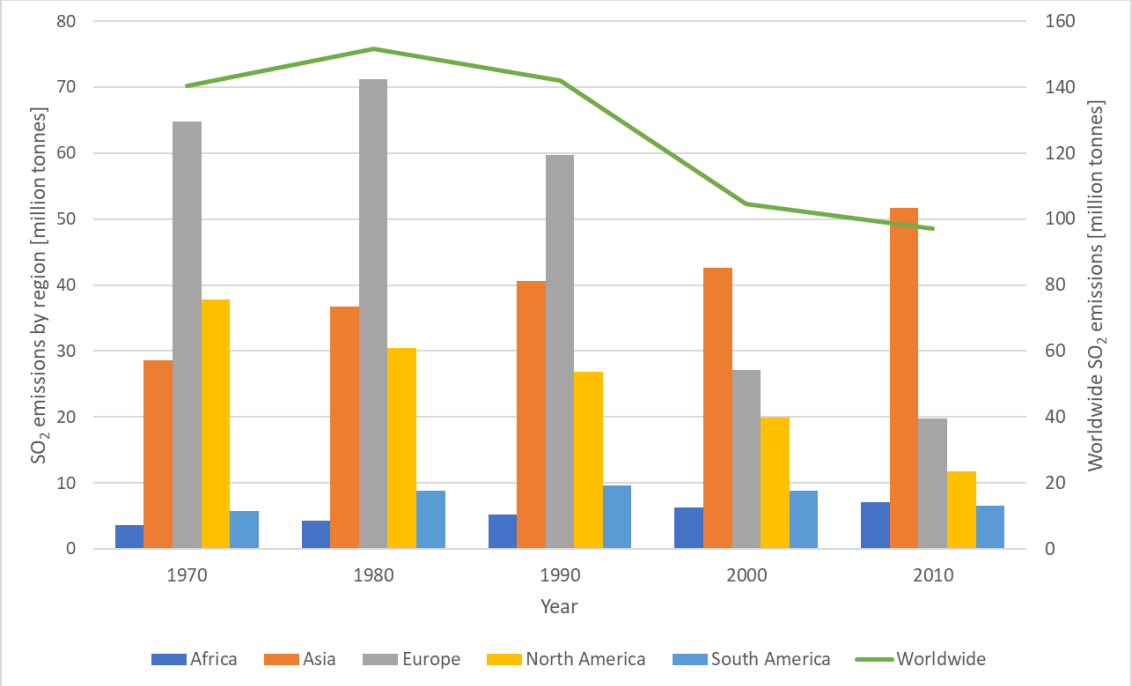

Figure 1.3: Global SO_2 emissions by world region 1970-2010

The nitrogen, sulfur and carbon (except CO_2) chemical compounds in the electro-energetic industry are mostly captured by advanced pollutants control devices. The APCDs have showed the remarkable capture efficiencies. The WFGD systems remove the SO_2 over 99%. The SCR systems remove the NOx over 90%. The ESP systems remove PM over 99%. Typically, the SO_2 emissions were declined greatly after 1980 (Fig. 1.3). This pollutant was most from energy production and industrial production which were applied the coal as the energy source (Walawska et al., 2014). However, the heavy metals are hardly to be removed by comparing with those mentioned pollutants, when heavy metals are partially emitted into environment and partially go to the solid wastes and industrial waters. In the gas phase they will be deposited via the wet or dry deposition process to the earth surface and objects. The microorganisms can transform and decompose some of heavy metal species. In some cases, the microorganisms transform the heavy metals into very toxic (much more then inorganic forms) organic molecules, as for instance the organic mercury compounds.

1. Mercury properties and its passthrough ways and fate in environment

Mercury could cause such huge environmental risk because of its unique physical and chemical properties. Mercury is a slivery, shiny metal. Mercury is in liquid form at the room temperature, which is unlike the other transition metals, like copper, zinc, iron. When dropped, elemental mercury breaks into smaller droplets. Mercury has the high surface tension; it can wet metals. The mean concentration of Hg in earth crust is around 50 ppb. In some regions, the concentration of Hg is up to 320 ppb (Canil et al., 2015). Mercury can be found in air, water and soil. It is classed to the 6^{th} period and 12^{th} (IIB) group of the periodic table of elements.

1.1. Physical and chemical properties of mercury

Mercury exists in various speciation forms, including elemental mercury (or metallic mercury, Hg(0)), inorganic mercury compounds (mercury salts), and organic mercury compounds. Mercury has three possible oxidation states in nature. Elemental mercury (Hg(0)) is electrically neutral.

Mercury also exists in two cationic states, Hg^{2+} (mercuric) and Hg_2^{2+} (mercurous) (Habashi, 2013), as mercury might exist in the form of Hg–Hg bonds. The mercuric cation is generally associated with inorganic molecules, including sulfur (in the mineral cinnabar), chlorine (mercuric chloride), oxygen, and hydroxyl ions. Toxic to living organisms is mercury. Hg^{2+} is also found in organic (carbon-based) substances such as dimethylmercury (Met_2Hg), which is significantly more toxic than inorganic mercury forms and bioaccumulates in the tissues of living organisms. Since mercury can be readily adsorbed onto small particles of matter, some scientists use the notation Hg(p) to denote mercury atoms that are attached to or absorbed by a particle.

The specific gravity of Hg is 13.5 times that of water. As it is a liquid at room temperature, its melting point is -38.89°C. On flat surfaces, liquid mercury droplets appear spherical and silvery-white with a high surface tension. Due to its low viscosity, the liquid is highly mobile and droplets combine easily. Mercury also combines with metals such as tin, copper, gold, and silver to form amalgams, also known as mercury alloys. Mercury does not amalgamate with titanium and iron, so it can be transported in standard iron flasks containing 34.5 kg of liquid mercury (Habashi, 2013). Mercury has relatively high vapor pressure and the highest volatility of any metals, transforming into an odorless, colorless vapors upon evaporation. The metal is an adequate electrical conductor but a poor heat conductor. There are additional mercury physical properties listed in table 1.1.

Table 1.1 Physical properties of mercury (Habashi, 2013)	
Melting point, ℃	-38.89
Boiling point at 101.3 kPa, ℃	357.3
Atomic weight	200.59
Density at 0℃, g/cm^3	13.60
Specific heat capacity at 0℃, $Jg^{-1}K^{-1}$	0.14
Heat of fusion, j/g	11.81
Heat of evaporation at 357.3℃, kJ/mol	59.45
Viscosity at 0℃, mPa·s	1.69
Surface tension, N/cm	480.3×10^{-5}

1.2. The toxicity of mercury

The toxicity of mercury is related to its chemical properties. Since the Minamata disaster, the whole society concerns about the mercury emissions, mercury contents in daily used product. Because it is an element, mercury is not biodegradable. It is converted among its various speciation forms through a range of abiotic and biogeochemical transformations and during atmospheric transportation. Although its form and availability to living organisms may change over time, mercury persists in the environment.

Mercury in all its forms is toxic to cellular function by altering the tertiary and quaternary structures of proteins and by binding with sulfhydryl and selenohydryl groups. Mercury can potentially impair the function of any organ or subcellular structure. Mercury vapor's primary target organ is the brain, but it also affects peripheral nerve function, renal function, immune function, endocrine and muscle function, and several types of dermatitis several types of dermatitis have been described in (Bernhoft, 2012).

(i) Elemental Mercury Vapors

Several organ systems, such as brain and kidneys, can be adversely affected by exposure to mercury vapor. Mercury readily crosses the blood-brain and placental barriers. Children are more susceptible to the toxic effects of mercury vapor than adults because their small stature places them closer to the ground, where dense mercury vapors settle (Clarkson et al., 2003).

When exposure at low levels of mercury vapor, the symptoms and signs of mercury vapor intoxication can be subtle and nonspecific, including weakness, pain, anorexia, weight loss, and gastrointestinal or neurologic symptoms (Bernhoft, 2012). After exposure the an acute high-level of mercury vapor, pneumonitis characterized by fevers, cough, and dyspnea may develop within hours and may lead to death from progressive hypoxia (Gungor et al., 2019; Johnson-Arbor et al., 2021). With massive acute mercury vapor exposure, erosive bronchitis and bronchiolitis leading to respiratory failure may be accompanied by central nervous system (CNS) symptoms such as tremor or erethism (Garnier et al., 1981).

(ii) Inorganic mercury

Mercurous (Hg^{1+}) mercury, such as calomel (Hg_2Cl_2) is still used in some regions of the world as a laxative. The absorption of mercurous mercury in the form of Hg_2Cl_2 is extremely low; however,

some absorption does occur during oxidation to more absorbable forms. In the body, it was proposed that mercurous mercury is converted to metallic mercury and mercuric mercury (Ozuah, 2000; Bernhoft, 2012; Farkhondeh et al., 2019).

Mercuric (Hg^{2+}) Mercury, mercuric chloride ($HgCl_2$) is regarded as the most toxic and corrosive mercuric mercury compound. It was used to be in the development of photographic film (Ozuah, 2000). Mercuric mercury cannot cross the blood-brain barrier; however, it can cross the placenta and deposit in fetal tissues (Farkhondeh et al., 2019; Safari et al., 2019). Mercuric mercury is deposited primarily in the kidneys and liver (Farkhondeh et al., 2019; Safari et al., 2019). There is extensive precipitation of enterocyte proteins, accompanied by abdominal pain, vomiting, and bloody diarrhea, with the possibility of mucosal necrosis. This may result in death from peritonitis, septic shock, or hypovolemic shock. Anuria and renal tubular necrosis are common in survivors (Bernhoft, 2012). Chronic mercury salt poisoning is uncommon and typically involves concurrent occupational exposure to mercury vapor. Either renal tubular necrosis or autoimmune glomerulonephritis, or both, constitute kidney toxicity (Bernhoft, 2012). Immune dysfunctions include hypersensitivity reactions to mercury exposure, such as asthma and dermatitis, as well as various types of autoimmunity, suppression of natural killer cells, and disruption of various other lymphocyte subpopulations (Bernhoft, 2012). Because mercury ions tend to increase the formation of reactive oxygen species (ROS) such as superoxide oxygen (O^{2-}), hydroxyl radical (OH^-), and hydrogen peroxide (H_2O_2), especially at high concentrations (Gallego et al., 2002). When ROS are present in cells at high concentrations, they have a detrimental effect on cell structures and cell components. Typically, a physiological process generates ROS at low concentrations, and they are crucial for cell signaling (Ferreira et al., 2018).

(iii) Organic mercury

Molecules, such as methyl mercury, reacts with sulfhydryl groups throughout the body, thus interfering with the function of any cellular or subcellular structure. Mercury interferes with DNA transcription and protein synthesis (Khan et al., 2019), including protein synthesis in the developing brain, resulting in the destruction of endoplasmic reticulum and loss of ribosomes (Bernhoft, 2012). Methyl mercury is linked to a decrease in the activity of natural killer cells (Park et al., 2000; Vimercati et al., 2001).

1.3. Sources of mercury emissions

Mercury is similar with the majority of pollutants, which has two types of emission sources: natural and anthropogenic. Mercury emissions from natural sources include contributions from primary natural sources and re-emission processes of mercury historically deposited on land and in oceans. Mercury emitted from volcanoes, geothermal sources, and mercury-enriched topsoil represents primary natural sources, whereas the re-emission of previously deposited mercury on vegetation, land or water surfaces is primarily a result of land use changes, biomass burning, meteorological conditions, and exchange mechanisms of gaseous mercury at air-water/top soil/snow-ice pack interfaces (Pirrone et al., 2010). The estimated total mercury emission from the natural source was 5207 Mg/yr in 2008. The majority of mercury emissions result from the evaporation of seawater, which was 2680 Mg/yr. And the second and third large sources of mercury emissions from natural sources were biomass burning (675 Mg/yr) and net evasion fluxes from desert/metalliferous/non-vegetated regions (546 Mg/yr), respectively (Pirrone et al., 2010). In the GMA 2018 report, the models differ primarily in their estimates of the mercury delivered to the ocean as a result of silver and gold mining in the New World between the 16th and late 19th centuries and in their estimates of how much natural mercury was already present in the oceans (UNEP, 2018). Natural mercury emissions are too difficult to reduce with current technology. Therefore, scientists and mechanists expended an excessive amount of effort to reduce mercury emissions from human-caused processes.

1.3.1. Point and non-point sources of anthropogenic mercury emissions

There are two pathways for mercury to enter the environment via anthropogenic processes. The first are point sources, while the second are non-point sources. These sources emit a substantial amount of mercury from a single location or region, making it easy to track and locate the source of mercury emissions from human activities. ASGM contributed 838 Mg of mercury to the atmosphere in 2015, accounting for 37.7% of total mercury emissions that year. The second and third largest sources of mercury emissions are stationary fossil fuel combustion power plants (294.8 Mg) and cement production (233 Mg), accounting for 13.23% and 10.5%, respectively, of total mercury emissions (UNEP, 2018). Additionally, there were other mercury emissions from point sources, such as non-ferrous metal production (228 Mg), waste from other products (147 Mg), vinyl-chloride monomer (58.2 Mg) and etc.

Anthropogenic processes contributed such high amount of mercury into atmosphere because the fuels, which were applied as energy source in production activities, content mercury (Mojammal et al., 2019; Kho et al., 2022). The table 1.2 showed the mercury contents in different kinds of fuels in some region of world (table 1.2).

Table 1.2. Mercury content in selected fuel

Fuel	Region	Mercury content	Source
Coal	China	124.84-647.42 µg/kg	(Zhao et al., 2019)
		112.1-292.6 µg/kg	(Su et al., 2021)
	India	110-800 µg/kg	(Mukherjee et al., 2008)
		120-1080 µg/kg	(Raj et al., 2017)
	Russia	20-900 µg/kg	(Mukherjee et al., 2008)
		10-2930 µg/kg	(Osipova et al., 2019)
	US	0-10000 µg/kg	(Finkelman, 1993)
		17.1-81.9 µg/kg	(Gingerich et al., 2019)
	Poland	52-125 µg/kg	(Wierzchowski et al., 2017)
		67.8-276 µg/kg	(Okońska et al., 2013)
Crude oil	China	14.4-19.3 µg/m^3	(Yan et al., 2017a)
		0.17-14.2 µg/m^3	
	Europe	8.7 µg/kg	(Littlepage, 2013)
	South America	5.3 µg/kg	
	Africa	2.7 µg/kg	
	Unit Sate	4.3 µg/kg	(S. Mark Wilhelm et al., 2007)
	Middle East	0.8 µg/kg	
Natural gas	China	15.43-296.763 µg/m^3	(Q. Liu, 2013)
		0.04-125.1 µg/m^3	(Yan et al., 2017b)
	Europe	100-150 µg/m^3	(Jian et al., 2020)
	South America	50-120 µg/m^3	
	North Africa	50-80 µg/m^3	

As mentioned before, one of sources Hg is from energy consumption. But there are other sources of Hg emissions. These mercury emissions are classified as non-point sources, which are difficult to track. And the biomass combustion contributed to relatively high mercury emission levels from the non-point sources. Nearly 2.3 billion people will continue to use biomass until 2030 (James et al., 2020), and the majority of them reside in rural areas, particularly in developing countries (Ravindra et al., 2019). In contrast, nearly 43% of the EU28's energy sources in 2017 (prior to the UK's exit from the EU) came from the combustion of solid biomass in household boilers and stoves. More than 50% of the burned biomass was used for residential heating (Jaworek et al., 2021). Wood contained between 0.4 and 7.3 g/kg of mercury, while bark and leaves contained between 2.7 and 65.9 g/kg (Dziok et al., 2020). Biomass combustion contributed to relatively high mercury emission levels. Up to 30% of mercury emissions were due to mercury bound to particulate matter (De Simone et al., 2017). Dziok et al. (2020) reported that the household heating boiler released nearly 99% of mercury from the combustion of hard coal and woody biomass (Dziok & Penkała, 2020).

1.3.2. The commercial products related with mercury

Between 2001 and 2005, 15,552 Americans were exposed to elemental mercury, according to the US Poison Center. In 91% of these cases, accidental exposure occurred (Caravati et al., 2008). Mercury has been intentionally used in many products and processes in different aspects because of its unique properties. That is the reason people exposure to mercury easily.

In the ancient time, three HgS products—namely cinnabar, metacinnabar and hypercinnabar—prevail were used as the pigments, medicines, etc. They were used for different kinds of purposes such as painting human bones and offerings, decorating architectural structures and mobile objects (Gliozzo, 2021). In the modern time, mercury is commonly used in - dental amalgam, batteries, discharge lamps, measuring equipment and electrical control and switching equipment because of its unique properties (Risk & Limited, 2002). The estimated annual mercury usage in 2004 was around 3300 Mg. ASGM used 1000 Mg of mercury to extract gold, accounting for 30% of total mercury consumption that year. The second and third largest sources of mercury utilization were Chlor-alkali processes in industries (700 Mg) and disposable batteries (600 Mg), accounting for 21% and 18%, respectively, of total mercury emissions (Swain et al., 2007). There were

additional mercury consumption from different sources, such as dental amalgams (270 Mg), catalyst for chemical production (250 Mg), measuring and control equipment (160 Mg), other usage (50 Mg) and etc. (Swain et al., 2007).

In the 50 Mg of mercury product, thimerosal (a mercury-based preservative) has a lot of controversy for decades. Because it is use in children vaccine for antiseptic and antifungal in a low cost by comparing with other preservative methodologies. Although thimerosal dose not still in body a long time and it decomposes into ethylmercury and thiosalicylate when it reaches harmful levels. And the ethylmercury and thiosalicylate, which are readily eliminated from the body (CDC, 2013). And the result from analysis the methylmercury and ethylmercury in hair samples of infants immunized with thimerosal-containing vaccines proofed the ethylmercury would be eliminated from body easily than methylmecury (Dórea et al., 2011). However, the mercury products in vaccines are an ignored source of mercury emission.

People are exposed to mercury not only via the commercial products containing mercury or mercury implementation devices, but also via the products contaminated by mercury. For instance, people frequently exposed to mercury are consuming the specific kinds of fish. In 2017, the estimated fish consumption rate was around 20.5 kg per capita (FAO, 2018). So, people who frequently consume the fish products can be poisoned by higher levels of methylmercury. Feingold et al. (2020) investigated people exposed to mercury via different factors, such as live region (ASGM-affected communities or not), household income (commercial, professional, transportation, employment), daily meal (consume rice, fish, fruit) and etc. The result was obvious and it proofed that the most important factors of mercury exposure to human were fishing activities and daily consumption of fish (Feingold et al., 2020). Except consumption of fish, human may expose to mercury by other food intake, such as rice, whey protein. Liang et al. (2015) analyzed the rice samples from 10 different regions in China. They found that the concentration of total mercury and methylmercury were in a range of 3.2 μg/kg—569 μg/kg and 2.1 μg/kg—144 μg/kg, respectively. The top rank of concentration of total mercury and methylmercury in rice samples were from the regions which are near the mercury mining (Liang et al., 2015). Nevertheless, Aquino et al. (2017) found the mercury present in 19 whey protein brands, and the concentration of mercury in the samples was in a range of 0.55 ng/g—9.41 ng/g. There is another unintentional route of human exposure to mercury—using cosmetics. Hamann et al. (2014) investigated mercury

content in 549 skin-lightening products from different brands and different countries. In their study, mercury presence in those 549 skin-lightening products. And 6% of they contained mercury in excess of 1000 ppm, 3.3% of lightening products purchased in the United States were found to contain mercury in excess of 1000 ppm. The FDA in U.S. prohibits the use of mercury as an active ingredient in cosmetics and limits mercury as an impurity to 1 ppm (Hamann et al., 2014). Elhag et al. (2015) also found the mercury present in the skin-lightening products from 8 different brands. And the mercury concentration in those 8 samples were in a range of 0.035 ppm—3.373 ppm. Mercury concentration in five of those samples were higher than the limitation of FDA in U.S.(Eldin.Elhag et al., 2015).

Most of the mercury concentrations are lower than the limit of 500 ng/g recommended by the International Organization for fish and seafood (WHO, 2010 ; Aquino et al., 2017). But based on dairy products and the multiple food intake routine, manufacturers should control the products in order to keep toxic elements at an absolute minimum.

1.4. Current stage of fossil fuels and biomass in China

Since China jointed the WTO in 2001, the economy, GDP, the annual per capita disposable income increased rapidly comparing with the ages before 2001. As the response, the industrial production such as concrete, steel and for instance car ownership number increased. As another constructing programs were waiting to start, the energy consumption also increased, as well as the fossil fuels usage. In 2003, the total coal consumption in China was 183,760.24 [10 Gg of SCE]. Till 2020, the total coal consumption has increased to 404,860 [10 Gg of SCE]. And the total energy consumption increased from 197,083 [10 Gg of SCE] to 498,314 [10 Gg of SCE] between 2003 and 2020, which were 2 times than 2003's coal consumption and energy consumption (Fig.1.4) (National Bureau of statistics of China).

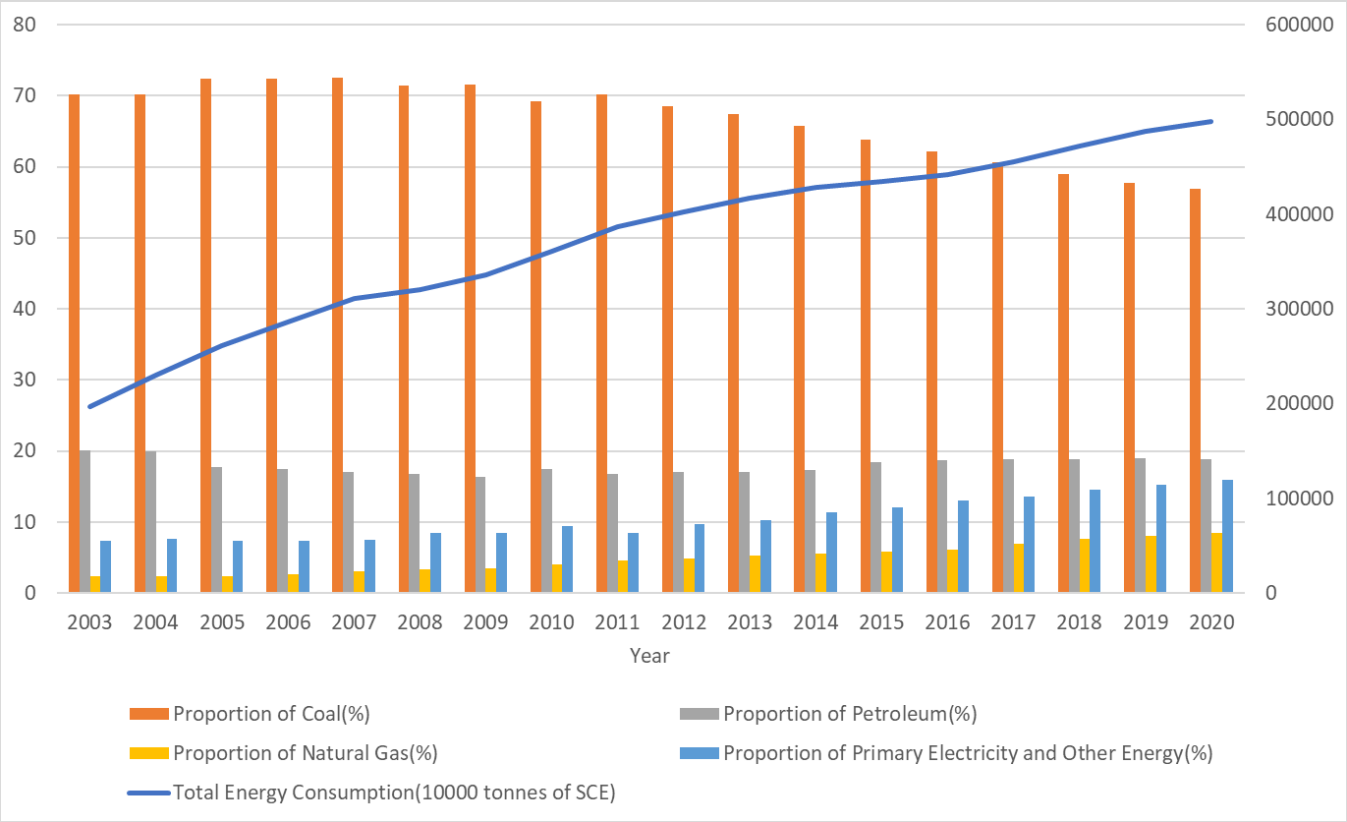

Figure 1.4: The energy consumption in China in 2003-2020

As the result, the total mercury emission in China also increased. In 1995, the total mercury emission was around 500 Mg, as it increased to 650 Mg till 2002 and around 842.2 Mg in 2010. So, within 15 years, the annual mercury emission increased almost 70% (Jiang & Wang, 2019). Realizing the large amount of pollution, since 2001 the society in China requested for a better living environment. The Environment Protection Ministry of China enhanced the standard of ambient air quality and implemented a branch of emission regulations starting from 2011. From 2010 to 2014, the number of coal-fired units increased by 30% in whole China, so annual increase was around 6% and annual capacity increase was 42790 MW. By the end of 2014, the National Statistical Bureau computed the whole capacity of all coal-fired units over 6 MW to be 897 230 MW. The majority of them were small and located in densely populated

areas (Environment Protection Ministry of China, 2016). Although, it is anticipated that the proportion of coal fuels in the China energy consumption structure will decrease as a result of the implementation of various carbon emission peak and neutrality policies (CSC 2022). The mercury emission limit (50 μg/m^3) was added for the first time to the *Emission Standard of Air Pollutants for Boilers* (GB 13271–2014) in China, in 2014 (Tong et al., 2022).

Assuming, the coal-dominated energy consumption structure will persist for a period of time and the reduction of the atmospheric mercury emissions from CFIBs in China continues to be an enormous challenge (Tong et al., 2022).

1.4.1. Countryside

China's remote, rural and suburban forests have total Hg inputs that are 2–4 times and 2.5–5 times higher than European and North American forests, respectively. The vast majority of the extremely elevated total Hg inputs come from the elevated atmospheric Hg concentrations and litterfall biomass. The total Hg emissions from forest ecosystems are significantly lower than atmospheric depositions. The annual total Hg retentions in subtropical forests range from 26.1 to 60.4 μg/m^2, and in temperate forests, from 12.4 to 26.2 μg/m^2. Given the extensive forest coverage in China, the total Hg retention in the forests is 69 Mg/year, which is significantly higher than global model estimates (J. Zhou et al., 2020).

Based on Shi et al. (2022) report, the total elemental mercury emissions in rural regions were lower than the emissions from the urban regions. The total mercury emission in the rural region of Changdao Island, Mt. Ailaoshan, Mt. Changbai were 2.52±0.82, 2.09±0.63, and 1.68±0.47 ng/m^3, respectively. And the total mercury emissions in urban regions of Lanzhou, Nanjing, Haidian were 4.48±2.32, 7.94±6.99, and 2.77±0.91 ng/m^3, respectively (Shi et al., 2022).

The mercury emissions from the scattered sources, especially from the households is hard to be calculated in terms of the total mercury emission. The residents who live in the rural regions use the agricultural wastes, such as straws and different kinds of wood, as an energy source to heat up their households in the winter season. In the Sichuan Basin in China, the quantity of black carbon released from low efficiency combustion household stoves was 640±245 Gg/y in 2014. Straw and wood contribute to 42±13% and 36±15% of total national emissions of black carbon, respectively

(W. Zhang et al., 2017). The mercury content in agricultural wastes, such as fuelwood, straws, and pellets, was determined at levels of 0.65-28.44 μg/kg, 3.02-12.05 μg/kg, and 5.22-8.10 μg/kg, respectively (Shen et al., 2021).

1.4.2. Urban area

Comprehensive city-level atmospheric mercury emission inventory from coal combustion was established by updating emission factors of using high-resolution information such as plant-specific air pollution control devices (APCDs) in 182 cities in China in 2010. The estimated atmospheric mercury total emission from coal combustion was 202.3 Mg, of which more than a half was concentrated in 36 cities such as Chongqing (megacity) and Ordos (city heavily dependent on coal), indicating that mercury emissions were unevenly distributed (Z. Wu et al., 2020). The metallurgy, non-metal products, the chemical industry, electricity and hot water production and supply, Civil constructions, are the industries with the highest mercury emissions in China. Metallurgy appeares three times among the top three BBA mercury emission sectors for Jiangsu, Shandong, and Henan. Jiangsu and Shandong's metallurgy primarily influences the sectors in their respective provinces. The Jiangsu metallurgy sector reveals 49.7 Mg of BBA changes in Jiangsu. Shandong metallurgy is responsible for 56.4 Mg of mercury emission changes in the Shandong province. Henan's metallurgy is responsible for 47.2 Mg of changes in BBA mercury emissions within its own province (K. He et al., 2021). Mercury emissions in China in 2014 are primarily concentrated in Henan, Hebei, and Shandong, among other regions, while the northern and western regions have relatively high mercury emissions overall. The evolution of mercury emissions in various regions of China from 2003 to 2014 (Jiang & Wang, 2019). Corresponding colors represent variations in mercury emissions throughout this time period. It can be observed that emissions in the western and eastern regions have increased substantially, while emissions in the northern regions have decreased proportionally (Tang et al., 2018). In case study of the period of Hg(0) analysis from 2012 to 2020 in Xiamen in China, the Hg(0) concentrations in January were highest in 2015 (4.47 ng/m^3) and decreased to 2020 (3.93 ng/m^3). The seasonal variation of Hg(0) was characterized by higher values in the winter than in the summer and at night than during the day, which is consistent with the values in the majority of urban areas (Shi et al., 2022). In Guiyang city, which located in the Guizhou province in Southwest China, some of local residents used the low combustion efficiency stoves to cook. Cui et al. (2019) pointed out that the annual total

mercury emission from households between 1990 to 2016 was 1.2—2.3 Mg/year. And these total mercury emissions from households were twice as high compared to the total mercury emissions from the CFFPs (Cui et al., 2019).

A series of policies have been issued by the Chinese government since 2013 to promote clean heating and address emerging issues. These policies plan to solve the winter heating problems, combat climate changes, and improve standards of living for rural residents. Clean heating is defined as heating methods with low emissions and low energy consumption that utilize natural gas, electricity, geothermal energy, biomass, solar energy, industrial waste heat, clean coal, nuclear, or another form of clean energy(Y. Li et al., 2022) . According to Cui et al. (2019), Wu et al. (2020), He et al. (2021), Shi et al. (2022) studies, the mercury emissions in China have continuously decreased in recent years. However, mercury emissions from industries and domestic sources are still a serious issue. It needs keep forward to reduce mercury emissions to meet the goal of zero emissions.

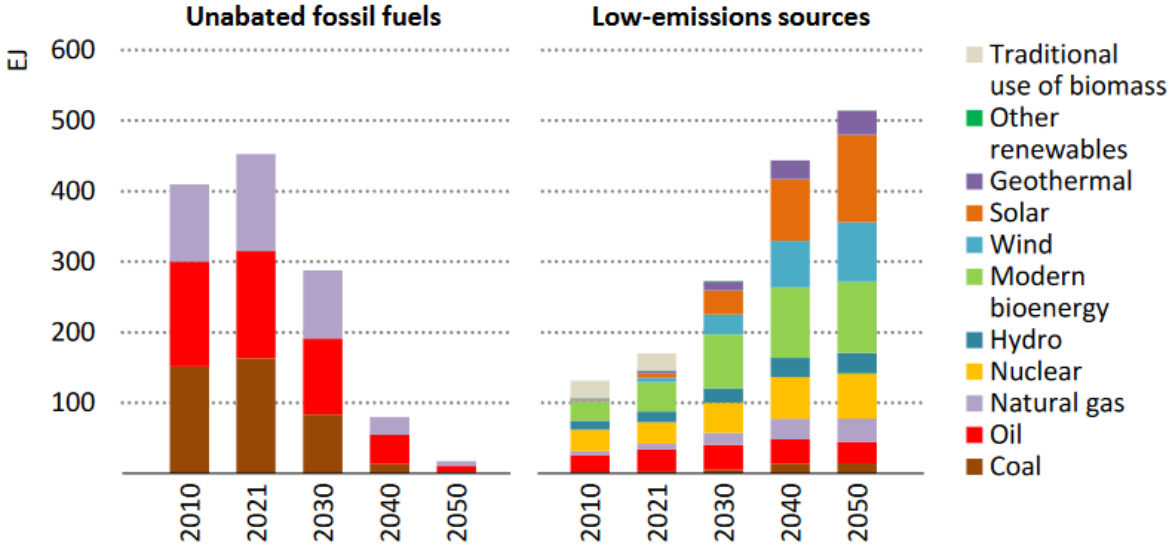

Figure 1.5: World-wide total energy supply of unabated fossil fuels and low-emissions sources in the NZE Scenario, 2010-2050

1.5. Future sight of mercury emissions

In recent years, the IGCC power plants or the coal gasification systems are an advanced and effective fossil fuel combustion technologies, comparing with the conventional CFPPs. Mercury

mainly remains in the form of Hg(0) vapors during the coal gasification process (Z. Wang et al., 2020; Zheng et al., 2021; Altaf et al., 2022). IGCC power plants will dominate the fossil fuel combustion in energy generation sectors. Hg(0) is a main pollutant from IGGC power plants exhaust emission. Therefore, Hg(0) reduction and atmosphere protection will have a serious issue. Fortunately, the whole society realized the significant environmental issues. The EU and OECD, developing countries made restrict regulations and acts to reduce the pollutants emissions from energy generation by using fossil fuel sources. The zero emissions policy was made according it to reduce air pollutions from their sources. According to the International Energy Agency analysis, the high pollutions energy supply which is from the fossil fuels would be end till 2050, when clean energy and zero emissions will dominant the sources of energy supply. The use of fossil fuels and traditional biomass will be limited after 2030, and the clean energy will dominate the energy production (Fig. 1.5) (International Energy Agency, 2022).

1.5.1. Mercury from the biofuels

Biofuels are converted from the biomass. The biomass includes the forestry or wood residues that have not been chemically treated, glued, or coated on the surface, excluding waste-derived fuels (Tsai et al., 2023). The 63.7% of the world's renewable energy supply in 2015 came from solid biofuels, as well as liquid biofuels, biogas, and renewable municipal waste accounted for 4.3%, 1.7%, and 0.9%, respectively. Biomass and renewable wastes account for even less in OECD countries, where biomass is widely used in modern systems, accounting for just 5.2% of total primary energy supply in 2015 and 36.1% of renewable energy supply (Sahoo et al., 2022). However, biofuel may also contain mercury because of the biomass grown on soil contaminated with mercury (Bilandžija et al., 2022). Dziok et al. (2020), Shen et al. (2021), Tsai et al. (2023) pointed out the mercury content in the biomass in their studies, which is present in Chapter 1.3 and 1.4. Mercury content in liquid biofuel (biodiesel) was 0.19 ppb, 2.6 ppb and 23.2 ppb (De Jesus et al., 2020).

1.5.2. Mercury re-emissions from ocean sources

The 75% of the mercury emitted by biomass burning was deposited in ocean basins, with global consequences for food chains and human health (De Simone et al., 2017). Mercury re-emission

from the ocean is a serious issue, because over 50% of the annual mercury release is currently coming from the natural sources. So, mercury re-emissions from the ocean dominated other natural sources of mercury emissions.

In recent years, the algal biofuels are a potential renewable energy source. As the feedstock of the third generation, algae are suitable for biodiesel and bioethanol production due to their rapid growth, high biomass yield, and high lipid and carbohydrate content (Saad et al., 2019). Certain algae species (Schizochytrium sp., Nitzschia sp., and Botyococcus braunii) contain over 50% of the oil reduced to dry biomass, which can be extracted and processed into fuel (Bošnjakovic & Sinaga, 2020). The mercury polluted ocean may cause the algal biofuel contamination and heavy metal emissions, interfering between the natural and anthropogenic cycles. The algal biofuel would contribute the high amount of mercury emission, when it is finally commercialized. Therefore, there is still a lot of effort to achieve the clean energy and zero emission in the future.

2. The mercury capture from emission sources

Hg(0) remains in the atmosphere even to 6 years. It can travel approximately 2500 km within 72 h (Glass et al., 1991). It covers to the Earth's surface from the atmosphere via wet and dry depositions with efficiencies of approximately 66%, 70% (Fitzgerald & Vandal, 1991; Lindberg et al., 1991). Therefore, mercury may occur at the earth surface, surface water or soils without the link to any specified mercury source from the industries (Hurley et al., 1991). At current state of technology, it is hardly to remove mercury from the atmosphere or oceans. It is the only way to reduce the mercury concentration in the environment by capturing mercury from its sources.

2.1. The techniques of mercury capture

There are different kinds of mercury capture commercial techniques in the market, ready for the industrial or household implementation. The fuel preparation is one methodology to remove mercury content from the fuel sources before the fuel utilization. This methodology includes the blending, physical or chemical treatment. The blending method is to mix the low-quality fuels (containing a high quantity of impurities) with the high quality fuel (containing a low quantity of impurities) to reduce the quantity of impurities (including mercury content). It is a compensative method to meet the requirements of low cost and low pollutants emissions.

The physical or chemical treatment method is to remove the impurities from the fuels. In coal washing, froth flotation is to remove hydrophobic impurities during a hydraulic process. In this process, hydrophobic and hydrophilic bubbles are injected to adhere to the impurities and remove the impurities. But this methodology may cause the water contamination after the fuel preparation process, and the organic bounded mercury is hardly to be removed (Dziok & Strugała, 2017). Therefore, there are other techniques required to capture mercury from the exhaust way to reduce the mercury emissions.

2.1.1. Beneficial devices

In the industries, there are kinds of APCDs to reduce the pollutants from the exhaust gas, such as SCR, WFGD, ESP or FF. They are used to reduce NOx, SO_2 and particulate matters from the flue gas, respectively. But those APCDs can reduce the mercury concentration in flue gas to some extent. It can be considered as a side benefit of APCDs. In the conventional CFPPs, the APCDs are implemented among the exhaust gas stream lines in the specific location (depends on the fuel utilization and capacity of electricity generation) (Fig. 2.1).

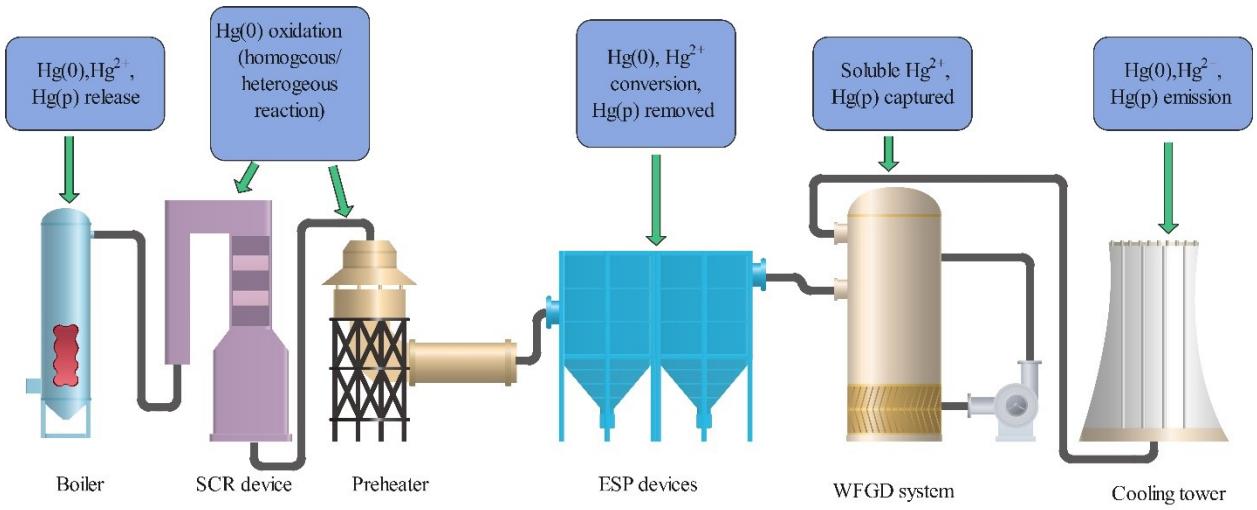

Figure 2.1: Mercury capture by APCDs in CFPPs (Deng & Macherzynski, 2023)

The SCR device with its efficient catalytic bed oxidizes Hg(0) with O_2, sulfur compounds, and halogen species under the heterogeneous (on particles) or homogeneous (in gas phase) reactions. After that, the remaining Hg(0) is emitted from SCR device into the preheater. In the preheater, Hg(0) may be continuously oxidized as the gas temperature degrease. Inside ESP devices, the high voltage electrical field captures the particles with oxidized mercury, halogenated mercury, particulate matter-bonded mercury, and a portion of Hg(0) may be exited and trapped in ash, but some untreated passes through. The mercury capture in FF undergoes a different scenario then in ESP. Fly ash collects onto filters and mercury is captured even with better efficiency than in ESP. The uncaptured mercury species enter the WFGD system, where the soluble mercury species of Hg(II) are captured and the non-soluble mercury species of Hg(0) and possible Hg(I) primarily escape. Mercury that has not been captured is then released into the atmosphere. More details and the principles of the mercury species capture in APCDs from process gases in different industries, were described in (Deng & Macherzynski, 2023). Wang et al. (2010), Liu et al. (2019) and Chou et al. (2021) analyzed the mercury capture effectiveness by the APCDs and the mercury species emissions from the selected CFFPs in China. According to their data, the APCDs were able to reduce the mercury concentration from the flue gas. But the APCDs were hardly to remove Hg(0) (table 2.1). Therefore, the additional techniques or devices are required to implement to capture mercury from the flue gas.

Table 2.1. Concentration of mercury species in flue gas after each APCD from 3 different power plants in China

Power plants	Hg species	Measurement point				Total Hg removal efficiency	Sources
		SCR inlet ($\mu g/m^3$)	ESP inlet ($\mu g/m^3$)	WFGD inlet ($\mu g/m^3$)	Stack ($\mu g/m^3$)		
P-1	Hg^T	1.92	1.89	1.44	1.22	36.5%	(Wang et al., 2010)
	Hg(0)	1.55	1.02	1.00	1.08		
	Hg^{2+}	0.15	0.40	0.44	0.13		
	Hg_p	0.22	0.47	0.00	0.00		
P-2	Hg^T	24.49	19.22	0.77	0.60	94.4%	(Liu et al., 2019)
	Hg(0)	5.73	0.75	0.33	0.49		
	Hg^{2+}	4.65	1.76	0.45	0.10		
	Hg_p	14.11	14.43	0.001	0.005		

P-3	Hg^T	2.984	2.852	1.090	0.240	92%	(Chou et al., 2021)
	Hg(0)	0.811	0.601	0.647	0.221		
	Hg^{2+}	0.07	0.192	0.397	0.008		
	Hg_p	2.102	2.058	0.047	0.016		

2.1.2. Ion-exchange

In other kinds of industries or small-scale institutions, they may install different kinds PCDs by comparing with CFPPs due to the economic reasons or waste treatment procedures.

Ion exchange is a reversible chemical reaction between ions in liquid phase and ions in solid phase. It can effectively treat wastewater containing mercury with a mercury ion concentration of less than 100 mg/L (Ghodbane & Hamdaoui, 2008). It has the benefits of good mercury removal efficiency, no secondary pollution, fast treatment process (Gode & Pehlivan, 2006). The ion exchange method is useful to remove the mercury from the wastewater or drinking water (Hua et al., 2019). There are different kinds of ion exchangers applied in the wastewater treatment processes, such as strongly acidic cation exchangers, weakly and strongly basic anion exchangers, and selective ion exchangers (Dujardin et al., 2000). The ion exchange resins, like chelating resins are widely utilized due to their abundant raw material source, large adsorption capacity, high selectivity, simple re-generation, and excellent stability. They are considered as ideal adsorbents for the removal of heavy metals from wastewater (Xiong et al., 2012). Strongly acidic resins with sulfonic acid groups (-SO_3H) and weakly acid resins with carboxylic acid groups (-COOH) are the most prevalent cation exchangers. Hydrogen ions in the sulfonic or carboxylic groups of the resin are exchangeable with Hg^{2+} (Hua et al., 2019). The total mercury removal resins are the macroporous, thiol-containing styrene–divinylbenzene copolymers. Thiols can react with mercury as well as other heavy metals, and they are known as mercaptans. The reactions of total mercury removal resins capture mercury is described by Equation (1), (2) (Dujardin et al., 2000).

$$2RSH + Hg^{2+} \rightarrow RSHgSR + 2H^+ \quad (1)$$

$$RSH + HgCl^+ \rightarrow RSHgCl + H^+ \quad (2)$$

2.1.3. Membrane separation methodology

When mercury in wastewater is present in particulate/colloidal form, membrane separation techniques are especially effective (Dean, 2009). They are extremely effective, achieving mercury concentrations below 100 ng/L (Urgun-Demirtas et al., 2012). The complex membrane was prepared by the methodology of semi-interpenetrated polymer networks. It consist in a matrix of polyvinylalcohol, crosslinked by gaseous dibromoethane. This complex membrane had over 99.4% of Hg^{2+} removal efficiency (Bessbousse et al., 2010). The microfiltration, ultrafiltration, nanofiltration processes and reverse osmosis membranes have the ability to remove Hg^{2+} from the wastewater in oil refineries (Urgun-Demirtas et al., 2012). The microfiltration and ultrafiltration membrane performed the high mercury removal efficiency in the pressure condition over 2.8 bar. The reverse osmosis (RO) and nanofiltration membranes separated mercury effectively at 20.7 bar to achieve the result of mercury concentration below 1.3 ng/L (Urgun-Demirtas et al., 2012). Since, the membrane separation is a pH sensitive method, its optimal adsorption performance can be achieved between pH 5.5 to 6.0 (J. Wang et al., 2016).

2.1.4. Activated sorbents

The activated sorbents have the most promise due to its simplicity, low cost, and efficiency in water and gas purification, they are capable to remove the mercury in wastewater and flue gas (Baran et al., 2017; J. Yang et al., 2018; Maiti et al., 2019; Nanusha et al., 2019). As well-known, ACs, zeolites, clays, are a high-surface-area, porous, and multi-tunnel substances. Therefore, they are frequently used to remove particles, ions, or microorganisms in water or gas, since in some mechanism, only particles and ions of a certain size can pass through its pores and tunnels. In addition, those sorbents' chemical properties are determined by the extra framework in its basic structures, which has the ability to exchange ions and absorb acidic or basic ions. However, the non-modified sorbents have the low capacity of mercury removal and weak binding affinity (Benhammou et al., 2005; S. Wang & Peng, 2010). The modified sorbents have the high capacity of Hg removal efficiency. The thiol/thio-functionalized adsorbents, such as clays, resins, mesoporous silica, activated carbons, mesoporous carbons, and chalcogenides are highly efficient for Hg^{2+} removal in aqueous solutions due to the soft-soft interaction (Shin et al., 2007; Tchinda et al., 2009; Bessbousse et al., 2010; He et al., 2012; Ie et al., 2012; J. Wang et al., 2016; O'Connor et al., 2018; Hernández et al., 2019).

The dithio-carbamate-functionalized Fe_3O_4 nanocomposite treated aqueous Hg^{2+} in contaminated seawater. The adsorption process occurred spontaneously, and the adsorption capacity of the adsorbent could be increased by increasing the pH (pH range: 2.0-6.5) according to thermodynamic studies (Behjati et al., 2018). In addition, theoretical calculations have been used to investigate the mechanism of mercury adsorption. Density-functional theory (DFT) calculations were utilized to investigate the mechanism of mercury adsorption by dendrimer-functionalized multi-walled carbon nanotubes, revealing that two oxygen atoms of the phosphate group played a significant role in mercury removal (Iannazzo et al., 2017).

In recent years, a new material techniques known as MOFs (metal-organic frameworks) and SPCs (sorbent polymer composite) have been created by combining inorganic and organic sorbent components. The SPC proved to be effective at removing pollutants from exhausted gas and waste water. It does not have the disadvantages of traditional sorbents such as high costs, low sorption capacities, low number of reusing cycles, non-degradable properties, and secondary pollution, that make it difficult to implement these materials on a large scale. In addition, SPC materials have properties that conventional sorbents lack, such as covalent or non-covalent bonding (hydrogen bonding, metal-ligand coordination, ionic and hydrophobic interactions) between polyelectrolytes and a variety of inorganic/organic partners. The SPC materials contain polymeric ionic chains consisting of a high number and distinct stimuli-responsive functional groups with regulated actions (detection, immobilization, release) toward various classes of air and water pollutants (Bucatariu et al., 2021; Gorecki et al., 2022). The SPC removed 99.5% of mercury within 42 days, while the SPC removes between 99.5% and 82.3% after 34 days (Gorecki et al., 2022). The MOFs containing free-standing sulfur groups have proven to be effective mercury sorbents in solid phase (J. He et al., 2011; Kobielska et al., 2018). This is a potentially potent strategy for the molecular design of MOFs; while carboxyl groups bind metal ions for network formation, sulfur groups can remain as free-standing secondary donor groups (Hua et al., 2019). The Zr- DMBD with the hard carboxyl and soft thiol functioned as an effective mercury sorption, and the synthesized thiol-derived Cr-MIL-101-AS via the post-synthetic modification method, which exhibited excellent mercury ion adsorption capacity (Yee et al., 2013; T. Liu et al., 2014). The polymer composite Fe-BTC/Polydopamine (nanostructured MOFs) attached to the inner surface of the MOF increased the porosity of the composite, resulting in an ultra-high mercury

adsorption capacity of the composite, which removed more than 99.8% of the Hg^{2+} in a 1 ppm solution and reached drinkable levels in others (Sun et al., 2018).

2.1.5. Biotreatment methodology

Biological treatment is the process of passively adsorbing or combining metal ions with biomass. Heavy metals can be removed by bacteria, actinomycetes, yeasts, and molds among prokaryotic and eukaryotic microorganisms, respectively. In addition, some seaweeds, including brown algae, green algae, and red algae, exhibited the ability to remove heavy metals (Menger-Krug et al., 2012). The biotreatment can be divided by the types of microorganisms, sulfur reducing types and non-sulfur reducing types.

The sulfur reducing microorganisms precipitate the soluble mercury into the insoluble mercury species. The SRB (sulfate-reducing bacteria) is applied to mix with FGD sludge to remove the heavy metals in the wastewater treatment process. The SRB acts as an electron acceptor to generate H_2S (Maiti et al., 2019; Liu et al., 2021; Okonji et al., 2021), the H_2S react with soluble mercury, Hg^{2+}, to form the non-soluble HgS. The mechanisms of SRB involved enzymatic reduction and oxidation of Hg(0) removal were described by the Equations (3) to (9). APS: adenosine 5′-phosphosulfate, AMP: adenosine mono-phosphate (Xu & Chen, 2020).

$$2CH_3CHOHCOO^- + SO_4^{2-} + 4H_2O \rightarrow 2CH_3COO^- + 2HCO_3^- + HS^- + H^+ \quad (3)$$

$$2CH_3CH_2OH + SO_4^{2-} \rightarrow 2CH_3COO^- + HS^- + H^+ + 2H_2O \quad (4)$$

$$CH_3COO^- + SO_4^{2-} \rightarrow 2HCO_3^- + HS^- \quad (5)$$

$$AMP^{4-} + SO_4^{2-} + H^+ \rightarrow APS^{2-} + HP_2O_7^{3-} \quad (6)$$

$$APS^{2-} + 2e^{2-} + H^+ \rightarrow HSO_3^- + AMP^{2-} \quad (7)$$

$$HSO_3^- + 6e^{2-} + 6H^+ \rightarrow HS^- + H_2O \quad (8)$$

$$Hg^{2+} + H_2S \rightarrow HgS + 2H^+ \quad (9)$$

The non-SRB, such as E. coli, also has the ability to treat the low mercury containing wastewater. It achieved the result of mercury reduction, down to concentration of 6.3 ng/L (S. Chen & Wilson, 1997). However, the mercury absorption rate of E. coli in wastewater is influenced by the high pH and other ions (Deng & Wilson, 2001). The Bacillus also can be used to remove mercury in

wastewater in the same performance conditions as the E. coli do (low mercury concentrations, the effective performance at pH between 4.5 to 6.0) (Green-Ruiz, 2006).

2.2. The principles of mercury (ad)sorption

The activated sorbents can be capable to capture the particles, ions, or heavy metals in wastewater or exhaust gas because their physical or chemical properties. Those activated sorbents are divided into two groups based on their adsorption type: physisorption and chemisorption.

2.2.1. Physisorption

Physical adsorption is accompanied by low heats of adsorption, with the surface undergoing no violent or disruptive structural changes during the adsorption. It can result in the formation of multiple layers of adsorbate on a surface. The adsorbate can completely fill pores for pore volume measurements. These pore condensation phenomena can also be used to determine pore size and distribution. Physical adsorption equilibrium is reached rapidly because activation energy is not required. Adsorption in small pores (less than 2 nm) can limit the adsorption rate. But mercury adsorption is an exception. Because mercury adsorption measurement can be measured in a pore size from 200 μm to less than 1.8nm (Lowell et al., 2004). Physical adsorption is fully reversible for the adsorption and desorption processes (Lowell et al., 2004).

In the adsorption process, sorbents adsorb pollutants from the wastewater or flue gas by the Van der Waal force. The Van der Waal force is important for the physisorption because it present in the dispersion forces, ion-dipole, ion-induced diploe, dipole-dipole and quadrupole interaction (Lowell et al., 2004). Therefore, the determination of surface area, pore size, and pore volume from physisorption isotherms, the application of appropriate theoretical models that accurately describe the underlying adsorption mechanism is crucial (Lowell et al., 2004; Thommes & Cychosz, 2014).

Kinds of sorbents applied for mercury capture

The granular activated carbon, zeolites, and sorts of metal oxide sorbents, reduced the mercury emission from exhausted gas by 90%, 87%, 95.3%, respectively (Wdowin et al., 2015; Xu et al., 2018), as well as reducing the mercury from waste water by 81%, 99%, and 70-90%, respectively (Tauanov et al., 2018; Pasinszki et al., 2020; Budihardjo et al., 2021).

The ACs impregnated or modified by selected metal compounds or elements, showed the related good mercury capture efficiency. The Fe_2O_3 and sulfur modified ACs (ACs/ Fe_2O_3 and AC-S) both showed over 60% of Hg(0) removal rate in the simulated flue gas (N_2 + 10% H_2 + 15% CO + 1500 ppm H_2S) at 150℃, respectively. However, the raw ACs removed only less than 20% Hg(0) from the simulated flue gas in the same conditions, when comparing with Fe_2O_3 and sulfur modified ACs (ACs/ Fe_2O_3 and AC-S) (J. Wang et al., 2022). The sulfur impregnated ACs showed the high Hg(0) removal efficiency because of the Hg(0) not only deposits on the ACs' surface, it also interacts with the sulfur functional groups (disulfide, thiophene, sulfoxide and sulfone groups) (W. Liu et al., 1998; J. Wang et al., 2009; Huo et al., 2019). Those functional groups have the high affinity to mercury chemical species, improve the overall mercury adsorption capacity and selectivity. The mercury adsorption capacity of modified activated carbons was 820 mg/g in simulated flue gas (Cai & Jia, 2010).

2.2.2. Chemisorption

Surface atoms frequently possess electrons or electron pairs that can form chemical bonds. This adsorption process involves valence forces of the same type as those operating in the formation of chemical compounds. SO, this adsorption process results from chemical bond formation (strong interaction) between the adsorbent and the adsorbate in a monolayer on the surface (Lowell et al., 2004). As majority of chemical reactions, chemisorption is frequently associated with an activation energy, and active sites that attracted molecules to a surface must overcome an energy barrier prior to forming strong bonds with the surface (Lowell et al., 2004). The sorbent surface is involved in the chain of reactions and interactions between molecules or atoms coming from a gas or aqueous phase, which adsorbed at neighboring areas create new bonds, and finally desorb. The reactions can occur between the adsorption layer and the atoms of sorbate, as well as direct collisions of gas molecules with adsorbed molecules or atoms on the sorbent surface. The chemical adsorption was defined by Langmuir as presented in the Equation (10):

$$\theta = KP/(1 + KP) \quad (10)$$

where P is the gas pressure and K is the equilibrium constant for adsorption-desorption (Prins, 2018).

In the chemisorption process, pollutants, such as heavy metals, molecules are adsorbed by sorbents, then it is followed with forming chemical bonds with the sacrificial ions of the sorbent. There are four mechanisms used to defined the chemical adsorption processes. They are so-called the Deacon process, the Eley–Rideal mechanism, the Langmuir–Hinshelwood mechanism, and the Mars–Maessen mechanism. Hg(0) adsorption processes in those four mechanisms are illustrated by the Fig. 2.2 (Deng & Macherzynski, 2023). Pollutant ions react with metals on the sorbent in two different routines. In the first one, pollutants deposited onto sorbents, then they continue to react with the surface oxygen on the metals sorbents to establish a stable molecule, which can then be removed in a subsequent procedure. In the second routine, pollutants react directly with metals placed on the surface of sorbent, forming a chemical bond without the adsorption or without the reaction with the surface oxygen. The Mars–Maessen process and the Langmuir–Hinshelwood mechanism are examples of the first chemisorption mechanism, while the Eley–Rideal and Deacon mechanisms are examples of the second.

Deacon mechanism

The Deacon reaction processes are based on the oxidation of hydrochloride or chlorine gas on the surface of the sorbent which occurs at a temperature of 400–450°C, in the presence of a selected adsorbents (Hisham & Benson, 1995; Cao et al., 2005; Q. Zhang et al., 2020). The copper, iron and manganese sorbents are suitable for the Deacon process (Du et al., 2014; Zhang et al., 2020). When HCl deposits onto the adsorbent, the surface oxygen or lattice oxygen converts a large quantity of HCl to Cl_2. And the Cl_2 is a critical factor in the oxidation of Hg(0) in the further steps of homogenous or heterogenous reactions. The Deacon reaction process consists of two independent steps: (1) HCl adsorption by the metal adsorbent to form metal chloride (or oxychloride) with water and (2) chloride oxidation by O_2 to regenerate the metal oxide and free Cl_2 (Fig. 2.2 A).

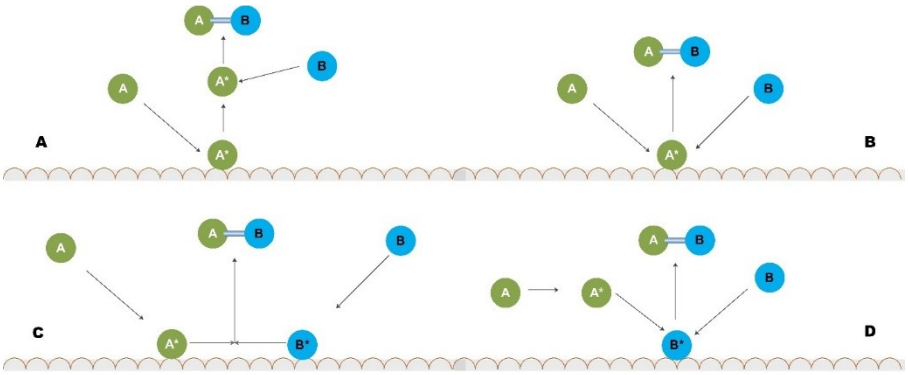

Figure 2.2 The mechanisms of atoms transformation, where A is Deacon mechanism, B is Eley–Rideal mechanism, C is Langmuir–Hinshelwood mechanism, and D is Mars-Maessen mechanism (Deng & Macherzynski, 2023)

Eley–Rideal mechanism

During the Eley–Rideal mechanism, there is only one kind of atom or molecule adsorbed onto the surface of sorbent, for instance the Hg(0) atom or HCl gas. Senior and Linjewile (2003) hypothesized that mercury oxidation may take place onto the solid surface, when the process gas passes though the SCR catalyst. This mechanism involves chlorine compounds as intermediates (Presto et al., 2008; Dranga et al., 2012; Zhang et al., 2016). Hg(0) atoms remain in the gas phase, they react with the hypothetical adsorbed chlorine to produce molecules, which readily desorb (Fig. 2.2 B).

Langmuir–Hinshelwood mechanism

In the Langmuir–Hinshelwood mechanism, Hg(0) and another molecule or atom (for instance HCl) deposit on the adsorption sites of adsorbent, and finally two compounds react there. The first step: Hg(0) in gas is attracted onto the adsorption site of a sorbent, and subsequently the adsorbed mercury and the surface oxygen or oxide radical interact on the sorbent surface resulting in the formation of Hg^{2+} (Ewers et al., 2017; Yoo et al., 2018). At the same time, the proposed HCl deposits onto the sorbent near by the Hg(0) adsorption site. The chemical bond of HCl is

disassociated, and in the second step, the disassociated radical reacts with mercury resulting in the formation of $HgCl_2$. The product desorb from the solid surface (Fig. 2.2 C).

Mars–Maessen mechanism

The Mars–Maessen mechanism is similar to the Langmuir–Hinshelwood mechanism. Hg(0) deposits on the surface of adsorbent, then it is oxidized by surface oxygen or lattice oxygen to form Hg^{2+}. It is boned by the weakly bond Hg–O–Metal–O_{x-1} on the metal sorbent surface, and then form HgO. In the further step, the gas-phase O_2 replaces the consumed lattice oxygen and/or surface oxygen from the metal sorbent surface (Ling et al., 2015) (Fig. 2.2 D).

More details of mercury capture mechanisms involving the oxidation of elemental mercury, in different industries, were presented in the review (Deng & Macherzynski, 2023).

Kinds of sorbents applied for mercury capture

Nanocrystal sorbents, such as metal sulfides, ZnS, Cu_2S, CdS and etc. have the high adsorption capacity for Hg^{2+} fixation. The ZnS nanocrystals sorbent has 2000 mg/g of adsorption capacity and it captures over 99.9% of Hg^{2+} from the wastewater. It reduced the Hg^{2+} concentration from 297.5 mg/L to 1.0 µg/L within 5 minutes (Qu et al., 2014). The nanostructured tubular copper sulfide (Cu_2S) was obtained in a wet-chemical reaction. As a highly effective substrate for mercury removal, the as-synthesized product provided an exceptionally high removal capacity towards Hg^{2+} with a maximum capacity of 3,096 mg/g (Ray et al., 2015).

The CdS nanocrystals were synthesized prior to the addition of Hg^{2+} containing reactants. Cd^{2+} was easily and rapidly replaced by Hg^{2+} in CdS nanocrystals (Gupta et al., 2013). This application is based on the intrinsic cation exchange properties of nanocrystals and opens a new application window for nanocrystals. It is a new strategy for preparing bright and compact quantum dots (QDs) based on mercury cation exchange in non-polar solvents (HgxCd1-xE, where E represents Te, Se, or S) (Smith & Nie, 2011).

The CuS can capture Hg(0) from process gas containing a high concentration of SO_2. When Hg(0) was presented in SO_2 gas of 500 ppm, 1000 ppm and 2500 ppm, the Hg(0) adsorption capacities of CuS were 16.25 mg/g, 15.93 mg/g and 15.88 mg/g, respectively. The Hg(0) adsorption capacity of CuS in pure N_2 was close to 17 mg/g (W. Liu et al., 2019). The $CuFeS_2$, CuS, FeS_2 showed the remarkable results towards mercury removal, in a temperature range between 40ºC to 100°C.

10 mg sample of $CuFeS_2$ removed almost 100% of Hg(0) from the simulated gas containing 68 $\mu g/m^3$ of Hg(0) and 2000 ppm of SO_2 (J. Yang et al., 2021).

3. The mercury chemical analysis systems

Although researchers and scientists designed many kinds of advanced sorbents, there is a need for advanced mercury analyzing systems. It is hard to analyze the sorbent capture efficiencies and the interference factors of mercury removal without these tools. Researchers and scientists analyze the mercury dedicated sorbents in the laboratory and industrial environment. These analysis systems are similar – the laboratory ones should simulate the industrial processes, and of course are of a different scale.

3.1. Industrial scale mercury analysis systems

The analysis of mercury capture efficiency from the industrial exhaust gas is quite complicated study because of the conditions of exhaust gas. Mercury analysis may be interfered by many factors as chemical character of the contaminants and the flow rate, which subjects to fluctuations. When switching from one impact factor component to another impact factor component, if the new impact factor component (such as SO_2, SO_3) is easier to oxidize and the concentration is high enough, then the process continues without any trouble (Trovarelli et al., 1999). The mercury analysis procedure and strategies is often adjusted to the specified process gas and industry. The most common methods for mercury analysis in industries are OHM method and EPA method 30B. The OHM is a standard mercury sampling method that can determine Hg(0), oxidized mercury (Hg^{2+}) and particulate-bound mercury (Hg_p) (Cheng et al., 2009). The EPA method 30B can greatly simplify the mercury determination process. It consumes less sampling time and costs, but can still give good, comparable results. However, Hg_p cannot be detected by this method, leading to the lack of Hg_T concentration.

Zhou et al. (2020) combined the SI and Hg-TPD methodologies to analyze the mercury capture efficiency for the industrial scale mercury analysis. In Zhou et al. (2020) procedures, they used the SI methodology to loading the sorbents into the industrial exhaust gas. The feeder first conveyed the sorbent from the hopper to the injectors. Then the sorbent was injected into flue gas by the

airflow from the compressed air tank. The airflow used in the experiments was controlled by pressure regulating valves. The sorbents were introduced into the upstream of FF system. After then, the sorbents from the downstream of FF system was collected to analyze the mercury capture efficiency. The mercury speciation measurement in the exhaust gas was achieved by the OHM and US EPA Method 30B. Therefore, the following discussion about mercury removal efficiency is based on data obtained by the OHM, and the data from EPA method 30B can verify the accuracy of OHM method results. These methodologies were used to quantify the mercury concentration in coal-fired flue gas (Y. Zhou et al., 2020). After the industrial test, Zhou et al. (2020) collected the two kinds of samples, samples obtained without the sorbent injection, and the samples obtained with SI. Then, all the samples were analyzed by Hg-TPD in the laboratory. It consisted of a thermal decomposition unit and an online mercury monitor (RA-915M). The thermal decomposition unit consisted of two furnaces. The first one was used to heat the samples from 30℃ to 700℃ at a stable heating rate of 5℃/min. In this furnace, various mercury species decomposed at specific temperatures. To reduce these mercury compounds into Hg(0), which can be detected by the mercury monitor, the second furnace was kept at 800℃ (Y. Zhou et al., 2020). Lou et al. (2019) used the similar methodology as Zhou et al. (2020). They tested their sorbents and analyzed the mercury capture by using SI in CFPPs. Mercury concentration was measured by the OHM method. And the mercury capture efficiency was achieved by the Hg-TPD in the laboratory (Luo et al., 2019).

In another methodology, Górecki et al. (2016) designed at the AGH University a portable mercury analysis system to be connected directly with the process gas stream. This portable system consisted of fly-ash heated filter, probe transfer line, T-connector and two mercury analyzers equipped with gas-conditioning scrubbers. It measures the mercury concentration by CVAAS, and the methodology results were compared to data simultaneously obtained from OHM in pc-fired boiler power plant stack gas. During the period of time, 36 speciation measurements were performed. The sampling points were placed before the electro precipitator (EPS), after EPS, and after the flue gas desulphurization installation (FGD). For measurements in complex matrices, the PC-AGH system allows the measurement by means of the Standard Addition Method (SAM). In order to perform the measurements of Hg with SAM the PC-AGH system was additionally equipped with a peristaltic pump, a 10 dm^3 Tedlar bag, 4 mm PTFE tubing, PTFE T-connector and an activated carbon filter. The procedure of measurement with a SAM was as follows. In the first

step the Hg(0) calibration gas was pumped from the Tedlar bag via peristaltic pump to the PTFE tee connector (here the calibration gas was diluted with filtered air) and then to EMP-2 (NIC) detectors. In the second step the diluted Hg(0) calibration gas was administered to the inlet of the probe to check the sorption of mercury. In the third step the probe was inserted to the flue gas tract (calibration gas was still administrated to the probe inlet). In this step the calibration gas was diluted with flue gas. In the fifth step the Tedlar bag was disconnected and filtered air was pumped to the probe inlet. In the last (sixth) step the peristaltic pump was stopped and the detectors measured mercury in flue gas only. The mercury concentration results were oriented on-line by the CVAAS detectors (Górecki et al., 2016).

3.2. Laboratory scale mercury analysis systems

In the laboratory scale mercury analysis, the most common used are CVAAS and CVAFS techniques to detect mercury in gas stream. The CVASS technique is applied to determine the total mercury content, measuring elemental mercury from the vapors. Either tin chloride1–3 or sodium tetrahydroborate(III)4,5 is used to reduce mercury to its elemental form. Mercury vapor is purged from solution by a carrier gas, such as air, nitrogen or argon. After passing through a gas-liquid separator, it is introduced into the optical path of an atomic absorption spectrometer (Kopyść et al., 2000). In the CVAFS technique, resonance fluorescence transitions involving the excitation of an atom by the absorption of a photon from the ground state to an excited state, followed by radiative de-excitation back to the ground state (fluorescence), is applied (Morita et al., 1995). This technique is around two orders of magnitude more sensitive than CVAAS.

There are two kinds of methodologies to analyze the mercury behaviors crossing the treatment system with the flue gas in laboratory. One is using the multiple gas sources to simulate the flue gas. Another one is combustion of fuels in small scale furnace to simulate the flue gas coming from different industries.

He et al. (2020) designed an advanced mercury analysis system to capture the mercury by using the modified catalyst sorbent. The source of simulated flue gas was consisted by multiple gases, such as NO, SO_2, O_2, N_2. The laboratory-scale fixed-bed system for the removal of Hg(0) and NO was composed of a gas distribution system, a mercury permeation, a catalytic reactor, a

temperature control system, a mercury absorption device, and an exhaust gas purification device. The catalytic reactor was placed in a temperature-programmed tubular electric furnace, and the prepared catalyst was placed in a quartz glass tube. The Na_2S solution was used to absorb the mercury vapors in the exhaust gas, as the NaOH solution was used to absorb the acidic gases in the exhaust gas. The Hg(0) concentration at the inlet and outlet of the reactor was obtained with use of an Hg(0) analyzer. More details were described in (Z. He et al., 2020).

Yang et al. (2019) used wheat straw as the material to prepare the activated sorbent. Then, it was modified further by an ultrasonic-assisted impregnation technique with iron nitrate and copper nitrate. They designed a mercury analysis system by using the multiple sources of gases to consist of the simulated flue gas. Their experimental setup for determining the Hg(0) capturing capacity of the prepared samples. The main components of the simulated flue gas were 5% O_2, 400 ppm NO, 600 ppm SO_2, 4% (vol) H_2O, 65 g/m^3 Hg(0) and N_2. The water vapors and mercury vapors were generated, by a water steam generator and a mercury vapor generator, respectively. The total flow rate of flue gas passing through the reactor was maintained at 0.8 dm^3/min, which corresponded to a GHSV of approximately 57000 h^{-1}. The testing system consists of the following components: a flue gas generation system, an online detection device for flue gas and Hg(0), a fixed bed reactor, and an exhaust gas purification device. A water steam generator, a mercury vapor generator, a gas mixer, and some gas cylinders comprise the flue gas generation system. The exhaust gas purification system consisted of an activated carbon trap capable of efficiently capturing any lingering pollutants in the tail gas. An online Hg(0) analyzer and a flue gas analyzer were used, respectively, to measure the concentration of Hg(0) and each component (especially SO_2, NO, and O_2) in flue gas at the reactor's inlet and outlet. A heating tape of 105°C was used to prevent the condensation of Hg(0) and water vapors in the system lines. The exhaust gas was introduced into a treatment system for efficient purification to prevent pollution. Before the mercury removal experiment, a blank test was conducted in the fixed bed reactor to evaluate the Hg(0) concentration stability in the simulated flue gas (W. Yang et al., 2019).

Dong et al. (2021) used the fixed-bed reactor system to perform the Hg(0) capture measurement. In their system, there were four main experimental modules: the simulated flue gas generation system, the Hg(0) generation system, the fixed-bed reaction system, and the Hg(0) detection system. They also used the multiple gas sources to get the simulated flue gas. And the composition

of the simulated flue gas included different concentration of each component in the gas, which was 0/12% CO_2, 0/5%/10% O_2, 0/300/500/1000 ppm NO, 0/500/1000/1500 ppm SO_2, and 78% N_2. Dong et al. (2021) used the total gas flow rate of 2 dm^3/min. The concentration of Hg(0) vapors in the flue gas was maintained at 90±0.5 g/m^3 by a Hg(0) generator. In their each test, 100 mg (40–60 meshes) of sorbent was used to remove mercury, along with a gas hourly space velocity (GHSV) of 4×10^5 h^{-1}. The quartz glass reactor with a length of 800 mm and a diameter of 8 mm was placed in a tube furnace. They also used the heating tape with 105℃ to prevent Hg(0) and water vapors condensation. The gas flowed first into the bypass line, and the Hg(0) concentration at the reactor's entrance was stabilized within 30 minutes. Then, the flue gas was diverted to pass through the sorbent to initiate the 200 minutes adsorption test. NaOH aqueous solution and silicone gel impingers were applied to prevent corrosion of the mercury analyzer caused by acidic gases and water vapor from the flue gas. Then, the exhaust gas containing Hg(0) and other gas components should be introduced into the activated carbon trap prior to being released into the atmosphere (Dong et al., 2021).

Zhou et al. (2015) designed an advanced mercury analysis system to simulate the ACI methodology in CFPPs. The source of the simulated flue gas was obtained by combustion of fuel in a laboratory scale boiler. The tests of in-duct mercury capture by sorbent injection were conducted in an entrained flow reactor. In their construction, the reactor consists of several separate components: simulated flue gas generating system, gas preheating and insulation system, sorbent injection system, mercury capture reaction system, sampling and test system, sorbent collection and gas purification system. The mercury concentration in the simulated flue gas was measured by using VM3000 and EMP-2 (NIC) mercury vapor analyzers. More details are described in (Q. Zhou et al., 2015).

Masoomi et al. (2020) designed a laboratory scale system to analyze the behavior of mercury across the flue gas treatment system in CFPPs. The idea of analyzing mercury concentration was similar with this presented in Zhou et al. (2015). Both of them used the combustion of fuel in a laboratory scale boiler to simulated flue gas, but in Masoomi et al. (2020) the post-combustion and analysis systems were different. They implemented the SCR, ESP and WFGD systems to treat the air pollutants. It was useful for analysis the interferences from different air pollutants on mercury behavior. More details are described in (Masoomi et al., 2020).

4. Mercury analysis system redesign and testing

The mercury analysis system is the key to the research and study. Many researchers have designed their own analysis systems to fulfill their research goals. Based on the references from the Chapter 3.2, many research teams use the multiple gas sources to generate the simulated flue gas, instead of using fuels to generate the simulated flue gas. Therefore, the primary goal of the first period of my study was to conduct reliable, reproducible, multiple analyses, under flue gas conditions. This could be a significant added value to my research.

4.1. The original mercury capture analysis system

In this study, the mercury capture analysis system was based on the version designed at AGH University in the group of my PhD supervisor. The idea of the original laboratory system was described in Macherzyński et al., (2015) and Macherzyński (2018), as the expanded mobile, industry version in (Gorecki et al., 2022). In these systems the laboratory scale furnace was implemented. It is combusting solid fuels to generate the exhaust gas simulating the process gases coming from industries. Furthermore, the flue gas was enriched with Hg(0) and directed through sorbents, which simulated the gas/sorbent contact as possible capture efficiency in the industries conditions. The acidic gas treatment system was used to determine whether the acidic gas (such as SO_2, H_2S) interfered the Hg(0) capture efficiency. All series of experiments were conducted by using CVAAS technique to detect the on-line concentration of Hg(0) in the gas streams. Two EMP-2 analyzers, each equipped with the scrubber conditioning system WLE-8 as detailed in (Górecki et al., 2016), were used to analyze Hg(0) in two process gas lines: containing reference and sorbent reactors. A total flow rate of simulated gas in both reactors was from 6 dm^3/h to 60 dm^3/h. Fuel load was maximum around 12 g/h, measurements were done at relatively low gas stream temperatures of (20-150°C), but the use of heating tapes for any lines outside the thermostatic cage is necessary (Macherzynski et al., 2015, 2020) and Macherzynski (2018). The original set-up was showed in Fig. 4.1 and second redesigned (improved) version was showed in Fig. 4.2. The second version includes a lab scale WFGD system to remove SO_2 and six-gas analyzer (testo) and was also the AGH scientist construction.

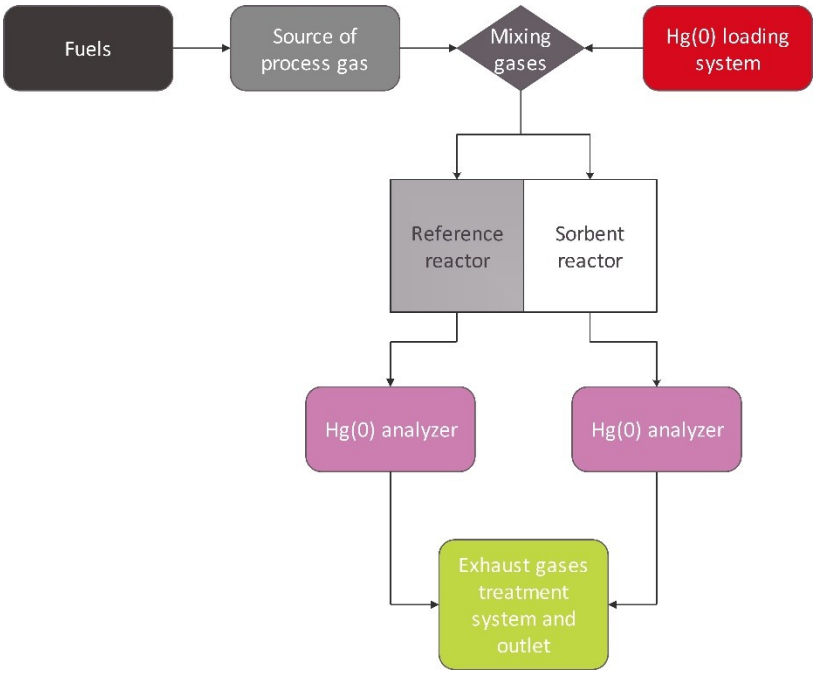

Figure 4.1: Scheme of the original, laboratory scale experimental set-up to determine Hg(0) capture by sorbents (description in the chapter)

Both versions of experimental set-up performed experiments in stable conditions and generated the reliable experimental results, when using different kinds of process gases, reactors and sorbents to capture Hg(0). The ACs and synthesized zeolites were tested in the original version, the Hg(0) capture efficiencies were over 80% and 70%, respectively (Macherzynski et al., 2015, 2020). And the polymer composite sorbents were tested in the second version of set-up, where the Hg(0) capture efficiencies were over 99%, respectively (Gorecki et al., 2022).

Although these two versions of set-up could generate the good results, there were still some limitations as well as some measurements could not be performed by using them. In the original version of set-up, the flow rate was only regulated by the restrictors which connected with mercury analyzers. There was no conjunction point after the reference and sorbent lines. Because the flue gas analyzer requires flow rate of 60 dm^3/h to analyze the composition of flue gas, the flow rate and Hg(0) concentrations in the reference and sorbent's reactors were interfered, when using flue gas analyzer (Gorecki et al., 2022). It resulted at an unstable on-time analysis data. It was hard to analyze the composition of simulated gas after the sorbent reactor. Some flue gas components such

as NO, SO_2 may compete with Hg(0) to deposit onto the sorbent which reduce the Hg(0) capture efficiency (Li et al., 2018; D. Liu et al., 2020; Xu et al., 2021).

4.2. Redesigned mercury analysis system

Based on the reasons pointed out in Chapter 4.1, the idea to redesign (developed) the mercury analysis system based on the previous two versions to obtain more useful and reproducible results, of the Hg(0) capture efficiencies by different sorbents.

The redesigned experimental set-up is shown in Fig. 4.3 and Fig. 4.4 (depicts a technique drawing with additional information about the experimental stand). The set-up was equipped with a laboratory-scale furnace (CZYLOK) together with double-pipe vertical boiler (AGH scientists constructed) and raw gas small fabric filter – (A). The filter is able to remove the fly ash from the

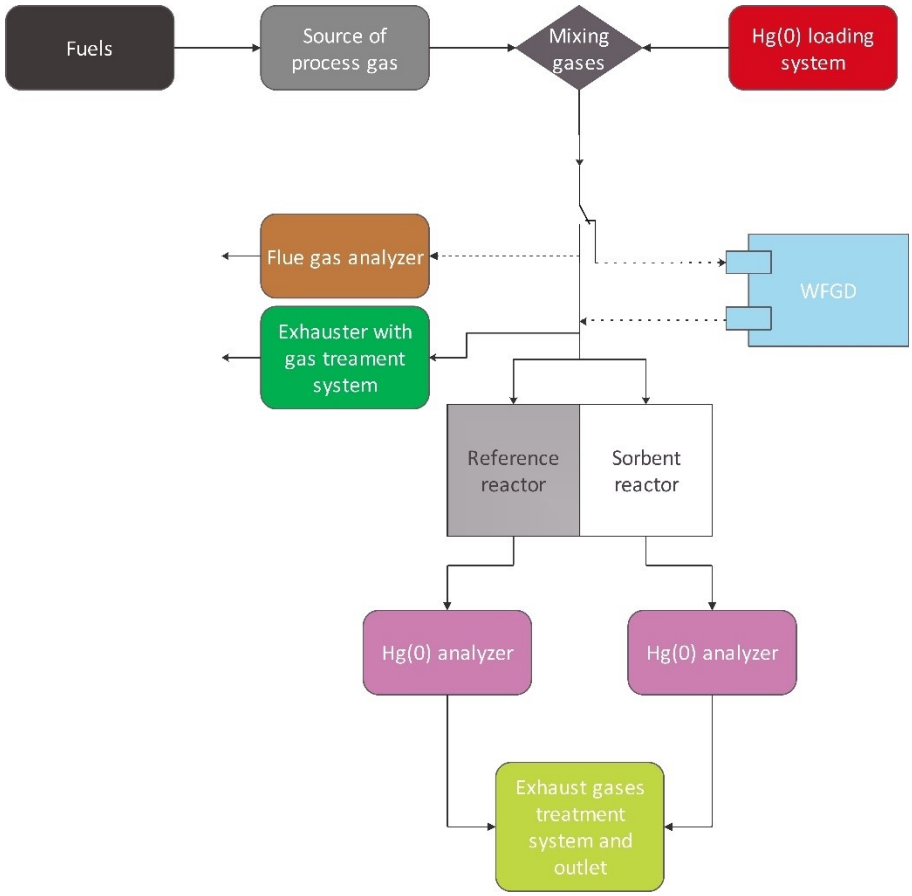

Figure 4.2: Scheme of the improved laboratory scale experimental set-up to determine Hg(0) capture by sorbents (description in the chapter)

simulated flue gas. The additional elemental mercury loading system (B) was used to set a concentration of mercury in exhausts. It was usually a 10 dm^3 Tedlar bag filled with a mixture of Hg(0) and N_2 gas as a carrier of elemental mercury, and the precise peristaltic pump transported the gas mixture to the thermostatic tee connector located behind the filter flue gas. So, the Hg(0) concentration was controlled by the peristaltic pump. The laboratory scale desulphurization (WFGD) system (AGH scientists constructed) could be occasionally implemented. $CaCO_3$ slurry was introduced into the extended scrubber system to remove most of SO_2. Otherwise, flu gas went directly to the thermostatic cage (E) containing sorbent reactors inside (AGH scientists constructed). Three exhaust fans were added in order to regulate the total flow rate in three different points. They were used to balance the system's total flow rate when the Testo 350 was turned on or off or when changing the flow rate through the sorption cells. One exhaust fan (H) controlled the flow in the main stream point, just after the WFGD system. Other two exhaust fans (I & J) controlled a flow in the outlet of reference and sorbent reactors. As previously, two EMP-2 analyzers (F & G), each equipped with the gas conditioning scrubber system WLE-8 (NIC), were used in two process gas lines containing reference and sorbent reactors. Teflon tubes were the best choice to be used at higher temperatures and to prevent the absorption of mercury. It is important to underline, that the use of heating tapes for any lines outside the thermostatic cage was necessary to prevent condensation of sulfuric acid and water inside the Teflon tubes of the experimental system. The gas mixture was transferred to the thermostatic oven, where it was separated into two streams. Each stream had a dedicated reactor. The implementation of three kinds of reactor set-ups, which is presented in Chapter 5, was investigated there in terms of improved Hg(0) capture. In the redesigned system the thermostatic oven was set to 125°C in the most series of experiments as well as the heating traps. That set-up secured the range of 125—130°C (a feedback loop), what prevents from acids, moisture and mercury condensation inside the streamlines. And the 3-way valve No.3 (Fig. 4.4) was used to change flow direction after the reference and sorbent reactors, respectively. It allowed the flue gas analyzer to analyze simulated flue gas condition gas passthrough reference reactor and sorbent reactor, respectively.

In the mercury analysis parts (F, G) each stream (line) had its own mercury analyzer and gas scrubber system. The 10% KOH solution was utilized in two from three WLE-8 system (NIC) scrubbers. The third scrubber was just empty to improve water condensation from the treated exhausts, as the whole scrubber system was cooled. As a consequence the acidic gases and

moisture were removed from the simulated flue gas prior to analysis. It prevents damage to the sensor cell and improves the analyzer precision.

In the redesign set-up one can measure 7 gases in a simulated gas mixture, in four different points, using a flue gas analyzer (Testo 350) - (C). The system was thought to measure the composition of raw gas, the gas passing through the WFGD system, and the gas from reference and sorbent lines after the thermostatic cage. It could have helped to assume, whether the flue gas components such as NO or SO_2 deposit onto the sorbent competing with Hg(0) (reduced Hg(0) capture efficiency). Two additional gas loading systems were added (H_2S - (K) and N_2 – (D)). The new set-up has a total flow rate of simulated gas through adsorbent bed and reference reactors in an ideal range of 12—240 dm^3/h (the use of three external exhausters (H, J, I)). The fuel loading rate could be up to 40 g/h.

In my study, the total flow rate was selected in a range of 108—144 dm^3/h. It consisted of 48 dm^3/h from two mercury analyzers and 60—84 dm^3/h of two exhaust fans which connected with mercury analyzers (depending on experimental aims). The fuel loading rate was set at around 14 g/h of commercial bituminous and 21 g/h of commercial lignite during experiments, which the mercury concentration was 1.35±0.32 ppb and 8.52±0.56 ppb, respectively. The temperature of the gas generator was set at 830—900°C. All the parameters of the experiments, including sorbent reactor, were flexible. Only few parameters were fixed in the same conditions during this series of experiments, such as flow rate of mercury analyzer and the temperature of thermostatic cage.

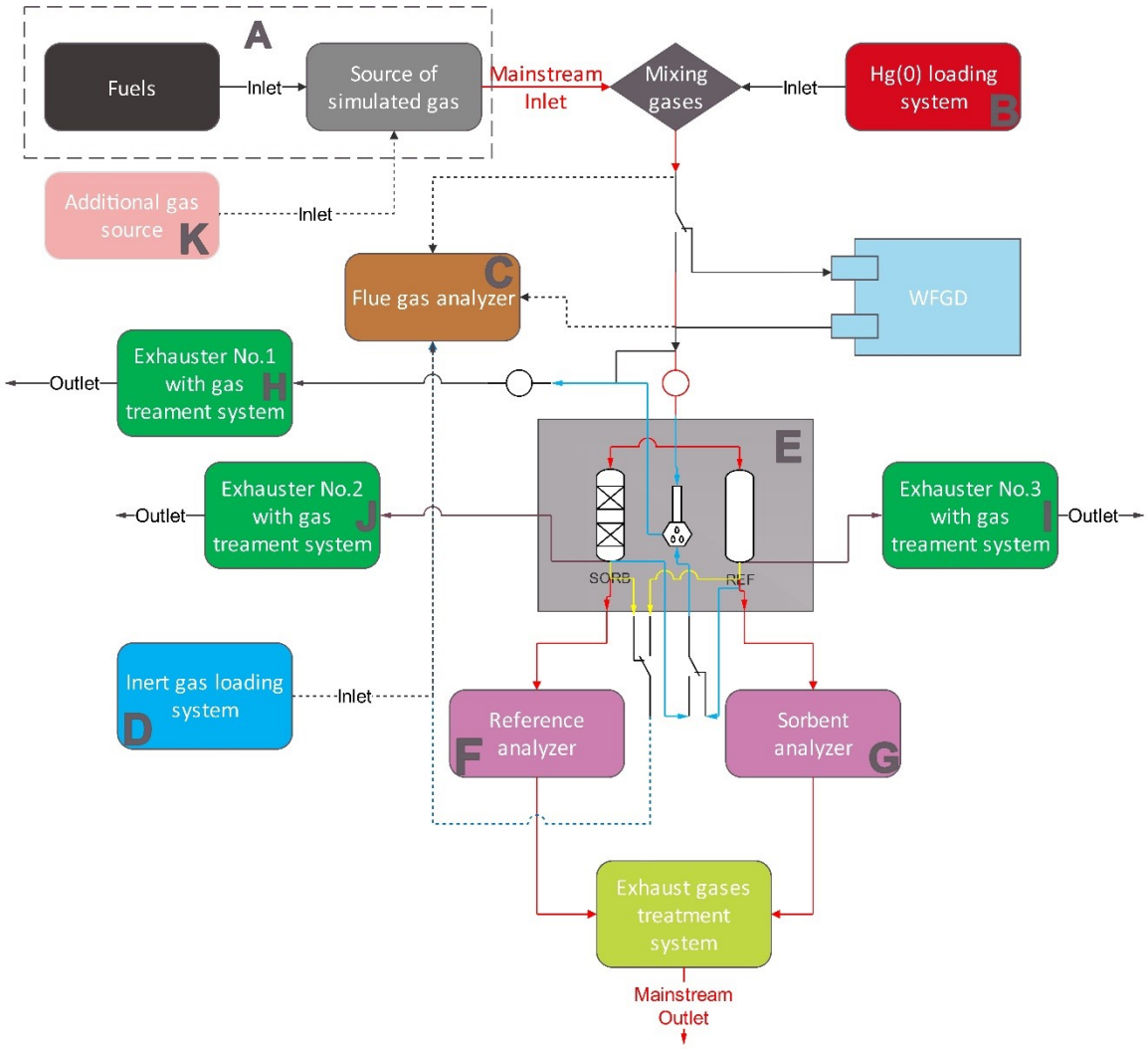

Figure 4.3: Simplified scheme of the redesigned experimental set-up

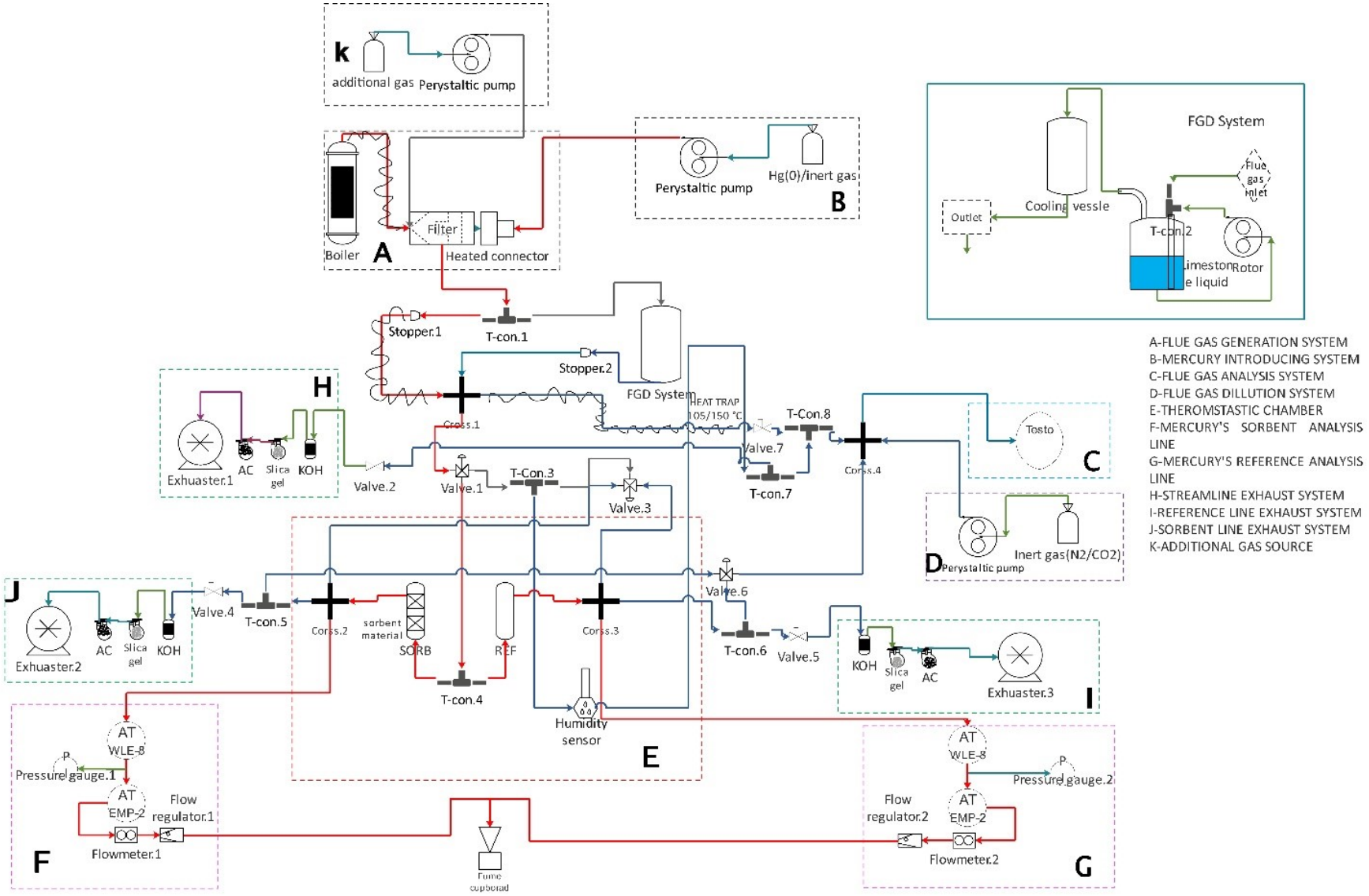

Figure 4.4: The technique scheme of redesigned experimental set-up

4.3. Controlment of simulated gas

In the industries, the composition of flue gas is influenced by multiple factors, such as the type of fuel, O_2 supply, the type of combustion method etc. to achieve a stable flue gas conditions (Fu et al., 2015; F. Lin et al., 2020). In the redesign version of the experimental set-up, simulated flue gas composition and concentration of each component (7 different gases) could be controlled by loading different fuels as well as flow rate, and combustion temperature control. The combustion pipe position inside the vertical furnace is also of prime importance. There are selected examples presenting the simulated flue gas controlling tests.

In the controlling test no. 1, the total flow rate was set at 156 dm^3/h, the temperature of combustion was set at 890°C. Fuel loading rate was increased from 9 g/h to 12 g/h. The selected fuel was commercial Bituminous-1, as the details of simulated gas composition are showed in table 4.1.

Table 4.1 Influence of fuel loading on mean concentrations of main gas components of simulated gas and excess air coefficient (**λ**)

Fuel loading [g/h]	**λ**	O_2 [%]	CO_2 [%]	CO [mg/m^3]	SO_2 [mg/m^3]	H_2S [mg/m^3]	NOx [mg/m^3]
9	2.76	13.34	7.47	83	1350	0	1330
10	2.68	13.18	7.64	88	1386	0	1336
11	2.51	12.56	8.24	88	1445	0	1246
12	2.28	11.81	8.97	73	1390	0	1278

In the controlling test no. 2, the total flow rate was set at 108 dm^3/h, flue loading rate was set at 9 g/h. The temperature of combustion was regulated from 830—890°C. The selected fuel was commercial Bituminous-1, and the details of simulated gas composition was showed in table 4.2.

Table 4.2 Influence of the combustion temperature on mean concentrations of main gas components of simulated gas and excess air coefficient (λ)

Combustion temperature [°C]	**λ**	O_2 [%]	CO_2 [%]	CO [mg/m^3]	SO_2 [mg/m^3]	H_2S [mg/m^3]	NOx [mg/m^3]

830	1.71	8.73	11.97	89	1581	0	900
850	1.68	8.51	12.19	89	1526	0	892
890	1.50	7.00	13.67	80	1341	0	591

In the controlling test no. 3, the fuel loading rate was set at 9 g/h, the temperature of combustion was set at 890°C. The total flow rate was regulated from 72—144 dm^3/h. The selected fuel was commercial Bituminous-1, and the details of simulated gas composition was showed in table 4.3.

Table 4.3 Influence of the total flow rate on mean concentrations of main gas components of simulated gas and excess air coefficient (**λ**)

Total flow rate [dm^3/h]	**λ**	O_2 [%]	CO_2 [%]	CO [mg/m^3]	SO_2 [mg/m^3]	H_2S [mg/m^3]	NOx [mg/m^3]
72	1.39	5.91	14.73	85	1114	0	360
84	1.42	6.21	14.43	32	1005	0	484
96	1.48	6.83	13.83	35	953	0	606
108	1.59	7.80	12.88	40	823	0	722
144	2.10	11.00	9.77	53	411	0	1141

Based on data from table 4.1, 4.2 and 4.3, λ is influenced by the flow rate, temperature of combustion and fuel loading. The λ represents the air-fuel ratio. It is the mass ratio of air and fuel in the combustion chamber. Therefore, λ and O_2 (CO_2) concentrations are the key factors to select the fuel loading, the total flow rate and combustion temperature in different experiments. Before each series of experiment, the composition of simulated flue gas was determined by the flue gas analyzer to control the value of λ between 1.5 to 1.8.

In the table 4.4, the selected conditions of simulated flue gas during each series of experiment are presented. In this controlling test, bituminous coal loading was around 9 g/h. When the total flow rate was selected at 108 dm^3/h, the λ was around 1.5 - 1.75. The concentration of each gaseous component was closer to the flue gas in power plants (λ= 1.22). Hence, the total flow rate and bituminous coal loading were selected as priority conditions to further experiments. On the other

hand, when lignite loading was around 21g/h, and the total flow rate was 108 dm^3/h, λ reached 1.45 - 1.7. These flue gases and its generation conditions, can be potentially used in some comparisons of the Hg(0) capture efficiency from bituminous coal-based and lignite-based simulated gas.

Table 4.4 Mean concentrations of main gas components of simulated process gas and excess air coefficient (λ) for different fuels and at different conditions

Fuel	Combustion temperature [°C]	Total flow rate [dm^3/h]	Fuel loading [g/h]	λ	O_2 [%]	CO_2 [%]	CO [mg/m^3]	SO_2 [mg/m^3]	H_2S [mg/m^3]	NOx [mg/m^3]
Bituminous -1-test 1	890	108	9	1.48	6.75	13.89	101	1212	123	885
Bituminous -1-test 2	890	108	9	1.75	8.99	11.72	113	1002	147	1315
Lignite-test 1	830	108	21	1.51	7.1	13.6	30	4949	62	816
Lignite-test 2	830	108	21	1.45	6.5	14.2	4	4815	45	736
Lignite-test 3	890	108	21	1.57	7.60	13.1	71	1157	87	311
Lignite-test 4	890	108	21	1.69	8.6	12.1	184	1102	43	159

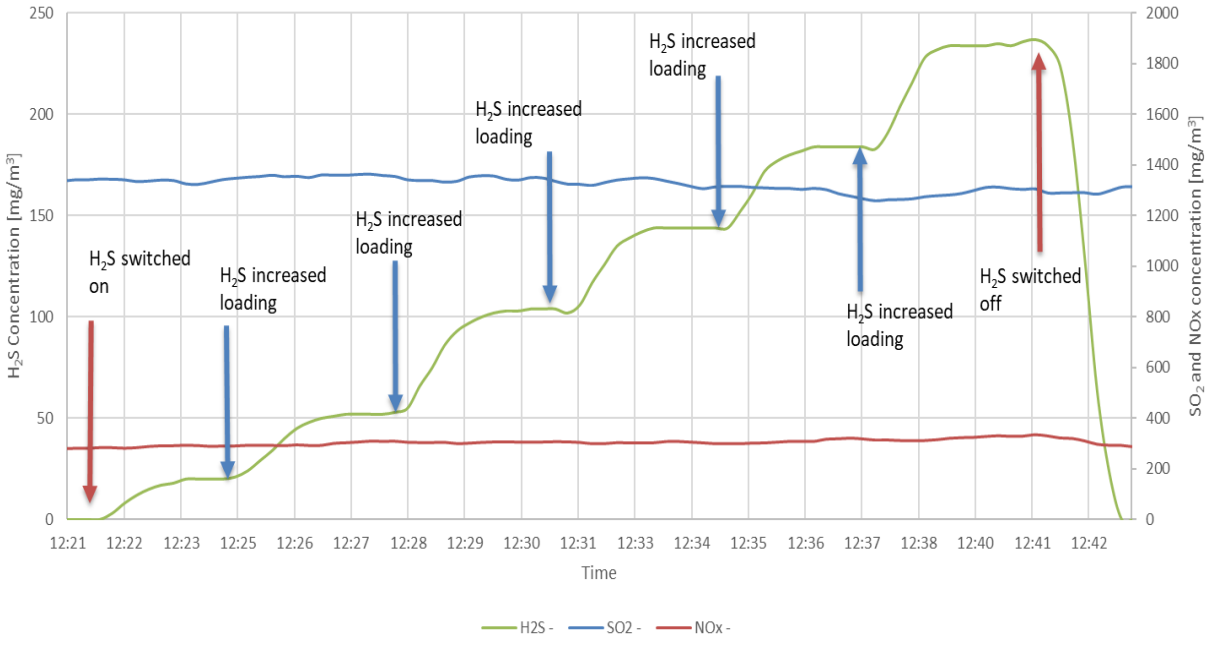

Figure 4.5: H_2S gas introduced and controlled in the simulated gas

The redesigned experimental set-up had a complex gas stream routine, it allows the additional gas was loaded into the system via selected points (D) and (K) shown in Figs 4.3 and 4.4. H_2S was used as the additional gas to load into the system to analyze whether it influence on Hg(0) concentration in the gas stream. H_2S and some specified sorbents undergo a synergetic mechanism to remove Hg(0) in flue gas (Guo et al., 2010). The H_2S was loaded into the system via connection (K) by peristaltic pump to control its concentration in simulated gas (Figs: 4.3, 4.4, 4.5).

The metal oxides or carbon based metal oxides are good sorbents which promote the surface area for the interaction between the H_2S and Hg(0) in the process gas, forming the non-water-soluble HgS (Z. Wang et al., 2020; Altaf et al., 2022). And the O_2—SO_2—H_2S equilibrium conditions under redox reaction can affect the effectiveness of Hg(0) capture in different temperature conditions (Steijns et al., 1976; Asadi et al., 2011). The laboratory WFGD system can break the O_2—SO_2—H_2S equilibrium conditions, when removing SO_2 from flue gas. H_2S is not removed by the WFGD system because the high concentration of CO_2 in the flue gas (Fig. 4.6 and table 4.5). SO_2 often inhibits Hg(0) oxidation by competing with HCl or Cl_2, occupying the adsorption sites or active surface of catalysts or even reacts with the sorbents (metal oxides, such as CuO or Al_2O_3) to influence Hg(0) capture (G. Li et a;., 2015; Z. He et al., 2020). The limestone slurry inside the WFGD system was used to remove SO_2 from the flue gas stream. The main compound of limestone suspension is $CaCO_3$. $CaCO_3$ reacts with SO_2 to form CO_2 and $CaSO_4$. The reaction of H_2S with limestone slurry to form CO_2 and CaS is described by Equation (11).

$$CaCO_3\ (s) + H_2S\ (g) \leftrightarrow CaS\ (s) + H_2O + CO_2\ (g) \qquad (11)$$

This is an equilibrium reaction, and its initial rate is low. The concentration of CO_2 in the lab simulated flue gas was around 11-15%. The released CO_2 gas and CO_2 from the simulated gas might inhibit the reaction between limestone slurry and H_2S (S. Lin et al., 1995). As the gas analysis in Fig. 4.6 revealed, the concentration of SO_2 significantly decreased, when the WFGD system was switched on. The concentration of other acidic gases was relatively stable except of H_2S which also dropped from 43.3 mg/m^3 to 3.0 mg/m^3 when lignite was used, and increased by 24% in case of bituminous coal (Fig. 4.6 and table 4.5).

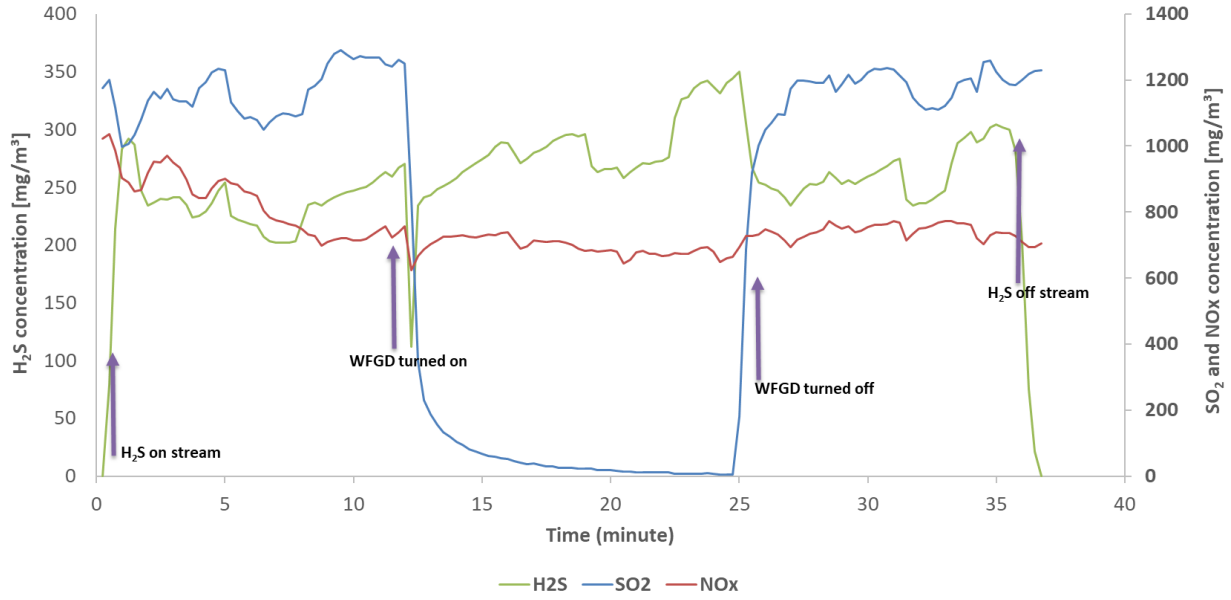

Figure 4.6: Acidic gas concentration in WFGD system off/on condition

Table 4.5 Mean values of acidic gases at the laboratory WFGD on/off conditions

WFGD conditions	Fuel	CO_2(%)	SO_2 (mg/m^3)	NOx (mg/m^3)	H_2S (mg/m^3)
on	Bituminous	11.34	1175	810	235
off		11.29	23	690	292
on	Lignite	12.1	1102	158	43.4
off		12.6	25	146	3.0

In some cases, the inert N_2 gas was loaded into system via connection (D) by peristaltic pump to balance and stabilize the total flow rate of simulated flue gas (Figs: 4.3, 4.4, 4.7). The inert gas was also used as a Hg(0) carrier in this series of study. When it influenced concentration of Hg(0)

and simulated flue gas, the loading amount of inert gas was necessary to be determined. table 4.6 shows simulated flue gas conditions when N_2 and H_2S loading systems were switched on or off. N_2 was used as a H_2S gas carrier to transfer it into experimental system. When the H_2S loading system was switched on, the small quantities of N_2 influenced the result of the simulated gas composition. The software of flue gas analyzer calculated (treated) the N_2 gas as CO_2, what resulted in misjudged concentrations of CO_2. When the N_2 loading system was switched on, that gas was diluting the simulated flue gas. It again resulted in misjudged, higher concentrations of CO_2 as well as SO_2, NOx and H_2S concentration decease in the system. This was taken into consideration and the proper calculations of gas concentrations (including dilutions) were additionally performed.

Table 4.6 Mean values of acidic gases at N_2 and H_2S supply on/off settings

N_2 loading system setting	CO_2(%)	SO_2 (mg/m^3)	NOx (mg/m^3)	H_2S (mg/m^3)	H_2S loading system setting
off	13.22	1116	443	0	off
off	14.57	1039	280	70	on
on	16.99	515	125	24	on
off	13.76	809	323	99	on

Although the N_2 and H_2S loading systems were not used frequently, these connections made the redesign version of the experimental system more complex than the previous one. However it let doing different kinds of analysis as gas composition influence on Hg(0) capture.

The redesign system lets to determine the components of simulated flue gas deposited on sorbents competitively with Hg(0) and to analyze the components of simulated flue, whether they interfere the Hg(0) capture efficiency.

Table 4.7 shows the composition of simulated flue gas passing through the sorbent reactor and the reference reactor. A gas analysis point was connected with the system through the valve no. 6 and the cross connector no. 4 (Fig. 4.4).

Table 4.7 Mean value of acidic gases at WFGD on/off settings when changing reference and sorbent reactors					
Reactor	CO_2 (%)	SO_2 (mg/m^3)	NOx (mg/m^3)	H_2S (mg/m^3)	WFGD setting
Reference	11.75	1213	856	0	off
Sorbent	11.39	1168	878	0	off
Reference	9.47	15	968	0	on
Sorbent	8.93	0	966	0	on

4.4. Controlment of mercury in simulated gas

In the original version and redesign version of the experimental set-up, the Hg(0) concentration in the simulated gas was regulated by the peristaltic pump – (B) in Fig. 4.3 and 4.4. The Hg(0) loading rate was controlled by the rotation speed of a pump. One may load Hg(0) into the system gradually to reach the required level of Hg(0). The result of Hg(0) concentration controlling test is illustrated in Fig. 4.7.

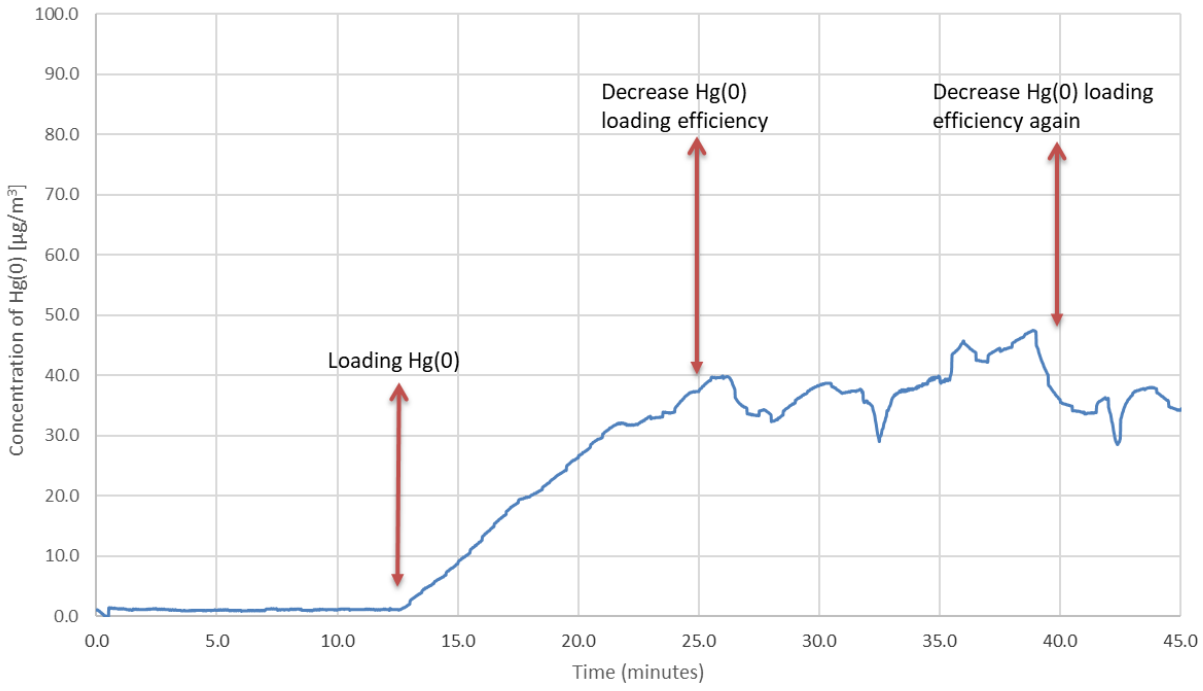

Figure 4.7: Concentration of Hg(0) in the controlling test in a reference line

In some cases, Hg(0) may be released from the often used limestone slurry. It may interfere the accuracy of the concentration of Hg(0) in the simulated gas. The Fig. 4.8 shows the result of hot air without Hg(0) when passing through the fresh and used limestone slurry of WFGD system. It is seen that some porsions of Hg(0) were released from the used limestone slurry. Because Hg^{2+} is dissolved in limestone slurry, it reacts with dissolved gaseous SO_2 to form mercury sulfites ($HgSO_3$), which are not stable in the desulphurization systems. In most conditions, $HgSO_3$ decomposes to Hg(0) immediately (C. Chen et al., 2014). Hg content in the used and fresh limestone slurry was analyzed by MA-3000 (NIC) total mercury analyzer (table 4.8). Therefore, the fresh limestone slurry was required to fill the WFGD system before each series of experiment, when it was in use.

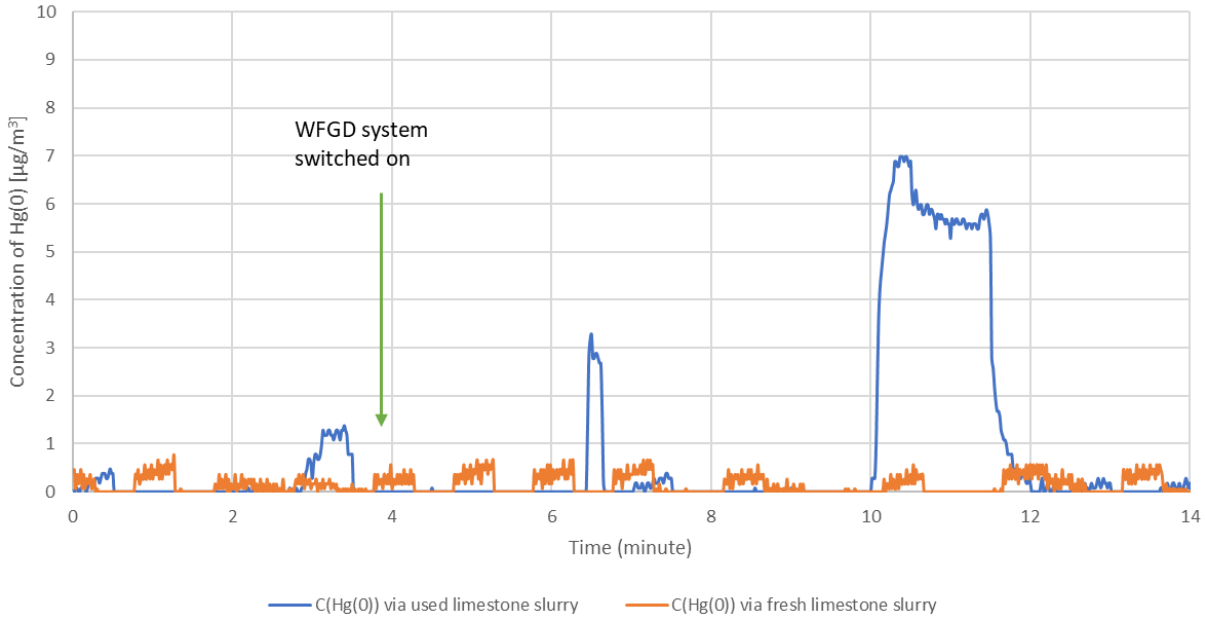

Figure 4.8: Hg(0) release tests of WFGD system limestone slurry

Table 4.8 Mean value of total mercury concentration in different WFGD slurries

	Hg_{tot} [ppb]	SD [ppb]	CV [%]	Increasing Hg [%]
Fresh WFGD liquid	294	1.3	0.44	N/A

WFGD liquid after test with AC based sample-1	497	64.5	12.97	69
WFGD liquid after test with AC based sample-2	451	26.7	5.91	53
WFGD liquid after test with AC based sample-3	640	30.0	4.70	117

5. Different kinds of reactors applied in the redesigned mercury analysis system

These series of experiments in this chapter were conducted by using the CVAAS methodology to detect the online concentration of Hg(0) in the gas streams. The mercury analysis system was tested in the previous studies. Two types of reactors (Chapters 5.1 and 5.2) were implemented in the following experiment: the fixed-bed reactor and two kinds of the immobilized sorbent reactors.

5.1. Fixed-bed reactor—vertical glass flow reactor

In the fixed bed reactor the sorbing bed is filled with the solid phase as an active material. The physical and/or chemical sorption takes place, and implemented technologies are compared from an environmental, engineering, and economic standpoint. The economic criteria are separated into three categories: capital costs (consisting of equipment, installation, engineering, etc.), operating costs (consisting of utilities, maintenance, and expected equipment lifetime), and total costs of ownership. Criteria for engineering are divided into five categories including reactor construction, pressure drop, heat distribution, particle abrasion, and recovery operations. Environmental criteria are divided into three categories including removal effectiveness, waste production and sound pressure level (Roshan & Mofidi, 2014; Coker, 2015).

The vertical flow glass reactor presented in Fig. 5.1 is a fixed bed reactor constructed by the AGH scientists (Macherzynski, 2018). It is consisted of three glass vessels with a diameter of 2.6 cm. These glass vessels separated with O-rings, are applied as the solid phase sorbent cells. One glass cylinder of 3.2 cm diameter serves as a main reactor to insert the sorbent cells. It has two side tubes with a diameter of 0.6 cm as the gas inlet from the bottom and outlet in the top side. The non-reactive stone chips (quartzite, barite) are placed in the bottom of a glass cylinder to hold the first

layer of O-rings and cells as well as to split the gas stream. The selected sorbents are placed onto the glass-sponge bed, inside in the bottom of each glass vessel. Gas flow was perpendicular to the sorbent bed (Fig. 5.1).

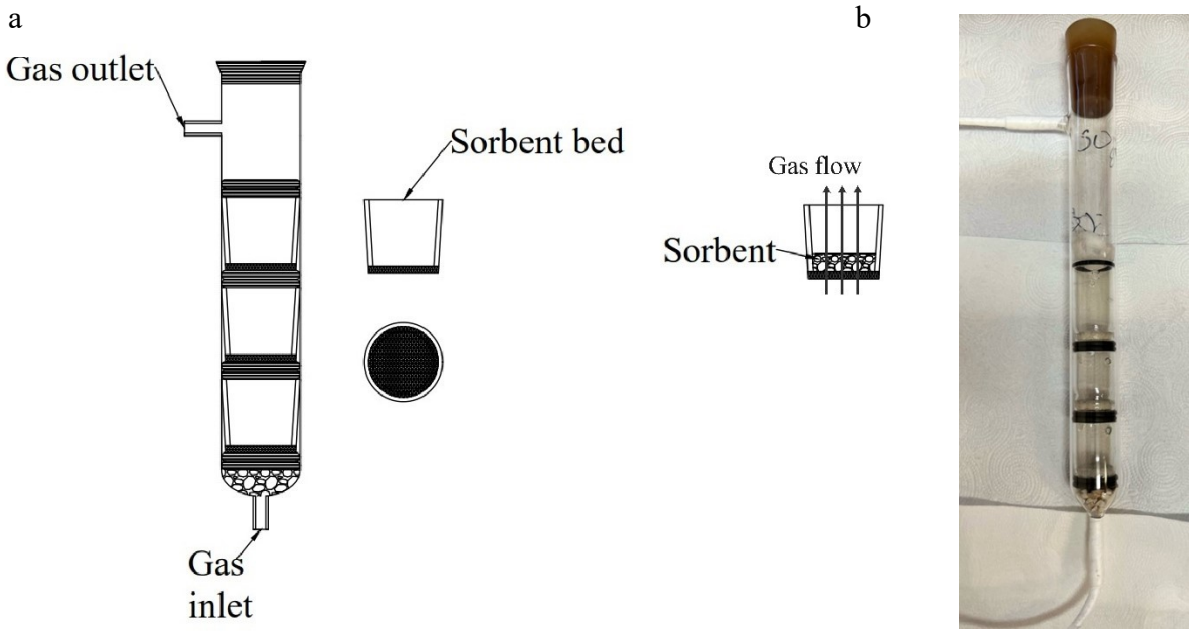

Figure 5.1: Schemes (a) and photo (b) of the vertical flow glass reactor and the sorbent cell

The gas rich in Hg(0) enters into the sorbent reactor from the bottom of reactor. Then, simulated gas crosses the rock chips and the glass bed, where penetrates the interface between the sorbent particles or the structure of a solid sorbent. During this process, Hg(0) was adsorbed by sorbents in physisorption/chemisorption processes. After this, the treated simulated gas moved out of the sorbent reactor and got into the PFTE pipe and was transferred to a scrubber and a mercury analyzer. In the reference line, the simulated gas rich in Hg(0) underwent the similar way as within a sorbent line, but there was no sorbent inside the reference reactor. So, the simulated gas from the empty reactor was directly transferred into a scrubber and a mercury analyzer. The advantages of a fixed bed reactor are: simple construction, small instrumentation and low costs and flexible operation.

Kinds of sorbents applied in a fixed-bed reactor

There is a branch of sorbents that can be applied in the VFGR, they are in granular or powder forms. The selected sorbents can be the physisorption sorbents, such as zeolites, activated carbons, or any kind of modified biosorbents. There are also the chemisorption sorbents, such as metal oxides (FeO, CuO, MnO) or metal sulfide (FeS, CuS, ZnS). The selected material such as composite sorbent can combine both the physisorption and chemisorption properties.

The drawback of vertical flow reactor

The vertical flow glass reactor has the same advantages as the fixed bed type reactor, but this reactor has some disadvantages to be unignored. The drawback of vertical flow glass reactor is that it is not made of glass. In fact, the transparent glass lets to observe the flow process inside of a sorbent cells. The main disadvantage was the "channeling effect" of solid sorbent. This effect may occur in the solid-liquid extraction because of the poor sorbent distribution or different particles size. There are some channels occurring on the interface between sorbent particles. The channels are of different sizes. Creation of those channels allow passing more gas through the material. But the phenomenon causes that the part of sorbent is not fully used and the sorbent contact area confined. Finally, it causes the poor capture rate of Hg(0). Another disadvantage is inability to fully control and change the contact time or contact area between sorbent and gas. According to the Equations (12) - (15), the velocity (v) and contact time (t) can be calculated:

$$Q = vA_{VFGR} \tag{12}$$

$$A_{VFGR} = \pi r_{VFGR}^2 \tag{13}$$

$$t_{VFGR} = \frac{l}{v} = \frac{l_{sorbent}}{\frac{Q}{A_{VFGR}}} = \frac{A_{VFGR} l_{sorbent}}{Q} \tag{14}$$

$$t_{VFGR} = \frac{\pi r_{VFGR}^2 l_{sorbent}}{Q} \tag{15}$$

Where Q was the selected flow rate in sorbent and reference reactors, A_{VFGR} was the cross section area of glass vessel, r_{VFGR} was the radius of glass vessel, $l_{sorbent}$ was the thickness of sorbent layer in glass vessel, respectively. Flow rate (Q) was selected in the beginning of the experiment, which was 54 dm^3/h. The glass vessel radius (r) was 1.3 cm. The cross-section area (A) was unchangeable as related to the radius of the glass vessel, which was 5.31 cm^2. The regulation of sorbent layer thickness (l) is adjusted to a limited extent related to the height of the vessel. For

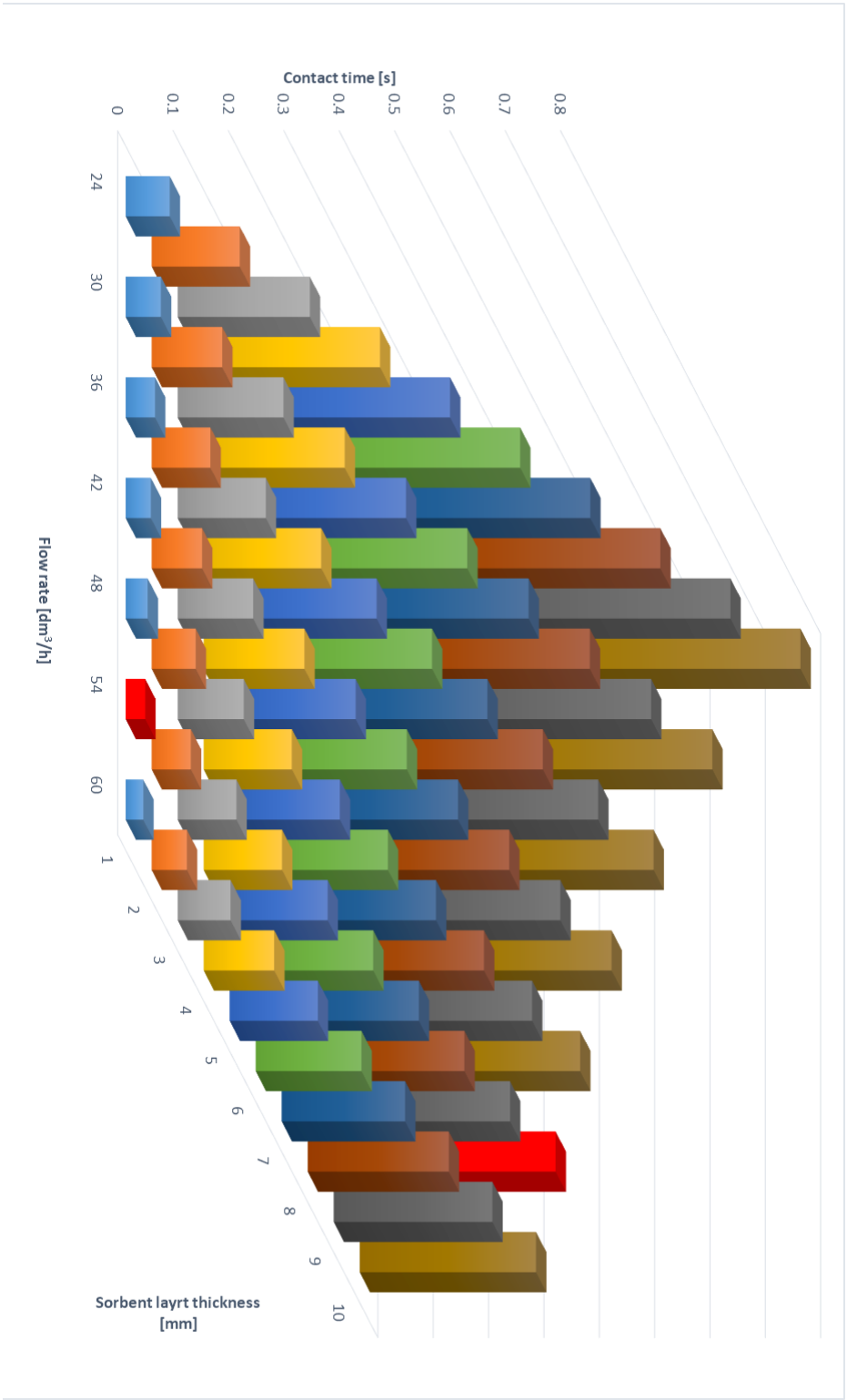

Figure 5.2: The contact time of simulated passes through sorbent cell in different flow rate and different thickness of sorbent in VFGR

instance, 1 g of commercial AC represented 1cm of thickness in the sorbent cell. Therefore, it was hard to significantly change the contact time (t) described in Equation (15). Based on calculations Equation (15), the gas-sorbent contact time was 0.345 s. Fig. 5.2 shows the contact time simulated

gas passes through the sorbent in different flow rate and different thickness of sorbent layer. The red bars are represented the results of contact time in the selected flow rate during my experiment.

The reason of design new reactor

If the tested sorbent requires more contact time to have a relative good Hg(0) capture efficiency, there are only two options to solve this issue in VFGR. One option is to decreasing the flow rate as meanwhile decreasing the fuel loading to keep the simulated flue gas compositions as well as the lambda at the previous settings. Another option is to increasing the amount of sorbent to enlarge the sorbent layer thickness. Therefore, it was hard to improve Hg(0) capture efficiency without changing the amount of sorbent. And it changes too many variables to keep the same parameters to control the experimental conditions. This issue is only solved by changing the structure of reactor. Therefore, I designed two reactors to enlarge the contact area without changing the mass of sorbents by comparing with VFGR. And both of two reactors provided longer contact time than VFGR when these two new reactors applied the same amount of sorbents as the VFGR, respectively.

5.2. Immobilized sorbent reactors

The immobilized sorbent reactors: the multiple pipe reactor and the multiple thin layer cubic reactor were designed for the planned experiments to compare with VFGR. In case of VFGR, the contact time was difficult to regulate, as these two types of immobilized sorbent reactors were designed to regulate the contact time without changing the amount of sorbent. These two reactors were made of PTFE polymer, which does not react with the gas components and Hg(0).

5.2.1. Multiple pipes reactor (MPR)

The prototype MPR was conceptualized using the Bernoulli Equation in a steady-state flow conditions. Several steams are separated from the one constant stream. These MPRs consist of two cylindrical modules and one to five PTFE pipes in between them. Each cylindrical module has two sides, one side with one hole and the other side with five holes. The side with a single hole serves as the gas inlet or outlet. The five-hole side is to connect sub-flow PTFE pipes (Fig. 5.3). The total amount of flows entering the reactor equals the total amount of flows leaving the system. Fig. 5.3 depicts the frontal view of the MPR. The two cylindrical modules of the gas inlet and outlet shared

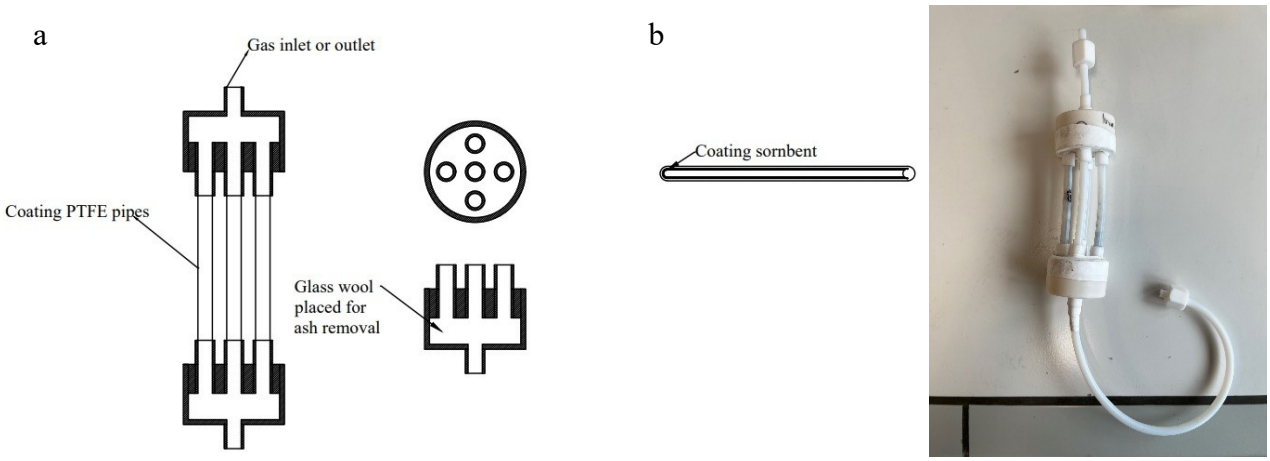

Figure 5.3: Schemes (a) and photo (b) of the MPR

the same diameter with the inlet and outlet of the main flow and the sub-flows. Consequently, the flow condition that entered and exited the cylindrical modules was described by the following Equation (16):

$$A_{(inlet)}v_{(inlet)} = NA_{(sub)}v_{(sub)} = A_{(outlet)}v_{(outlet)} \quad (16)$$

Where $A_{(inlet)}$ and $A_{(outlet)}$ were the cross section area of inlet and outlet of MPR, $A_{(sub)}$ was the cross section area of selected PTFE pipes, $v_{(inlet)}$ and $v_{(outlet)}$ were the velocity of simulated gas passed into and out off the MPR, $V_{(sub)}$ was the velocity of simulated gas in selected PTFE pipes, N was the total number of selected PTFE pipes in MPR, respectively.

In the MPR, selected sorbents were coated onto the internal surface of the PTFE pipes. The length of coating region inside of the PTFE pipelines was depended on the coating efficiency. The contact (coated) area in one pipe, $A_{(sub)\,coated}$, can be calculated by the Equation (17)

$$A_{(sub)\,coated} = 2\pi r_{pipe} l_{coated} \quad (17)$$

Where r_{pipe} was the radius of selected PTFE pipe for coating, l_{coated} was the length of sorbent coating inside of PTFE pipe, respectively. For instance, the length of CuS and CuO coating inside the PTFE pipe were 5 cm and 3.5 cm, respectively. The calculated coating areas of CuS and CuO, inside the PTFE pipes, are 6.28 cm^2 and 4.39 cm^2, respectively. When in the three-pipe MPR, the total contact area of CuS was 18.84 cm^2, the total contact area of CuO is 13.19 cm^2., respectively.

Then the contact time of simulated flue gas passing through the one coated MPR, $t_{(MPR)}$, can be calculated by Equation (18).

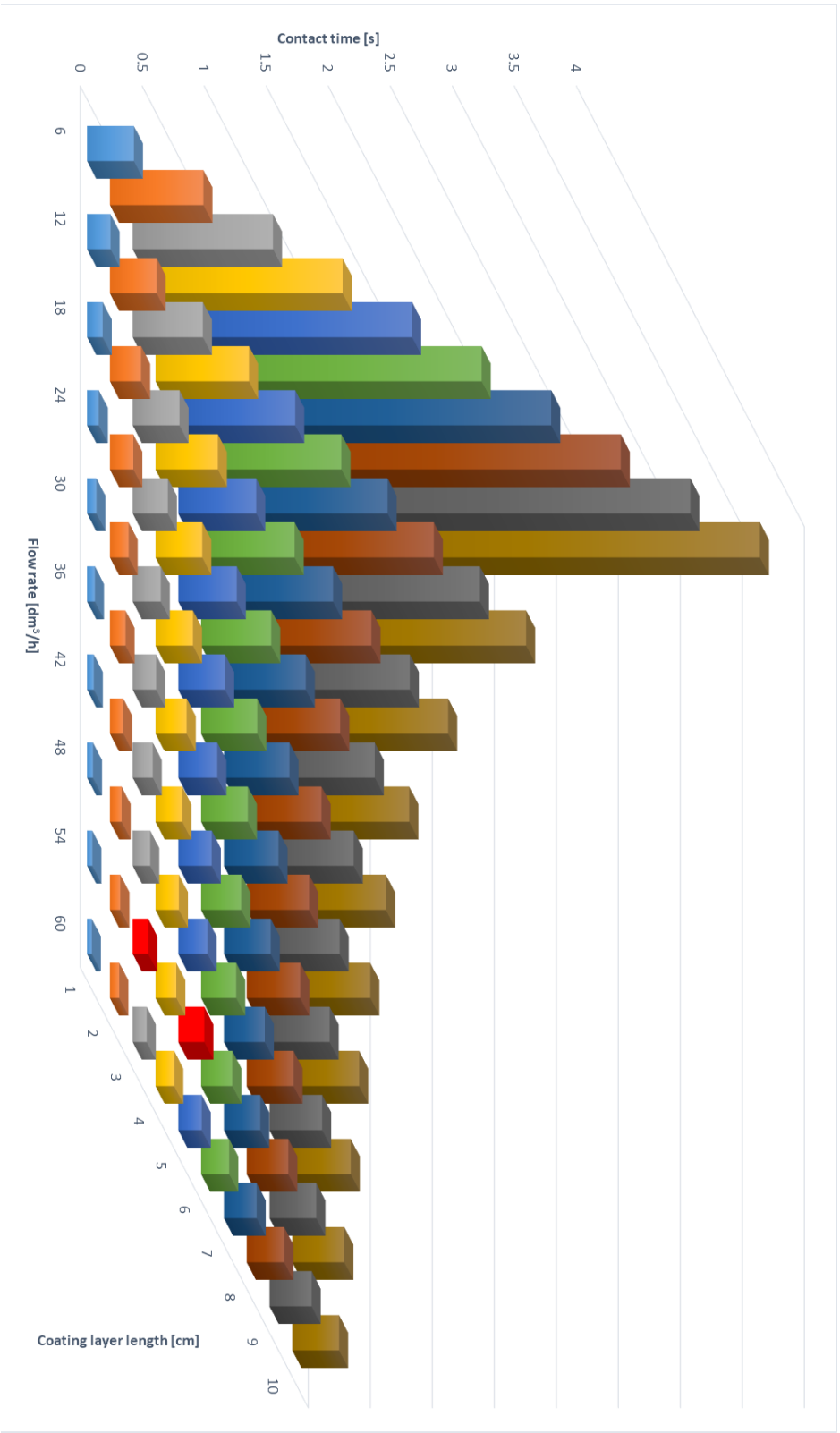

Figure 5.4: The contact time of simulated passes through coated sorbent in different flow rate and different length of coated sorbent in one coated pipe conjugation of MPR

$$t_{(MPR)} = \frac{n\pi r_{pipe}^2 l_{coated}}{QN} \quad (18)$$

Where r_{pipe} was the radius of selected PTFE pipe for coating, l_{coated} was the length of sorbent coating inside of PTFE pipe, N was the total number of selected PTFE pipes in MPR, n was the total number of coated PTFE pipes in MPR, respectively. Therefore, in the five-sub pipes conjugation of MPR, the contact time of simulated gas passed through one CuS and CuO coated pipe were 0.21 s and 0.15 s, respectively. If the MPR has three CuS and CuO coated pipes, the total contact time were 0.63 s and 0.44 s. By adding more coated PTFE pipes into the MPR's setting, the $t_{(MPR)}$ between the sorbent and Hg(0) is increased. According to the Bernoulli Equation, the velocity of flow in MPR is calculated by Equation (19).

$$v_{(sub)} = \frac{Q}{A_{(sub)}N} \quad (19)$$

Where $A_{(sub)}$ was the cross section area of selected PTFE pipes, N was the total number of selected PTFE pipes in MPR, respectively. The velocity of gas passing through the one pipe of MPR is 1.19 m/s and the velocity of gas passing through the five pipes of MPR is 0.239 m/s. Fig. 5.4 shows the contact time simulated gas passes through the coated sorbent in different flow rate and different length of coated sorbent in one pipe conjugation of MPR. The red bars are represented the results of contact time in the selected flow rate during my experiment.

The MPRs were horizontally placed inside the thermostatic oven. The reactor connected to the coated pipes was a sorbent stream, and the reactor connected to the non-coated PTFE pipes was a reference stream (Fig. 5.3). The PTFE pipe with 6 mm of outer diameter and 4 mm of inner diameter was connected with the mainstream and the selected reactor. Five of the same size PTFE pipes were used as the core of the MPR.

Kinds of sorbents applied in multiple pipes reactor

Because the sorbent must be well attached on the internal surface of the PTFE pipe, there is a limited number of sorbents successfully be implemented in this kind of reactor. Only the sorbents suitable to be synthesized inside of the PTFE were useful for the MPRs.

The drawback of MPRs

MPRs are not easily sorbent coated inside the PTFE pipes. This process requires a long time to season the sorbent with moisture. Sorbents often do not equally coat the internal surface.

a

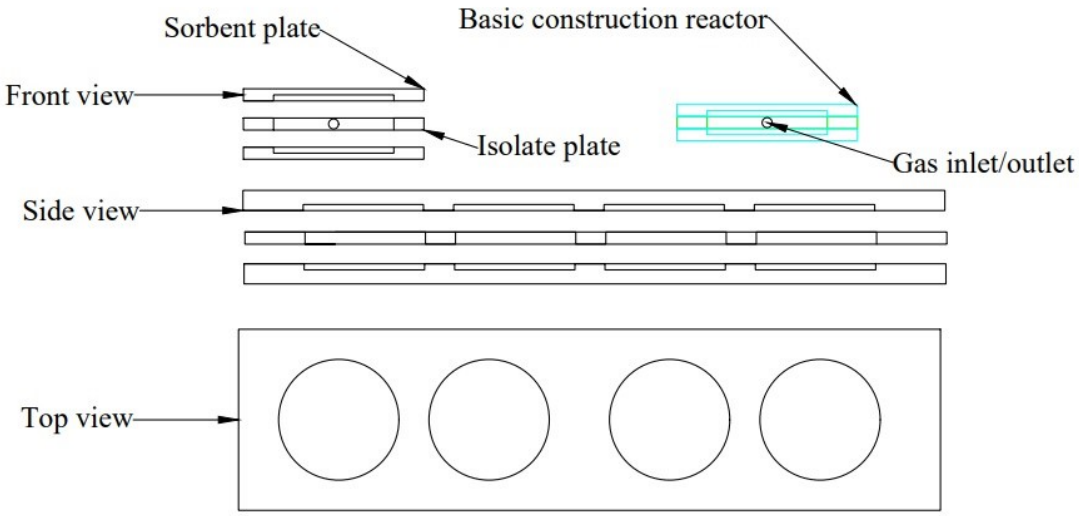

b

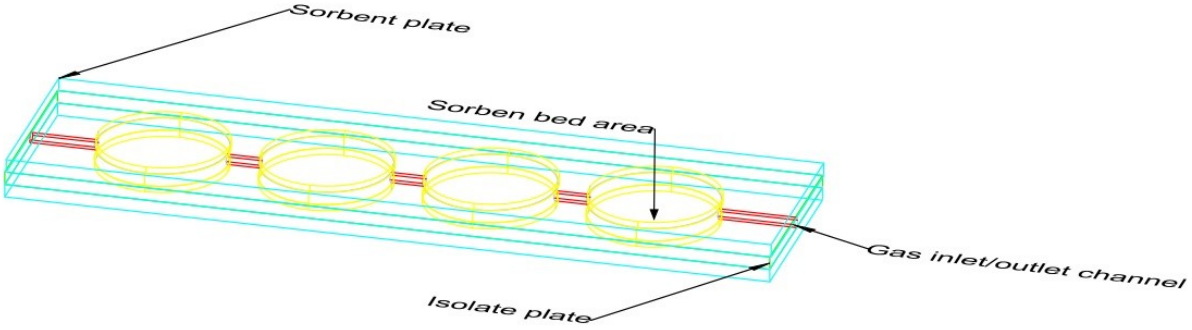

c

Figure 5.5: 2D (a), 3D (b) schemes, photos (c) of MTLCR and single module of MTLCR with metal supporter

5.2.2. Multiple thin layer cubic reactor (MTLCR)

The immobilized sorbent reactor—MTLCR, consists of multiple plates with different inner structures. The basic MTLCR construction has 3 plates: 2 sorbent plates with 8 sorbent beds (flat cylinders) within each sorbent plate, and one isolating plate with 4 circle-shape areas to assure the contact between process gas and sorbents. There is a 6 mm channel in the middle of each isolating plate to allow the gas passing through the whole construction (Fig. 5.5).

The selected sorbent was placed in the sorbent bed, covering its whole area. If required, the selected amount of sorbent can be equally shared and placed inside the rest of sorbent beds to enlarge the contact area between sorbent and gas. And our MTLCR can be also expanded from basic construction (2 sorbent plates and one isolate plate) to expanded version (4 sorbent plates and 2 isolate plates or 2 sorbent plates and 2 isolate plates and etc.). The direction of a gas flow is parallel to the long side of the MTLCR. When the Hg(0) rich gas passes through the inlet, it enters into the empty spaces of an isolate plate, and the larger space reduces the velocity of a gas flow. The longer retention time promotes the chance of sorbent to efficiently react with Hg(0). The area of sorbent bed can be calculated by Equation (20)

$$A = \pi r_{sorbent\ bed}^2 \tag{20}$$

Where r was the radius of sorbent bed inside of MTLCR. The sorbent bed has the dimeter of 6 cm, and its surface area is 28.27 cm^2. According to the Equation (21) and (22):

$$Q = A_{(inlet)} v_{(inlet)} = A_{(outlet)} v_{(outlet)} \tag{21}$$

$$v_{outlet} = \frac{Q}{A_{outlet}} \tag{22}$$

Where $A_{(inlet)}$ and $A_{(outlet)}$ were the cross section area of inlet and outlet of MTLCR.

The flow rate (Q) was constant - 54 dm^3/h, and the same at the gas inlet and outlet. Therefore, the velocity of gas getting in/out the MTLCR can be calculated by the Equation (22). However, the velocity of gas inside of sorbent area was more complex than the velocity of gas getting in/out the MTLCR. The cross section area of sorbent bed (A) is perpendicular to flow of gas direction. The front view of the cross section area is a rectangle. This area of rectangle is relate to simulated gas passthrough on the specific point of sorbent bed. It will change while the simulated gas passes through sorbent bed. Hence, figuring out of the specific point on the sorbent bed is the first step of calculation of cross section area of sorbent bed. The specific point, $f(x, y)$, can calculated by the Equation (23) to (25):

$$x_{point}^2 + y_{point}^2 = r_{sorbent\ bed}^2 \tag{23}$$

$$y_{point} = r_{sorbent\ bed} \sin\theta\ ,\ \theta \in \left[0 \quad \frac{\pi}{2}\right] \tag{24}$$

$$x_{point} = \sqrt[2]{r_{sorbent\ bed}^2 - y_{point}^2} \tag{25}$$

Where x_{point} and y_{point} were the coordinate of specific point on sorbent bed, $r_{sorbent\ bed}$ was the radius of sorbent bed, θ was the angle of between the x axis and distance of the specific point, respectively. The distance of specific point to y axis, $d_{y\ axis}$, can be calculated by following Equation (26):

$$d_{y\ axis} = \sqrt[2]{(x_2 - x_1)^2 - (y_2 - y_1)^2} = \left|x_{point}\right| \tag{26}$$

Where x_2 and y_2 were coordinate on sorbent bed, x_1 and y_1 were coordinate point on y axis, respectively. Assume the simulated gas pass the sorbent bed via y axis. Hence, the width of the cross section area is equal to 2 times of distance of specific point to y axis. Therefore, the simulated gas passes through the selected cross section area, $(A(y)_{ponit})$,can be calculated by the following Equations (27) to (28):

$$A(y)_{ponit} = wh_{gap}, \quad w = 2\left|x_{ponit}\right| \tag{27}$$

$$A(y)_{ponit} = 2\left|x_{ponit}\right|h_{gap}$$

$$= 2h_{gap}\sqrt[2]{r_{sorbent\ bed}^2 - y_{point}^2}$$

$$= 2h_{gap}\sqrt[2]{r_{sorbent\ bed}^2(1 - \sin^2\theta)} \tag{28}$$

Where w was the width of cross section area, h_{gap} was the gap between the sorbent in bottom of sorbent area to the sorbent or empty sorbent bed on the top of sorbent area, $\left|x_{ponit}\right|$ was the distance of selected specific point to the y axis, respectively.

In addition, the cross section area is changing while the coordinate is changing. The sum of cross section area, $\sum_{i=0}^{\frac{\pi}{2}} A(y)_{ponit}(i)$, can be calculated by following Equations (29) to (31):

$$\sum_{i=0}^{\frac{\pi}{2}} A(y)_{ponit}(i) = \int_{-r}^{r} A(y)_{ponit}\, dy \tag{29}$$

$$d(y)_{ponit} = r_{sorbent\ bed} \cos\theta\, d\theta \tag{30}$$

$$\sum_{i=0}^{\frac{\pi}{2}} A(y)_{ponit}(i) = \pi h_{gap} r_{sorbent\ bed}^2 \tag{31}$$

Where $d(y)_{ponit}$ is the distance of specific point on y axis to the center of sorbent bed. The step by step calculation procedures of sum of cross section area, $\sum_{i=0}^{\frac{\pi}{2}} A(y)_{ponit}(i)$, is showed as Equation (32):

$$\sum_{i=0}^{\frac{\pi}{2}} A(y)_{ponit}(i) = \int_{-r}^{r} A(y)_{ponit}\, dy$$

$$= \int_{-r}^{r} 2h_{gap} \sqrt[2]{r_{sorbent\ bed}^2 - y_{point}^2}\, d(y)_{ponit}$$

$$= 4h_{gap} \int_{0}^{r} \sqrt[2]{r_{sorbent\ bed}^2 - y_{point}^2}\, d(y)_{ponit}$$

$$= 4h_{gap} \int_{0}^{\frac{\pi}{2}} \sqrt[2]{r_{sorbent\ bed}^2 - (r_{sorbent\ bed} \sin\theta)^2} r_{sorbent\ bed} \cos\theta\, d\theta$$

$$= 4h_{gap} \int_{0}^{\frac{\pi}{2}} r_{sorbent\ bed}^2 \cos^2\theta\, d$$

$$= 4h_{gap} r_{sorbent\ bed}^2 \int_{0}^{\frac{\pi}{2}} \frac{1+\cos 2\theta}{2}\, d\theta$$

$$= 4h_{gap} r_{sorbent\ bed}^2 \left(\frac{1}{2}\theta + \frac{1}{4}\sin 2\theta\right)\Bigg|_{0}^{\frac{\pi}{2}}$$

$$= 4h_{gap} r_{sorbent\ bed}^2 \left(\frac{\pi}{4}\right)$$

$$= \pi h_{gap} r_{sorbent\ bed}^2 \qquad (32)$$

The $r_{sorbent\ bed}$ was 3 cm, h_{gap} was 1.8 cm. Hence, the sum of cross section area was 8.48 cm^3. And the sum of point of simulated pass through the cross section area from gas inlet to gas outlet, $\sum f(x,y)$, can be calculated by Equation (33):

$$\sum f(x,y) = \int_{-r}^{r} f(0,y)\, dy$$

$$= 2\int_{0}^{\frac{\pi}{2}} r_{sorbent\ bed} \cos\theta\, d\theta$$

$$= 2r_{sorbent\ bed} \qquad (33)$$

Therefore, the average cross section area, $\overline{A(y)}$, can be calculated by following Equation (34):

$$\overline{A(y)} = \frac{\sum_{i=0}^{\frac{\pi}{2}} A(y)_{ponit}(i)}{\sum f(x,y)}$$

$$= \frac{\pi h_{gap} r_{sorbent\ bed}^2}{2 r_{sorbent\ bed}}$$

$$= \frac{\pi h_{gap} r_{sorbent\ bed}}{2} \quad (34)$$

Therefore, the average of velocity of simulated gas, $\overline{v}$, can be calculated by following Equations (35):

$$\overline{v} = \frac{Q}{\overline{A(y)}}$$

$$= \frac{Q}{\frac{\pi h_{gap} r_{sorbent\ bed}^2}{2 r_{sorbent\ bed}}}$$

$$= \frac{2Q}{\pi h_{gap} r_{sorbent\ bed}} \quad (35)$$

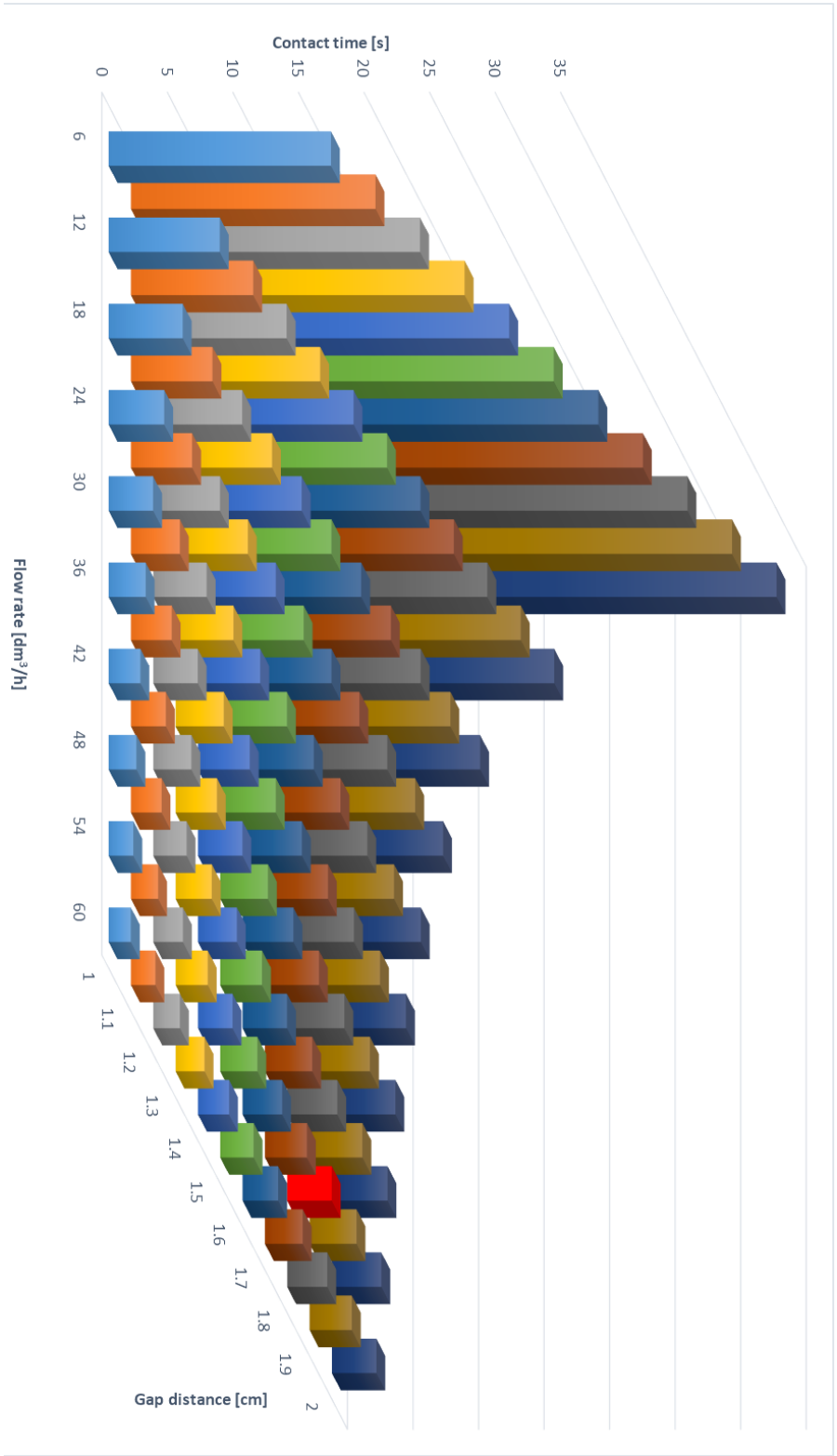

Figure 5.6: The contact time of simulated passes through one sorbent bed in different flow rate and different gap distance between two sorbent layers in MTLCR

The Q was 54 dm^3/h in one basic construction. Therefore, $\overline{v}$ was 0.018 m/s. And the velocity of simulated gas passthrough the selected cross section can be calculated by Equation (36)

$$v = \frac{Q}{A(y)_{ponit}}$$

$$= \frac{Q}{2h_{gap}\sqrt{r^2_{sorbent\ bed}(1-\sin^2\theta)}} \quad (36)$$

And the contact time between the gas and sorbent, $t_{sorbent}$, in the MTLCR can be calculated by the Equation (37):

$$t_{sorbent} = \frac{S_{sorbent\ area}}{\overline{v}} \quad (37)$$

Where $S_{sorbent\ area}$ was the distance between the gas inlet and outlet, which was 6 cm, $\overline{v}$ was the average of velocity of simulated gas in sorbent bed, which was 0.018 m/s. Therefore, the contact time was 3.40 s in one single sorbent bed. Fig. 5.6 shows the contact time simulated gas passes through one sorbent bed in different flow rate and different gas distance between two sorbent layers in MTLCR. The red bars are represented the results of contact time in the selected flow rate during my experiment.

Kinds of sorbents applied in MTLCR

The sorbents applied in the MTLCR are similar to these tested in VFGRs, most of solid form and powder form sorbents can be placed inside the MTLCR. The powder form may be tamped in the sorbent bed to cover the whole area of the sorbent bed. Unlike the VFGR, the MTLCR can implement the polymer composite sorbents. The polymer composite sorbent can be placed onto the both sides of each sorbent bed, unlike the solid form and powder form sorbents.

The drawbacks of MTLCR

The main drawback of the MTLCR is the weight of the reactor. It is built from solid Teflon blocks, and consists of several layers. The construction has the additional support cage to make the whole reactor temperature stable and tight. The weight of full version (include the support cage) is around 15 kg. On the other hand the PTFE material has the thermal expansion issue. When the PTFE material is kept at higher temperatures over 100℃, the structure of PTFE may expand and change its shape in specified parts of a reactor. When the MTLCR is in the full version the prolonged time is required to heat the whole reactor up.

5.3. Experiments and results

In these series of experiments, three reactors and the redesign Hg(0) analysis system were used to test the sorbent and analyze the Hg(0) removal efficiency. Some details of the three reactors are showed in the table 5.1.

Table 5.1 Comparison the experimental set-up conditions in the three kinds of reactors

Rector's type	**VFGR**	**MPR**	**MTLCR**
Total flow rate (Q)	108 dm^3/h	108 dm^3/h	108 dm^3/h
Flow condition	Laminar flow, static to semi-fluidized conditions, gas flows perpendicularly to the sorbent bed	Laminar flow, gas flows parallelly along the sorbent wall	Laminar flow, gas flow parallelly along the sorbent bed
Total number of beds or pipes in the reactor (N)	3	5	4
Number of used beds or coated pipes in the reactor (n)	1 to 3	1 and 3	1 and 2
The selected sorbent	Granulate or powder form sorbents	Synthesized metal sorbents	Granulate or powder form, synthesized and polymer composite sorbents
Mass of sorbent	200 mg to 6 g	50 mg in 1-coated pipe set-up 200 mg in 3-coated pipes set-up	2 g and 4 g
Radius of sorbent bed (r_1)	13 mm	N/A	30 mm
Radius of PTFE pipe (r_2)	N/A	2 mm	N/A

Sorbent thickness (l_1)	Depends on the mass of sorbent, max. about 2 cm	N/A, but less than 0.1 cm	Depends on the mass of sorbent, max. 0.5 cm
Coating sorbent length (l_2)	N/A	35 mm in CuO-coating pipes 50 mm in CuS-coating Pipes	N/A

The selected sorbents for Hg(0) capture study are as follows:

(1) Synthesized adsorbents: CuS, FeS, Fe-Cu-ACs, CuS-ACs, Fe-ACs.

(2) Sorbents from different cooperating institutions such as biosorbents (bio-H and bio-S), carbon base sorbents (C-1, C-2, C-3), polymer material (H-1, H-2), metal oxides modified polymer material (H-M1, H-M2), modified zeolite sorbents (X-M, A-M).

H_2S gas was prepared in the laboratory. The synthesis procedure can be described in the following steps:

(a) 2 g of iron sulfide (FeS) powder was placed inside a flask with rubber stopper.

(b) 200 ml of 10% H_2SO_4 was transferred using a syringe to the flask which FeS.

(c) When bubbles appeared, the peristatic pump transferred the gas inside a flask to a beaker with $CuSO_4$ solution till the black precipitation occurred.

(d) Then, using the peristatic pump, the gas was transferred into a 5 L Tedlar bag.

(e) H_2S was collected and mixed/diluted with nitrogen gas (Fig. 5.7).

The reaction between FeS and H_2SO_4 solution is described in Equation (38).

$$FeS_{(s)} + H_2SO_{4(aq)} \rightarrow FeSO_{4(aq)} + H_2S_{(g)} \quad (38)$$

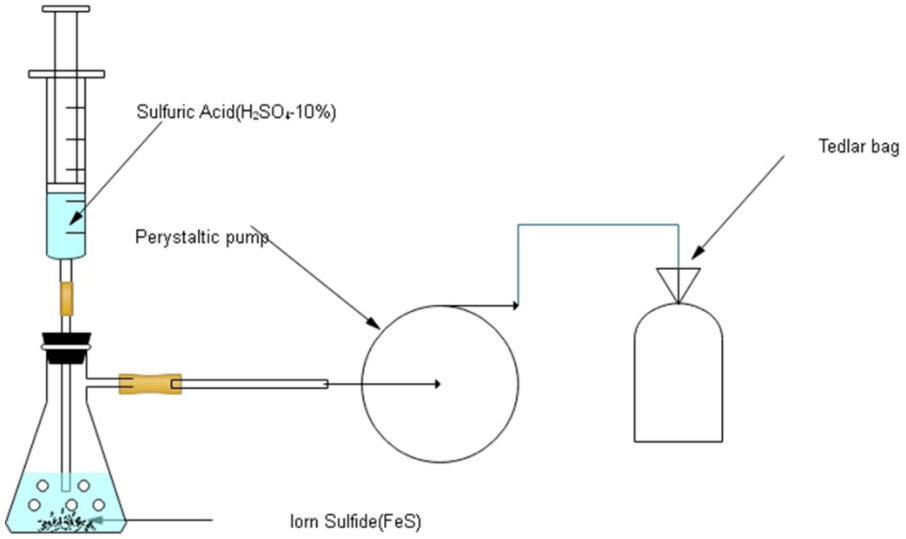

Figure 5.7: The on-line data of Hg(0) passed through the reference and sorbent mercury analyzer

5.3.1. Preparation of sorbents

The selected sorbents applied in the VFGR were partially from cooperating institution and partially were synthesized by me in the AGH laboratory. The details of sorbents and synthesis procedures are described as follows:

(1) The selected adsorbents were placed in the glass cell(s) of the VFGR reactor in the adsorbent line; the same but empty glass reactor was a reference in a reference line.

(2) The selected adsorbents were raw Acs (Baqua 1), synthesized granulate metal sulfides (CuS, FeS) and transition metals (Fe, Cu) loaded on AC: ACs were covered with different amounts of impregnation materials or pure powder

(3) Granulated forms of sulfide sorbents were used:

(a) the granulate forms of CuS and FeS were synthesized in a laboratory by using copper(II) acetate hydrate, $Cu(CH3COO)_2 \bullet H_2O$ and iron(II) chloride tetrahydrate, $FeCl_2 \bullet 4H_2O$ to react with sodium sulfide hydrate, $Na_2S \bullet 9H_2O$;

(b) 15.7 g of $Cu(CH_3COO)_2 \bullet H_2O$ and 12.5 g of $FeCl_2 \bullet 4H_2O$ were dissolved in 150ml of deionized water (DW). 16 g of $Na_2S \bullet 9H_2O$ was dissolved in 100ml DW;

(c) $Cu(CH_3COO)_2$ and $FeCl_2$ solutions were stirred around 250-300 rpm and heat up to around 60℃, then titrated with Na_2S solution drop by drop, and stirred for another 2 hours till reaction was completed;

(d) the product was filtrated, rinsed with DW and the filtrate dried at room temperature;

(e) after drying process, the synthesized sorbent was grounded in a short time to break bigger particles into a small granulate form (1-3 mm) as in that form they were used in the series of experiments.

(4) Cu^{2+} and Fe^{2+} modifications onto the AC surfaces were performed as follows:

(a) 1.3 g of $Cu(CH_3COO)_2 \cdot H_2O$ and 1.4 g of $FeCl_2 \cdot 4H_2O$ were dissolved in 100ml of DW;

(b) each of prepared solution was mixed with 12 g of AC (Baqua 1);

(c) the mixture was stirred at 250-300 rpm and heat up to around 60℃;

(d) the mixture was titrated with 50ml of Na_2S solution (16 g of $Na_2S \cdot 9H_2O$ in 100ml DW) drop by drop, and stirred for 2 hours till reaction was completed;

(d) the product was filtrated, rinsed with DW, and the filtrate was dried in room temperature, in that impregnation process 5% of Cu^{2+} and Fe^{2+} were loaded onto the AC surface.

(5) In order to prepared the granulate CuO sorbent:

(a) 15.7 g of $CuSO_4 \cdot 5H_2O$ was dissolved in 150 ml of DW;
(b) 11 g of potassium hydroxide, KOH, was dissolved in 100 ml of DW;
(c) $CuSO_4$ solution was stirred at 250-300 rpm and heated to 60℃ before being titrated with KOH solution;
(d) it was stirred for 2 hours till the reaction was completed;
(e) the obtained filtrate was filtrated and rinsed with DW;
(f) the solid residue was dried at room temperature;
(g) the sorbent was then quickly grounded to break larger particles into small granules (1-3 mm) and heated in an oven to 110℃ to remove moisture.

(6) The other synthesized and/or modified sorbents were obtained from cooperating institutions.

5.3.2. Preparation of coated pipes for MPR

There were two methodologies for synthesizing the coating sorbent inside of the PTFE pipes (A and B). The difference between methodologies A and B was the sulfur source of synthesized CuS.

In the methodology A the CuS sorbent coating was produced using the subsequent procedure:

(a) 15.7 g of $CuSO_4 \cdot 5H_2O$ was dissolved in 150 ml of deionized (DW) water;

(b) 16.0 g of $Na_2S•9H_2O$ was dissolved in 100 ml of DW;
(c) using two syringes, the $CuSO_4$ solution and Na_2S solution were transferred into the selected PTFE pipes at room temperature, respectively. And mixing $CuSO_4$ solution and Na_2S solution inside of selected pipes several times. Drying prepared pipes at room temperature, and then slowly rinsed with DW;
(d) prepared PTFE pipes were placed horizontally in the oven over 110℃ to remove moisture;
(e) the CuO-coating of PTFE pipes was obtained by substituting 11.0 g of potassium hydroxide, KOH, for $Na_2S•9H_2O$ and repeating the above procedure.

In the methodology B the selected adsorbents were coated with CuS in the reaction of $CuSO_4$ solution with H_2S gas instead of Na_2S solution:

(a) in a flat glassware (e.g. Petri dish), the PTFE pipes were immersed in a $CuSO_4$ solution;
(b) 3.0 g of iron(II) sulfide, FeS powder was placed in an Erlenmeyer flask;
(c) this Erlenmeyer flask was poured with 200 ml of 10% sulfuric acid to produce H_2S gas, which was transferred to a Tedlar bag using a precise peristaltic pump;
(d) H_2S gas was directed inside the PTFE pipes, where reacted with $CuSO_4$ solution;
(e) the coated pipes were removed from the flat glassware (e.g. Petri dish), and placed coated pipes in an oven. And heated to 110℃ to remove moisture. The pipes were then rinsed with DW, and re-dried them at 110°C in an oven.

As described, methods A and B differed in terms of drying temperature and time and residues (co-products). In the method A, CuS was completely precipitated along the pipes, and the coated pipes were dried at room temperature or low oven temperature (30–50°C). Because the CuS particles were not firmly adhered inside of coated pipes. When the coated pipes were dried at related high temperature (such as 105—160°C), the unstable CuS particles were expelled from the pipes by water vapor. The residues might stay inside of coated pipes were the Na^+ and SO_4^{2-} ions.

In a contrast with the method A, the drying time was shorter in the method B. CuS was firmly adhered to the PTFE pipe's interior surface. It was not expelled from the pipes at the high temperature (over 100°C). The remaining ions were H^+ and $SO4^{2-}$. The DW could be rapidly pumped through coating pipes to eliminate residues.

In the MPR, the coating of PTFE pipes is interchangeable. The PTFE is resistant to acid or alkenyl solutions. After use, the PTFE pipes or other kinds of cylindrical modules could be cleaned with 10% HNO_3 to remove the remaining coating and mercury. PTFE pipes can then be recoated using the same technique (described previously).

5.3.3. Experimental result from VFGR, MPR, MTLCR

The fixed bed designed in the VFGR provides the Hg(0) capture without any interferences. It is suitable to analyze the performance of powder sorbents. The VFGR provide the reliable data of Hg(0) removal by the sorbent in exhaust gas. Therefore, the particularly selected sorbents were tested in the VFGR. It was used as a reference to compare the results from two other self-designed reactors.

The testing system details are presented in Fig. 4.4. Before each series, after longer break, the system pipes and connections should be cleaned with 10% nitric acid solution and DW. Then dried and heated for longer period of time at 108 L/h and 140-150°C.

The details of each experiment are described as follows (names of the system elements refers to Fig. 4.4):

i. Using an exhaust fan after and a flow meter before the system, the possible leak was checked. If the leak of system occurred, the reactor corks at first, and then each T-connector and pipe connections were checked.
ii. Preparation of fresh limestone liquid loads to a WFGD system.
iii. Preparation of 10% KOH to load WLE-8 scrubbers and as protecting solutions before exhausters. Preparation of $SnCl_2$ and 5% H_2SO_4 solution to load a WLE-8 scrubber (only for measuring total elemental mercury).
iv. Preparation of selected sorbents to load reactors.
v. Preparation of Hg(0)/N_2 mixture gas in Tedlar bags.
vi. Switching on all devices including heat-traps, heating-filter etc.
vii. Setting up EMP2 analyzers and WLE-8 scrubbers, exhaust fan No.3, switching on Hg(0) source and determination of its base level in the whole system.
viii. Switching on WFGD system. Checking Hg(0) concentration in simulated gas passthrough reference reactor, sorbent reactor, respectively.
ix. Turning on the boiler, and pre-heating for 15 mins. Afterwards, turning on a coal feeder.

(ix-b. Switching on the Tedlar bag with H_2S.)

x. Turning on the Testo 350 analyzer for 2 min to measure flue gas composition, and then switching off. And then, turning on the exhaust fan No.3 instead of Testo 350.
(x-b. Switching 3-way valve to ref. site, sorb. site and switch off 3-way valve, respectively. Checking Hg(0) concentration and flue gas composition in different conditions. Each step shall be conducted in 5 mins for stabilization of Hg(0) concentration. In each step, the Testo 350 analyzer is used for 2 min to measure flue gas composition, and then switched off, as the exhaust fan No.3 is used instead of Testo 350.)

xi. Switching on the WFGD system.

xii. Turning on the Testo 350 analyzer for 2 min to measure flue gas composition, and then switching off. And then, turning on the exhaust fan No.3 instead of Testo 350. Observation of Hg(0) concentration and flue gas composition.
(xii-b. Observation of Hg(0) concentration and flue gas composition. Each step shall conducts in 5 mins for stabilization of Hg(0) concentration. In each step, the Testo 350 analyzer is used for 2 mins to measure flue gas composition, and then switched off, as the exhaust fan No.3 is used instead of Testo 350.)

xiii. Turning off the coal feeder.
(xiii-b. Switching off the Tedlar bag with H_2S)

xiv. Observation of Hg(0) concentration till stabilization.

xv. Switching off the Tedlar bag with $Hg(0)/N_2$. Observation of Hg(0) concentration till stabilization.

xvi. Stopping EMP2 analyzers and cleaning WLE-8 scrubbers with DW. Switching off all devices.

The procedures ix-b, x-b, xii-b, xiii-b were applied in the specific experiments.

Calculation of results from three reactors

In the mercury analysis procedures, the results were measured by the online EMP-2 mercury analyzers and the data can be illustrated in a graph. The mercury concentration curves from the reference and sorbent lines are obtained separately, and are analyzed as in Fig. 5.8.

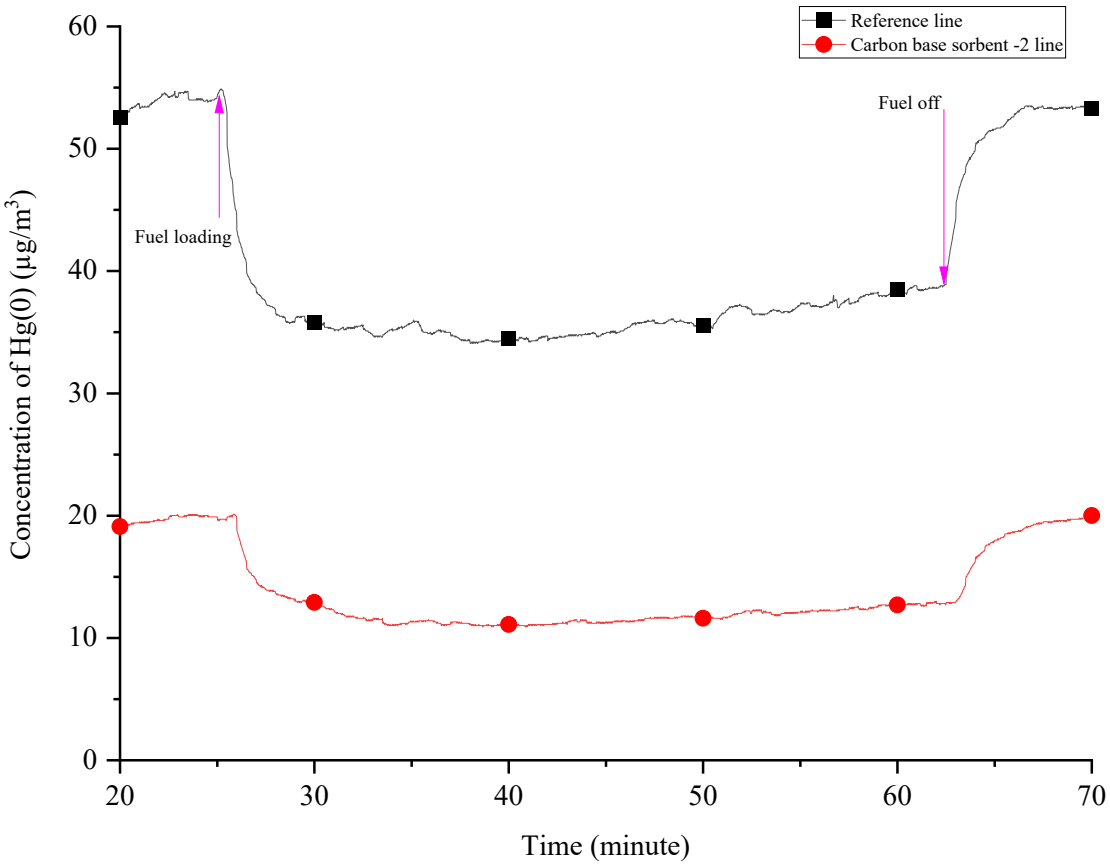

Figure 5.8 Online data from Hg(0) analyzers of mercury passing simultaneously through reference and sorbent lines

When the Hg(0) in N_2 gas mixture was loaded into system, the concentration of Hg(0) increased rapidly in both lines. The signal stabilization is observed and the reference concentration is easily set. The concentration of Hg(0) in the reference line was much higher than the Hg(0) in the sorbent line. The difference is related to many factors, however most important are quality of sorbent, quantity and speciation form of mercury and simulated flue gas composition (kind of fuel, combustion conditions). After the simulated gas was loaded into the system, the Hg(0) concentration drop in both lines was observed. Gaseous chemical compounds coming from F, Cl, Br, S, N in fuel may have oxidized mercury from Hg(0) to Hg(II) or interact with a sorbent (activation or deactivation paths). Presumably, some amounts of the Hg(II) may interact with a sorbent, but clearly the most of that Hg(II) was trapped in scrubbers, reacting with NaOH. The Hg(0) concentration drop was 20 µg/Nm^3 in the reference line opposite to less than the 10 µg/Nm^3

drop in the sorbent line, but removal rate (in %) remained at the similar level (64-67%) – Fig. 5.9. This fact indicates that using two separate measurement lines (one reference) may be an effective way to eliminate the influence of external conditions on the measured mercury capture efficiencies. Oxidation of mercury in exhaust gases is a widely known phenomenon, and this speciation form of mercury is effectively captured by fly ash and in flue gas desulfurization systems. Therefore, in these studies mainly Hg(0) was analyzed, because it is the main component of gaseous mercury emissions from power plants and other factories. The presence of uncaptured Hg(II) in clean gas transferred into EMP-2 analyzers is rather hypothetical, and would not be measured with an AAS method. When the flue gas production was stopped, the concentration of Hg(0) in both lines returned to the initial levels, which confirms previous assumptions.

The Hg(0) concentration gap between the reference and sorbent lines (Fig. 5.8) is related to the amount of Hg(0) captured by the sorbent, which as the Hg(0) capture efficiency is illustrated by the curve in Fig. 5.9. It demonstrates the sorbent performance in different stages during experiments. The online (temporary) Hg(0) capture efficiency ($\eta_{Hg(0)}$) could be calculated via Equation (39).

$$\eta_{Hg(0)} = \frac{C_{Ref} - C_{Sorb}}{C_{Ref}} \times 100\% \quad (39)$$

Where the C_{Ref} and C_{Sorb} are the Hg(0) concentrations from reference and sorbent lines at selected time, respectively.

According to Fig. 5.9, the Hg(0) capture efficiency of the C-2 sorbent was in a steady condition, both during the Hg(0)/N_2 loading and simulated gas/Hg(0) mix stages. There were two fluctuations occurred when the simulated gas was loaded into/removed from the system, but the Hg(0) capture efficiency line returned to steady condition quickly. These fluctuations were most likely related to the transient instability of the simulated gas composition (for example, a temporary, uncontrolled increase of CO concentration) The C-2 sorbent showed match more than 60% of Hg(0) online capture efficiency. It increased closely to 70% when the simulated gas was loaded.

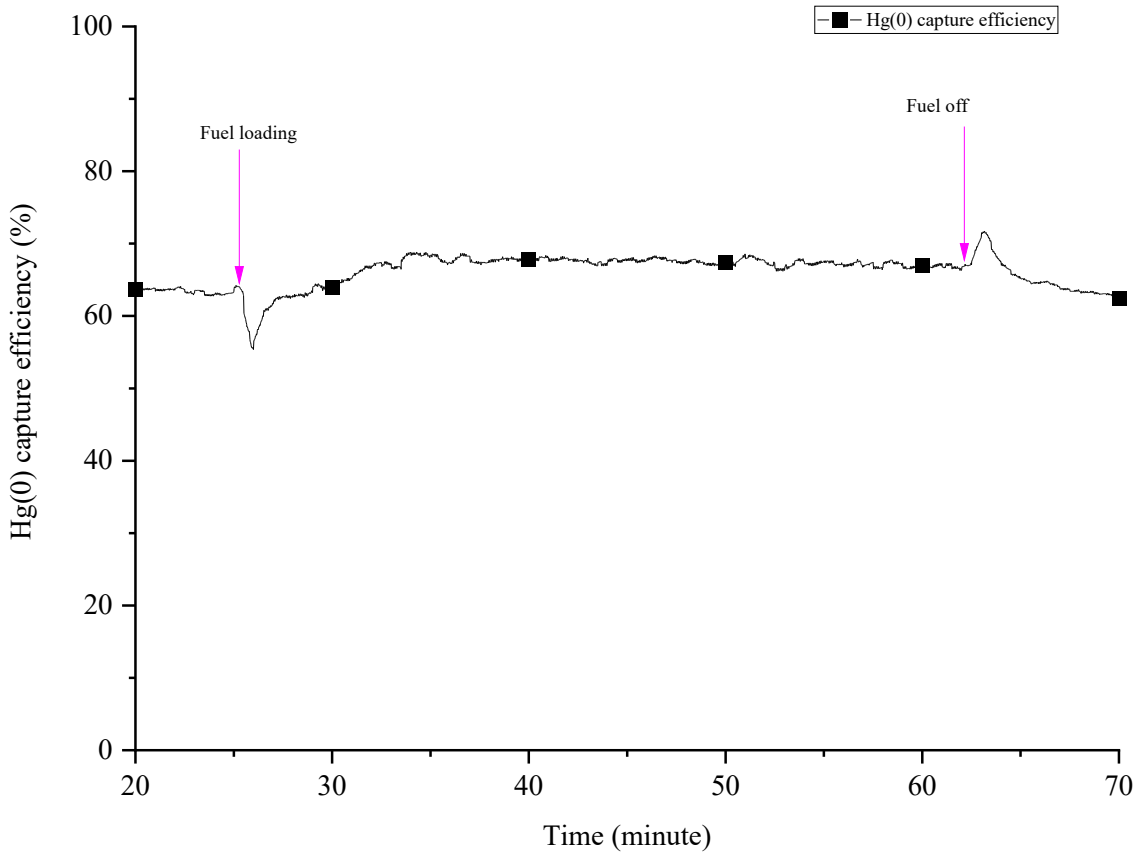

Figure 5.9 Online Hg(0) capture efficiency of carbon base sorbent-2

The results and graphs presented in Figs 5.8 and 5.9 may not be intuitive and easy to understand for readers. Hence, I applied I applied some mathematical transformations to present more intuitive data, such as mean Hg(0) capture efficiency in different stages (table 5.2), total Hg(0) capture rate (Fig. 5.14) and etc. The mean Hg(0) capture efficiency, $\bar{\eta}_{Hg(0)}$,in different stages represents a sorbent performance condition in a selected time range and it is calculated via Equation (40):

$$\bar{\eta}_{Hg(0)} = \frac{\sum_{n_s}^{n_e}\left(\frac{C_{Ref}-C_{Sorb}}{C_{Ref}}\times 100\%\right)}{n_e - n_s} \quad (40)$$

Where the C_{Ref} and C_{Sorb} are the Hg(0) concentrations from reference and sorbent lines, respectively, the n_s and n_e are the starting and ending measurement points in a selected time range (often the range between Hg(0) loading in and removing off the system), respectively.

The mean Hg(0) capture efficiency ($\overline{\eta}_{Hg(0)}$) can also evolves into two different Equations (41) and (42), which were used to calculate the total Hg(0) capture efficiency ($\eta Hg(0)_{total\ capture}$) or the total Hg(0) penetration rate ($\eta Hg(0)_{total\ penetration}$) through sorbent at a current time, respectively. These two measures demonstrate sorbent performance in a selected time range.

$$\eta Hg(0)_{total\ capture} = \frac{\sum_{t_s}^{t_e}(C_{Ref} - C_{Sorb})}{\sum_{t_s}^{t_e} C_{Ref}} \times 100\% \quad (41)$$

$$\eta Hg(0)_{total\ penetration} = \frac{\sum_{t_s}^{t_e} C_{Sorb}}{\sum_{t_s}^{t_e} C_{Ref}} \times 100\% \quad (42)$$

Where the t_s and t_e are start and end times of an experiment (often the time between Hg(0) loading in and removing off the system), respectively.

The mass of Hg(0) capture capability ($c_{sorbent}$) represents the mass of Hg(0) captured by selected mass of sorbent. It indicates that sorbent performance ability and effectiveness of Hg(0) capture. It can be calculated by the Equation (43):

$$c_{sorbent} = \frac{Q(t_e - t_s)\sum_{t_s}^{t_e}(C_{Ref} - C_{Sorb})}{m_{sorbent}} \quad (43)$$

Where Q is the selected flow rate in a sorbent reactor and $m_{sorbent}$ is the total mass of sorbent applied in a sorbent reactor.

The Hg(0) mass capture rate ($\eta(m)_{Hg(0)}$) represents the total mass of Hg(0) captured by selected sorbent in a given time. It indicates the average mass of Hg(0) captured in a specified time range. It can be calculated by Equation (44):

$$\eta(m)_{Hg(0)} = Q\sum_{t_s}^{t_e}(C_{Ref} - C_{Sorb}) \quad (44)$$

In addition, the Hg(0) mass capture rate ($\eta(m)_{Hg(0)}$) can also evolves into three different Equations (45) to (47), which were used to calculate the mass of Hg(0) passed through ($m(Hg(0))_{pass}$), captured ($m(Hg(0))_{capture}$) through sorbents in a specified time range and $\eta_t(m)_{Hg(0)}$, mass of Hg(0) passthrough per mass of sorbent in a specified time range, respectively.

$$m(Hg(0))_{pass} = Q(t_e - t_s)\sum_{t_s}^{t_e} C_{Sorb} \quad (45)$$

$$m(Hg(0))_{capture} = Q(t_e - t_s)\sum_{t_s}^{t_e}(C_{Ref} - C_{Sorb}) \quad (46)$$

$$\eta_t(m)_{Hg(0)} = \frac{Q\sum_{t_s}^{t_e}(C_{Ref} - C_{Sorb})}{m_{sorbent}} \quad (47)$$

The experimental results from the VFGR set-up

The table 5.2 presents data related to the Hg(0) capture efficiency, Hg(0) capture capability and Hg(0) capture rate from various sorbents by using VFGR set-up. The commercial AC (Baqua-1) performed a remarkable result of the Hg(0) capture in this series of experiments (78% mean Hg(0) capture efficiency). 1 g of AC captured 3.9 mg of Hg(0) from the exhaust gas, and its Hg(0) removal rate was 53.18 μg/min. Therefore, the Hg(0) capture performance results of commercial AC could be used as an high performance reference material to qualify results from other sorbents.

In the next series of experiments, 1 g of commercial AC and 1.5 g of CuS, FeS, CuS-ACs, Fe-ACs sorbents were placed at one sorbent cell. Furthermore, 2 g of materials, such as polymer material (H-1, H-2), metal oxides modified polymer material (H-M1, H-M2) zeolites modified sorbent (X-M,A-M), were placed at two sorbent cells. Each sorbent cell contained 1 g of material.

CuS, FeS, CuS-ACs, Fe-ACs sorbents showed the best Hg(0) capture capability among materials presented in table 5.2. The 1.5 g of these 4 sorbents had mean Hg(0) capture efficiencies and Hg(0) mass capture rate over 99% and between 0.11-0.18 mg/min, respectively. They showed the mass of Hg(0) capture capability over 10 mg/g except the CuS, which was 7.25 mg/g. The strong sorption processes, which were presented in Chapter 2.2 are responsible for the remarkable result of metal sulfide and metal-modified sorbents. By comparing with the AC, the results from 2 g of A-M, X-M and H-M2 were acceptable. Two metal modified zeolite sorbents, A-M and X-M, had similar Hg(0) capture performances. The Hg(0) capture rate was over 30 μg/min, and the mass of Hg(0) capture capability was over 1.8 mg/g. But the X-M had a good Hg(0) capture performance only at hot air/Hg(0) conditions, where the Hg(0) capture efficiency was higher than for A-M. The A-M performed the higher Hg(0) removal than X-M in simulated gas conditions. Hg(0) capture performance of H-M2 was lower than two zeolite sorbents. Its Hg(0) capture rate and mass of Hg(0) capture capability was 18.2 μg/min and 0.87 mg/g, respectively.

Table 5.2 The Hg(0) capture efficiency, capability and mass capture rate from selected sorbents								
Sorbent	Mass of sorbent [g]	Capture efficiency [%]				Mean Hg(0) capture efficiency [%]	Mass of Hg(0) capture capability [μg/g]	Hg(0) mass capture rate [μg/min]
		Hot air + Hg(0) (1st)	Simulated gas + Hg(0)+ WFGD off	Simulated gas + Hg(0)+ WFGD on	Hot air + Hg(0) (2nd)			
Commercial AC	1	80.5%	77.5%	N/A	72.7%	78.0%	3.9 (mg)	53.18
bio-H	2	N/A	N/A	N/A	N/A	N/A	-516(X)	-17.49(X)
bio-S	2	47.7%	N/A	N/A	13.6%	N/A	-28(X)	-0.52(X)
H-1	2	N/A	N/A	N/A	N/A	N/A	-393(X)	-14.3(X)
H-2	2	N/A	N/A	N/A	N/A	N/A	-307(X)	-5.44(X)
H-M1	2	13.3%	N/A	N/A	27.6%	N/A	-1.18 (mg)(X)	-15.71(X)
H-M2	2	23%	28.4%	55.7%	49.4%	33.7%	874	18.20
A-M	2	33%	41%	49%	34%	44%	1.95 (mg)	39.02
X-M	2	45%	37%	16%	52%	41.7%	1.85 (mg)	32.19
Fe-AC	1.5	99.1	99.4	99.6	99.7	99.04	10.47(mg)	0.11(mg/min)
CuS	1.5	99.9	99.9	99.6	99.7	99.7	7.25(mg)	0.14(mg/min)
FeS	1.5	99.7	99.9	99.7	99.4	99.5	10.98(mg)	0.18(mg/min)
CuS-AC	1.5	99.9	99.9	99.9	99.9	99.9	10.52(mg)	0.17(mg/min)

(X) Negative results – some comments are below Fig. 5.10.

According to the Fig. 5.3 and Equation (40), the Hg(0) concentration from the reference line shall be always higher than the Hg(0) concentration from the sorbent line, when Hg(0) is loaded into a system. Because there is no sorbent or any material in a reference reactor. However, the negative results coming from bio-H, bio-S, H-1, H-2, H-M1 materials were obtained. Fig. 5.10 is an example illustrating the negative result occurred with the H-1 material. The concentrations of Hg(0) in both reference and sorbent lines were closed to 1 μg/Nm^3 in the initial stage. The concentration of Hg(0) in the sorbent line was slightly higher than the in reference line. When the simulated gas was loaded into the system, the both curve lines reached steady conditions. But after 5 min, the concentrations of Hg(0) in both lines increased by around 5 and 3 μg/Nm^3 in the sorbent and reference lines, respectively. This may occur in the beginning stage, some Hg(0), which deposited on the untested sorbent, is released from the sorbent's surface. When the Hg(0)/N_2 gas mixture was loaded into the system, the concentration of Hg(0) increased rapidly in both lines. But the concentration of Hg(0) in the sorbent line was significantly higher than in the reference line, which were around 45 and 30 μg/Nm^3 in the peak point of the sorbent line and reference line, respectively. This experiment was conducted over 40 minutes, then the simulated gas was removed from the

system to observe the concentration of Hg(0) in both lines. After slight decrease, the concentration of Hg(0) in both lines the Hg concentrations increased again. There was still a significant gap between the reference line and sorbent line. When this experiment conducted till 60th minute, I loaded the simulated gas into the system again, the both curve lines dropped as the same as in Fig. 5.10. Meanwhile, a group of sharp peaks occurred in the graph. One of the reasons may be the particles coming from the material, which blocking the last filters by mercury analyzers. It resulted in pressure changes and unstable flow. In the 80th minute the Hg(0)/N_2 gas mixture was removed from the system. The concentration of Hg(0) in both lines dropped back to the initial stage (1 µg/Nm^3) intermediately.

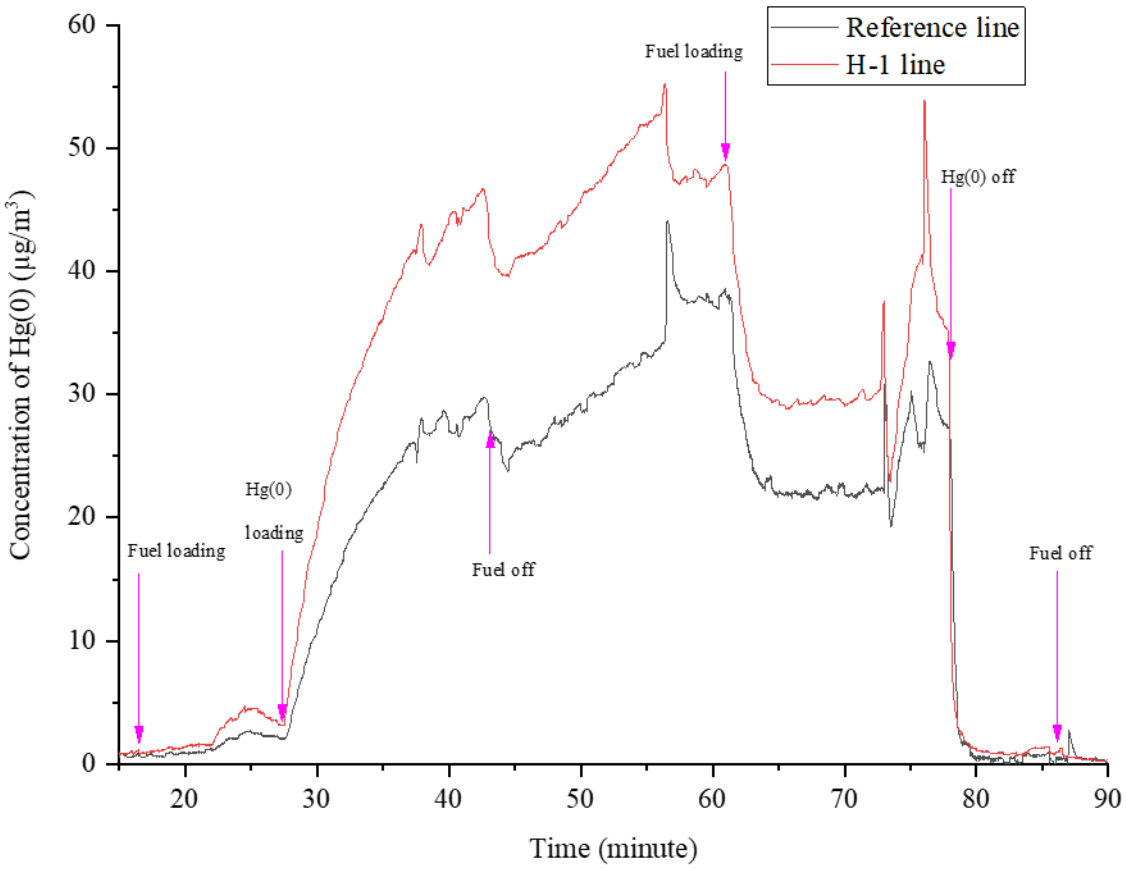

Figure 5.10. Online data of Hg(0) concentrations from the reference and 2 g of H-1 sorbent lines

During the whole experiment with 2 g of H-1, 786 µg of Hg(0) was determined coming out the system and the mass release rate (negative sorption rate) was 14.3 µg/min. The other materials: bio-H, bio-S, H-2, H-M1, had the similar Hg(0) concentration curves as in the H-1's case. 2 g of bio-H, bio-S, H-2, H-M1 materials did not efficiently adsorbed Hg(0) releasing from the system: 1032, 56, 614 and 2360 µg of Hg(0) during the whole process, respectively (table 5.2).

Table 5.3 shows the total mercury concentrations of specified sorbents (tested and untested (raw) materials) determined by the MA-3000 analyzer. Data clearly reveals that the mercury concentration in the tested materials exceeded those in the raw ones. The total mercury concentration of materials in a first (bottom) cell were higher than in a second (upper) cells, except the bio-S. For instance, the total mercury concentration of 1 g of H-1 in the first and second cell is 645.68 and 298.61 ppb, respectively. But these results are higher than the un-test H-1, which is 127.18 ppb. It meant that bio-H, bio-S, H-1, H-2 and H-M1 materials captured the certain amount of Hg(0) from the simulated flue gas during the experiment. But some unknown phenomena must have occurred between the Hg(0) and testing materials, which resulted in a faulty or incorrect readings of mercury analyzers. Some side effects can be presumed for polymer materials:

- They have high initial Hg conc. and release Hg, but it is not the case.
- They generate significant Hg release from the system, which is always - in some extent - contaminated with Hg, but during most of experiments the systems are in equilibrium. No research was done to get reliable results how chemistry of polymer material and its modifications may do so.
- They cause some chemical or physical disturbances that make the measurement in the sorbent line faulty or incorrect. I assume that Hg(0) may deposit on bio-H, bio-S, H-1, H-2 and H-M1 materials' surface (occupying active sites) during the Hg(0) loading stage. But the structure of these sorbents could not bear the thermostatic temperature, which is over 120℃. Their structure decomposes, what results that the deposited Hg(0) is released together with some material from surface. Then the new inner structure adsorbs the Hg(0) from the simulated gas and decomposes again to release the Hg(0). There were some evidences showed that the formation and deposition of the solids inside of the clean PTFE pipes in the sorbent line. Also the PTFE filter protecting a mercury analyzer of the sorbent line was often blocked with a tiny dust, which led to the flow rate disturbances and faulty reads, like in Fig. 5.10 between 73-

78 min. It influenced the reference line too, because pressure of a whole system was unstable then.

Table 5.3 Mean values of the total mercury concentration in sorbents (n=3 to 5)

	Hgtot [ppb]	SD [ppb]	CV [%]
SRM coal-1 (179.0 ppb)	175.26	12.18	6.95
SRM coal-2 (37.3 ppb)	30.60	2.56	8.38
SRM ash (2100 ppb)	2160.96	101.57	4.70
H-1 raw	127.18	0.80	0.63
H-1 (1st cell) (1g)	654.68	38.22	5.75
H-1 (2nd cell) (1g)	298.61	5.75	1.93
H-2 raw	11.77	2.78	23.61
H-2 (1st cell) (1g)	749.09	244.40	32.63
H-2 (2nd cell) (1g)	46.71	5.20	11.14
bio-H raw	< determ. limit	-	-
bio-H (1st cell) (1g)	725.12	32.59	4.49
bio-H (2nd cell) (1g)	568.02	9.11	1.60
bio-S raw	3.50	0.72	20.61
bio-S (1st cell) (1g)	149.99	4.09	2.73
bio-S (2nd cell) (1g)	378.69	114.78	30.31
H-M1 raw	0.82	0.06	7.74
H-M1 (1st cell) (1g)	239.64	3.41	1.42
H-M1 (2nd cell) (1g)	92.41	5.32	5.76
H-M2 raw	238.82	21.12	8.84
H-M2 (1st cell) (1g)	724.28	202.55	27.97
H-M2 (2nd cell) (1g)	701.73	119.10	32.63
A-M raw	33.55	1.27	3.78
A-M (1st cell) (1g)	1147.14	651.17	56.76
A-M (2nd cell) (1g)	177.33	38.68	21.81
X-M raw	10.25	0.23	2.28
X-M (1st cell) (1g)	788.50	58.93	7.47
X-M (2nd cell) (1g)	144.02	10.36	7.20

The experimental results from the MPR set-up

In the following series of experiments, I used the synthesized CuO and CuS sorbents to capture Hg(0) from the simulated flue gas. MPR was a tested reactor vs. the VFGR giving the controlling

group of results. The temperature of thermostatic oven was set at 120°C and the flow rate was 108 dm^3/h. The mercury basic concentration in this series of experiments was 30.0 ± 6.2 $\mu g/m^3$. 200 mg of sorbents was used both in VFGR and 3-pipe MPR configurations.

Table 5.4 shows the comparison results of Hg(0) capture efficiency and Hg(0) capture capability between VFGR and MPR. In the VFGR set-up, 200 mg of CuO or CuS granulates removed average 51% and 67% of Hg(0) during whole experiments, respectively. The maximum Hg(0) capture efficiency was 62.2% for CuO (Hg(0) loading stage) and 85% for CuS (Hg(0)/simulated flue gas loading stage), respectively. After that, the Hg(0) capture efficiency tended to decline. It decreased while increasing the testing time in both CuO and CuS granulates. These results were caused by a flow bypass due to the local porosity near the glass bed wall. On the other hand, the flow possibly does not pass the whole cross-section of a sorbent bed. This area of sorbents was a failure in a long-time experiment when a small amount of sorbent was applied in VFGR. In MPRs, one pipe covered with CuO or CuS sorbents removed 24.35 and 59.38% of Hg(0) during whole experiments, respectively. When three coated pipes were applied in the MPR construction, the average Hg(0) removal efficiency increased to 65.23 (by 268%) and 93.93% (by 158%), when using CuO and CuS, respectively. The Hg(0) mass capture capability of 3-pipe MPRs coated with CuO or CuS was 15.74 and 22.09 μg/mg, respectively, while in the VFGR the Hg(0) mass capture capability of CuO or CuS sorbents was 20.27 and 30.36 μg/mg. It indicates that the MPR set-up do not only promote Hg(0) capture efficiency, it also decreased the Hg(0) capture capability. It meant that the MPR provided more free space to capture Hg(0) than VFGR. In addition, the 3 coated pipes conjugation of MPR reduced the Hg(0) capture capability by comparing the 1 coated pipe conjugation of MPR. This is an advantage when MPR treat simulated flue gas contained high concentration of Hg(0). Because the 3 pipe conjugation of MPR splits the main gas stream into 3 sub-stream as well as the Hg(0). And selected sorbents in 3 coated pipes treat the decreased concentration of Hg(0) in 3 sub-stream is more efficiency than 1 coated pipe.

Table 5.4 The Hg(0) capture efficiency [%] of specified sorbents in different reactors and at different stages

Sorbent	Reactor	Mass of sorbent [mg]	Hot air + Hg(0) (1)	Simulated gas +Hg(0)	Hot air + Hg(0) (2)	Mean Hg(0) capture efficiency	Mass of Hg(0) capture capability [μg/mg]
CuO (granulate)	VFGR	200	62.2%	59.6%	33.6%	50.85%	20.27
CuO (coating)	MPR (1 pipe)	50	13.3%	24.8%	13.9%	24.35%	23.03
	MPR (3 pipes)	200	49.6%	77.3%	55.8%	65.23%	15.74
CuS (granulate)	VFGR	200	74.2%	85%	47.6%	66.70%	30.36
CuS (coating)	MPR (1 pipe)	50	67.4%	54.9%	55.83%	59.38%	75.91
	MPR (3 pipes)	200	97.9%	92%	92.1%	93.93%	22.09

The Hg(0) passthrough rate and mass of Hg(0) passing through selected sorbents during entire experiment are shown in table 5.5 and Fig. 5.11. In the initial stage (20—40 min), Hg(0) was loaded into the system and was stabilized. Small amounts of Hg(0) passed through the sorbents between 20—30 min. Then, it increased rapidly in VGR with CuO and CuS and MPRs with 1 coating of CuO and CuS between 50—90 min, respectively. The mass of Hg(0) passing through CuO and CuS within 3 coated-pipes conjugation of MPR was slow and stable in the 80 minutes of experiment. By contrast, the mass of Hg(0) passing through CuO and CuS in VFGR set-up was fast and unstable. If the experiment would be continuously conducted, the mass of Hg(0) passing through CuO and CuS in VFGR might increase rapidly.

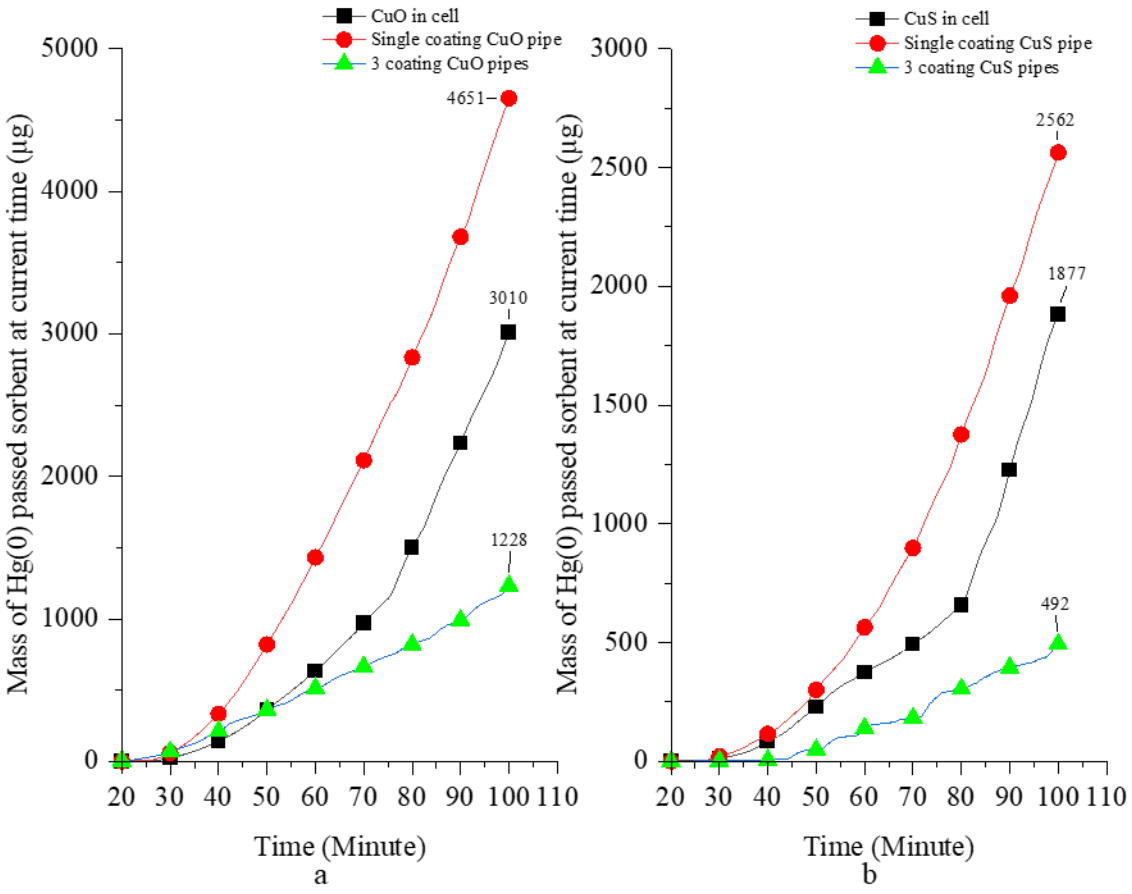

Figure 5.11. Total mass of Hg(0) passed through the CuO (a) and CuS (b)

Table 5.5 The time mass of Hg(0) passing through the selected sorbents in each 20 min

Sorbent (reactor)	20-40 min [µg/g·min]	40-60 min [µg/g·min]	60-80 min [µg/g·min]	80-100 min [µg/g·min]	Mean [µg/g·min]
CuO (VFGR)	35.5	123	216.3	377.8	188.1
CuO (MPR) (1 coating pipe)	332	1096	1402	1820	1162.5
CuO (MPR) (3 coating pipes)	51.8	75.3	77	103	76.8
CuS (VFGR)	20	73.3	70.8	305.8	117.4
CuS (MPR) (1 coating pipe)	115	449	811	1187	640.5

CuS (MPR) (3 coating pipes)	1.5	33.5	41.3	47	30.8

The CuO and CuS are the sorbents which are extremely suitable for Hg(0) capture. They capture Hg(0) from a gas stream in chemisorption processes, which are described in Chapter 2.2.2. But the Hg(0) capture efficiencies from the CuO sorbent are lower than results from the CuS sorbent in these series of experiments. There was some KOH solution remains that resided on the CuO crystals to form a thin layer (Fig. 5.12). Possibly the rinsing process after CuO synthesis was incomplete. It blocked the activation sites of Hg(0) oxidation. It also might affect the Hg(0) capture efficiency in CuS sorbent, if the rinsing process was incomplete. Another reason is the SO_2 competition with Hg(0). It deposits on CuO sorbent's surface and reacts with CuO surface active sites to form $CuSO_4$ and to block the Hg(0) adsorption (Y. Xie et al., 2015; Z. He et al., 2020).

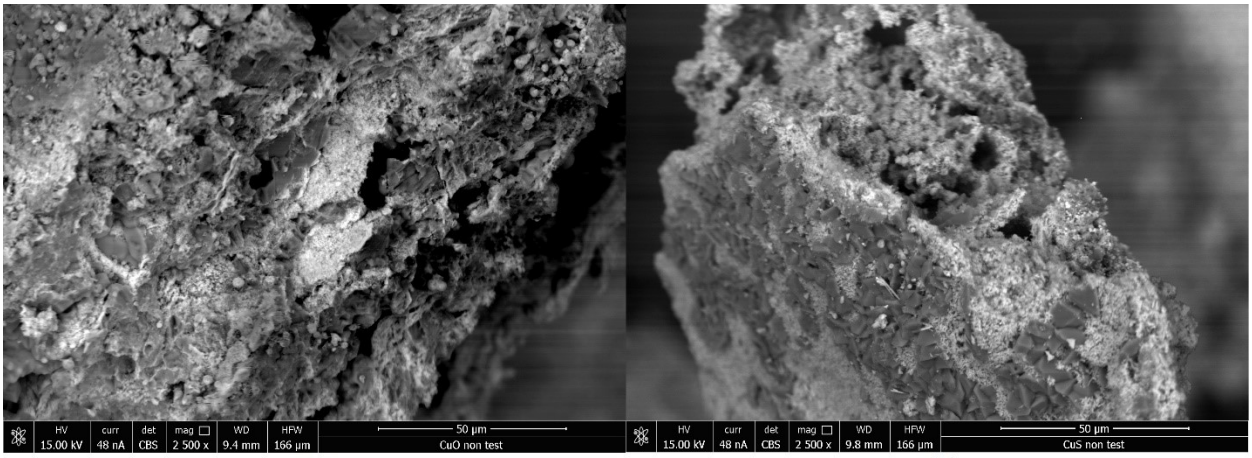

(a) **(b)**

Figure 5.12. The field emission-scanning electron microscopy images of CuO (a) and CuS (b) at 2500 magnification

To avoid the incomplete rinsing process influence on the Hg(0) capture, I used different methodologies to prepare the CuS sorbent in the PTFE pipes. The methodologies A and B were presented in Chapter 5.3.2. The comparing experiment between methodologies A and B was conducted in a MPR set-up. The Hg(0) capture efficiency was shown in Fig. 5.13. In the initial stage, a pipe coated with CuS_Na_2S (methodology A) captured more Hg(0) than a pipe coated with CuS_H_2S (methodology B). CuS_H_2S coating pipe captured more Hg(0) from the simulated flue gas than CuS_Na_2S coating pipe after 20 minutes. Nonetheless, the Hg(0) capture efficiency in two-CuS-coated pipe configurations were similar. In the beginning, the Hg(0) capture efficiency of CuS_H_2S and CuS_Na_2S were comparable. During a continuous experiment, the Hg(0) capture efficiency from CuS_Na_2S-coated pipes gradually decreased. The Hg(0) absorption rate of two CuS_H_2S-coated pipes remained unchanged in a 30-minutes experiment. The CuS_Na_2S and CuS_H_2S capture results were comparable for this configuration. The results in the system with

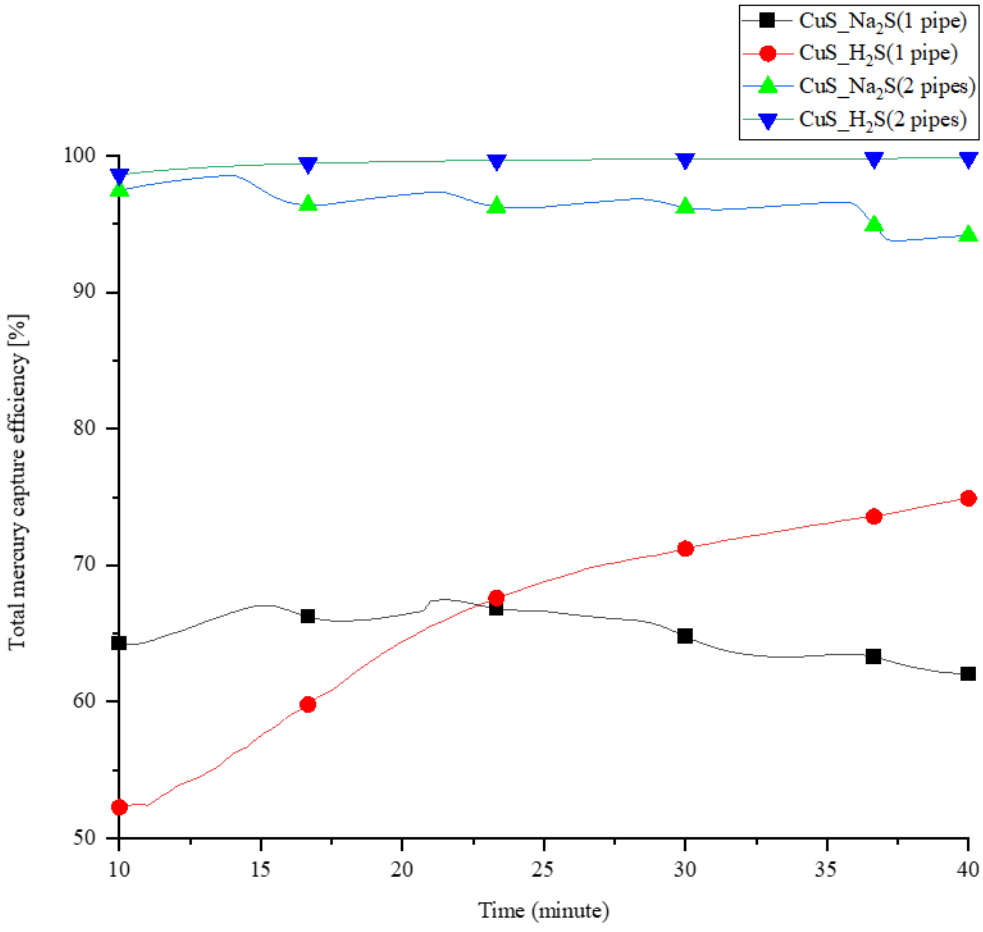

Figure 5.13. The total Hg(0) capture efficiency from CuS by using coating methodologies A (Na_2S) and B (H_2S)

one tube are less stable. This may be due to the fact that the production of layers is not entirely repeatable, and in the system with two tubes the amount of sorbent is sufficient to remove Hg(0) by almost 100%. The method B possibly produced a thinner CuS coating inside the pipe than the method A. A thick layer of coated sorbent may affect the velocity of sub-flows passing through PTFE pipes. In addition, small amounts of H_2S deposited and remained inside of PTFE pipes. H_2S has a higher Hg(0) affinity than Na_2S. It can easily react with Hg(0) in homogenous way.

The experimental results from the MTLCR set-up

In the following series of experiments, I used the carbon base sorbents (C-1, C-2 and C-3) to capture Hg(0) from the simulated flue gas. The selected reactors were the VFGR and MTLCR options. MTLCR was a tested reactor vs. the VFGR giving the controlling group of results. The temperature of thermostatic oven was set at 120°C and the flow rate was 108 dm^3/h. The mercury concentration in this series of experiments was 30.0 ± 6.2 μg/Nm^3.

During the experiments with carbon base sorbents in VFGR, 2 g of selected sorbent was placed in one glass vessel. Therefore, 4 g and 6 g of selected sorbents were equally placed on two or three glass vessels, respectively. According to the table 5.6, the Hg(0) capture capability of C-1, C-2 and C-3 was similar to each other. Hence, I chose the C-3 as an example to illustrate their Hg(0) capture abilities. In Fig. 5.14, 2 g, 4 g and 6 g of C-3 captured 31%, 42% and 53% of Hg(0) from the exhaust gas in the beginning, respectively. After 30 minute, the Hg(0) capture efficiency slightly dropped. Finally, the Hg(0) capture efficiency from 2 g, 4 g and 6 g of C-3 remained 27%, 37% and 50%, respectively. The data from C-3 was similar to C-1 and C-2, where 2 g of selected sorbent showed the lowest Hg(0) capture efficiency and 6 g the highest Hg(0). The total mercury capture efficiency in the same VFGR experiment was calculated by Equation (41). C-3 had 30, 36.5 and 49.2% Hg(0) capture efficiency on average, respectively. These results were the best Hg(0) capture efficiencies in these three carbon base sorbents. The C-3 had the smallest Hg(0) capture capability if compared with C-1, C-2. It meant that C-3 still had more unused pores and active sites for mercury capture. The C-3 had a highest Hg(0) mass capture rate, which was 19.08 μg/min, in these three carbon base sorbent.

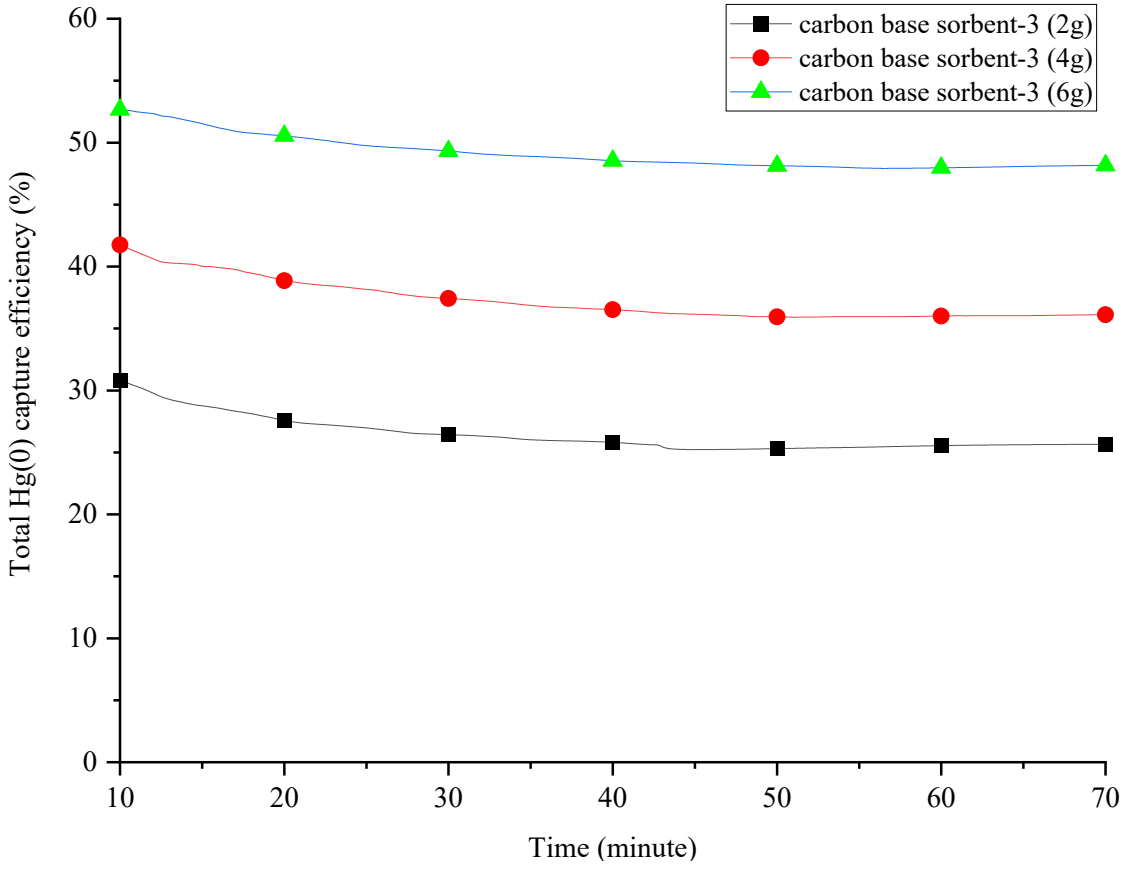

Figure 5.14. Online total Hg(0) capture efficiency by the carbon base sorbent-3 in VFGR

Table 5.6 The Hg(0) capture efficiency [%] of carbon base sorbents at different stages in VFGR and MTLCR

Sorbent	Reactor	Mass of sorbent [g]	Hot air + Hg(0) (1)	Simulated gas +Hg(0)	Hot air + Hg(0) (2)	Mean Hg(0) capture efficiency	Mass of Hg(0) capture capability [µg/g]	Hg(0) mass capture rate [µg/min]
C-1	VFGR	2	26%	18%	15%	18.2%	375	7.89
		4	37.7%	28.8%	35.5%	34.1%	859	31.24
		6	48%	44.6%	36.9%	43.7%	584	38.5
	MTLCR	2	38.9%	32.5%	40.7%	36.7%	1803	48.73

		4	70.4%	68.7%	70.8%	69.7%	982	53.10
C-2	VFGR	2	39.7%	20.2%	8.7%	22.4%	972	20.68
		4	28.2%	35.7%	21.5%	29.9%	733	25.5
		6	21.2%	29.2%	22.9%	22.6%	283	18.84
	MTLCR	2	31%	35.8%	38%	35.7%	1234	33.81
		4	63.4%	66.5%	63.8%	65.1%	907	49.01
C-3	VFGR	2	31.3%	26%	23.9%	30%	400	19.08
		4	38.3%	35%	34.2%	36.5%	80	7.13
		6	52%	47.5%	46.8%	49.2%	136	15.34
	MTLCR	2	23.9%	23%	27%	24%	765	21.85
		4	58.5%	57.3%	57.7%	57.7%	686	36.58

The Hg(0) capture efficiency was increasing along each additional 2 g VFGR glass with C-1, C-2 and C-3 except C-2 (6 g) case. However, the Hg(0) capture efficiency from the 6 g of C-1, C-2 and C-3 was always less than 50% (max. 49.2% in case of C-3). In case of C-1, the difference between 2 g (18,2%) and 6 g (43,7%) was 240%, and 164% for C-3. 6 g of selected sorbents could not obtain 3 times Hg(0) capture efficiency than the 2 g of these sorbents. Therefore, I selected 2 g of C-1, C-2 and C-3 and placed these three sorbents into three glass vessels to perform the experiment in the same condition as previously. Fig. 5.15 showed that the online Hg(0) capture efficiency was less 30% in the beginning. Although the online Hg(0) capture efficiency remained stable, it was continuously decreasing with experiment conducted time. The total Hg(0) penetrating rate was continuously increasing and finally was close to 80%. Data in Fig. 5.15 reveal that the three different carbon base sorbents could not promote the Hg(0) capture efficiency. The Hg(0) capture efficiency of 2 g of C-1, C-2 and C-3 was less than 6 g of single carbon base sorbent.

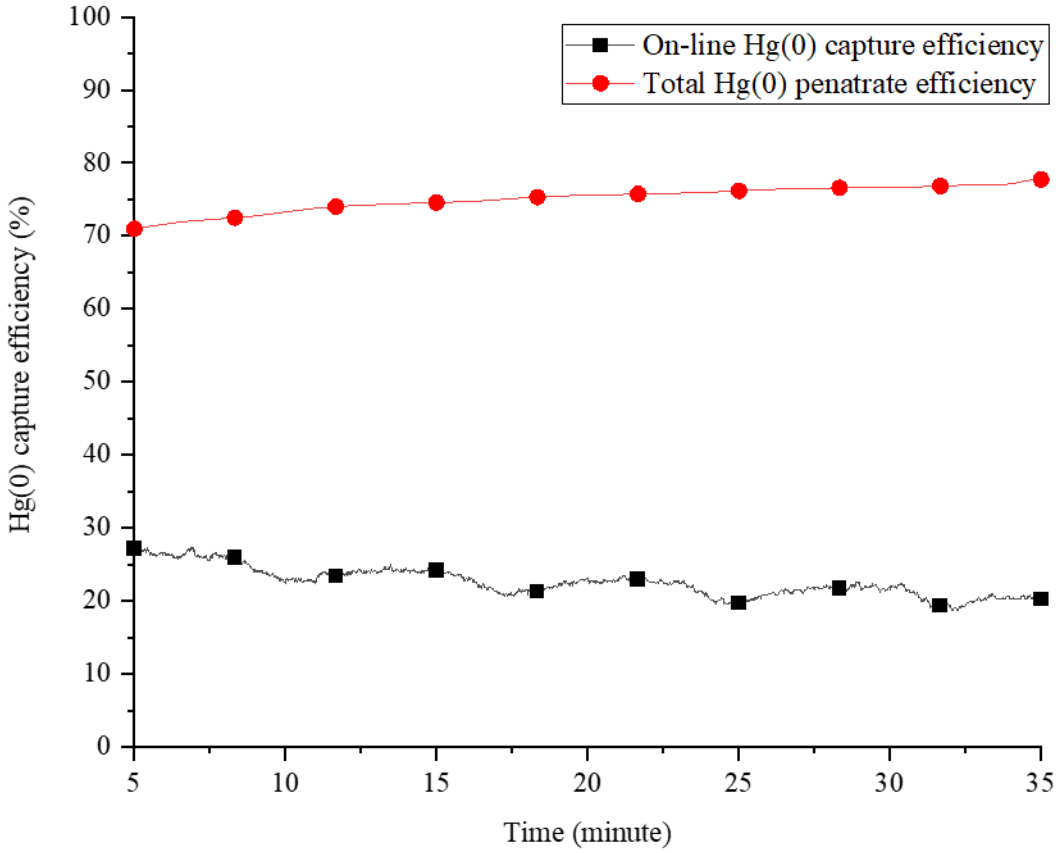

Figure 5.15. On-line total Hg(0) capture efficiency and Hg(0) penetration rate by the 2 g of carbon base sorbent-1, sorbent-2 and sorbent-3

In the next step, effectiveness of carbon base sorbents was determined in a MTLCR set-up by using the same amounts of sorbents than in the VFGR. 2 g of C-1, C-2 and C-3 had the total Hg(0) capture efficiencies 37, 36 and 24%, respectively. These results were higher than the results of 2 g sorbent samples in a VFGR set-up (expect the C-3). 4 g of carbon base sorbents had the total Hg(0) capture efficiencies from 57 to 70%, which was higher than for 6 g of the sorbents in a VFGR set-up. Fig. 5.16, illustrates the time required to capture a given mass of Hg(0) by different quantities of C-1 in MTLCR and VFGR set-ups. 4 g and 6 g of C-1 took 52 and 37 minutes to capture 1000 µg of Hg(0) in VFGR set-up, respectively. In the MTLCR, 2 g of C-1 was placed in one sorbent bed. And 4 g of C-1 was placed in two sorbent beds, each sorbent contained 2 g of C-1. The 2 g and 4 g of C-1 captured 1000 µg of Hg(0) in 42 and 35 minutes, and 2000 µg of Hg(0),

was captured in 52 and 57 minutes, respectively. In the three-glass system (6 g) of the VFGR, 2000 µg of Hg(0) was removed from flue gas in 55 minutes. Hence, both MTLCR configurations and VFGR with 6 g, showed the best and comparable Hg(0) removal efficiency. The similar situation occurred for materials C-2 and C-3. MTLCR promoted the Hg(0) capture capability (table 5.6). 2 g of sorbents C-1 and C-3 captured from 900 to 1800 µg/g and C-3 around 700-750 µg/g. These results were about two times higher than mean values in the VFGR set-up. Crucial to explain that data is contact time in both reactors and conditions of contact between the simulated flue gas and the sorbent in both systems. The long contact time in MTLCR is based on its unique conjugation. It provides a large sorbent bed and a large space for simulated gas passthrough its structure.

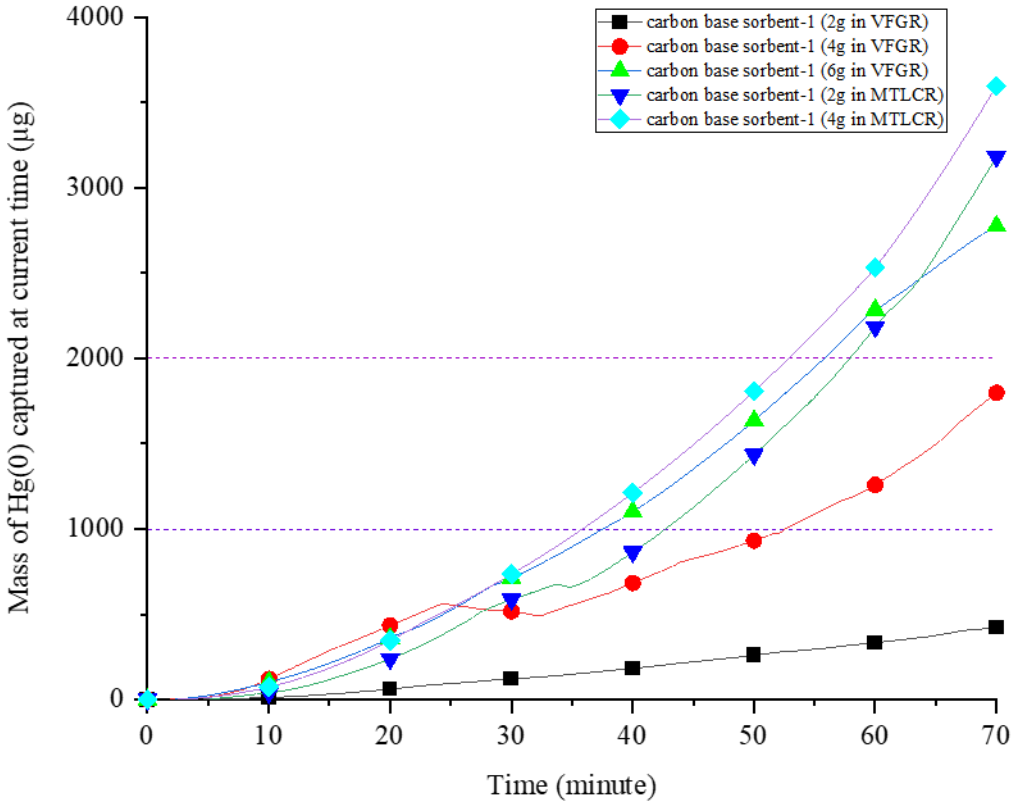

Figure 5.16. Total mass of Hg(0) captured by the C-1 sorbent in VFGR and MTLCR configurations vs. time

Again, the multiple layers of selected sorbents could not reach twice of Hg(0) capture efficiency of a single layer (table 5.6). The mass of Hg(0) capture capability was lower in a second sorbent bed configuration (4 g) in both VFGR and MTLCR set-ups (except one case). These observations were proofed by the total mercury analysis results in sorbents (table 5.7). When Hg(0) penetrated two layers of each sorbent, the concentration of Hg(0) in the second one was always much lower. When the selected sorbent has the noticeable Hg(0) mass capture capability, the similar Hg(0) capture efficiency as in the previous layer of sorbent, would not be obtained. In general, but not always in that series of experiments, the capture efficiency for each subsequent layer becomes lower.

Table 5.7 Mean values of total mercury concentrations in carbon base sorbents in VFGR

	Hgtot [ppb]	SD [ppb]	CV [%]
C-1 raw	421.17	78.45	18.63
C-2 raw	298.62	75.06	25.14
C-3 raw	356.41	108.94	30.5
C-1 - two cell test (1st cell) (2g)	1284.03	82.23	6.40
C-1 - two cell test (2nd cell) (2g)	674.76	62.75	9.30
C-2 - two cell test (1st cell) (2g)	945.00	106.47	11.27
C-2 - two cell test (2nd cell) (2g)	669.19	54.76	8.18
C-3 - two cell test (1st cell) (2g)	1173.21	71.65	6.11
C-3 - two cell test (2nd cell) (2g)	601.77	96.02	15.96
C-1 - three cell test (1st cell) (2g)	1162.77	99.34	8.54
C-1 - three cell test (2nd cell) (2g)	758.25	54.71	7.21
C-1 - three cell test (3rd cell) (2g)	785.25	3.90	0.50
C-2 - three cell test (1st cell) (2g)	1109.57	17.63	1.59
C-2 - three cell test (2nd cell) (2g)	519.80	85.08	16.37
C-2 - three cell test (3rd cell) (2g)	895.34	64.77	7.23
C-3 - three cell test (1st cell) (2g)	812.81	79.94	9.83
C-3 - three cell test (2nd cell) (2g)	506.76	117.65	23.22
C-3 - three cell test (3rd cell) (2g)	620.81	133.04	21.43

In a three-layer VFGR set-up the concentration of Hg(0) in a first and second layer of sorbents was similar to the two-layer VFGR configuration. The third layer of sorbent contained similar or even higher quantities of Hg(0) than the second layer (table 5.7). It might be caused by the partial Hg(0) release from the sorbent surface during the experiment. The released Hg(0) would compete with the uncaptured Hg(0) in simulated gas to deposit in the next, third layer of sorbent. This capture/release process can be proofed by the Hg(0) concentration curves in Fig. 5.17. When the Hg(0)/N_2 mixture gas was removed from the system, Hg(0) concentration in both reference and sorbent lines decreased rapidly to 10 µg/Nm^3. But it was slightly higher in the sorbent line. The Hg(0) was continuously released from the sorbents and elevated concentration peaks are observed during small increases in temperature inside the thermostat.

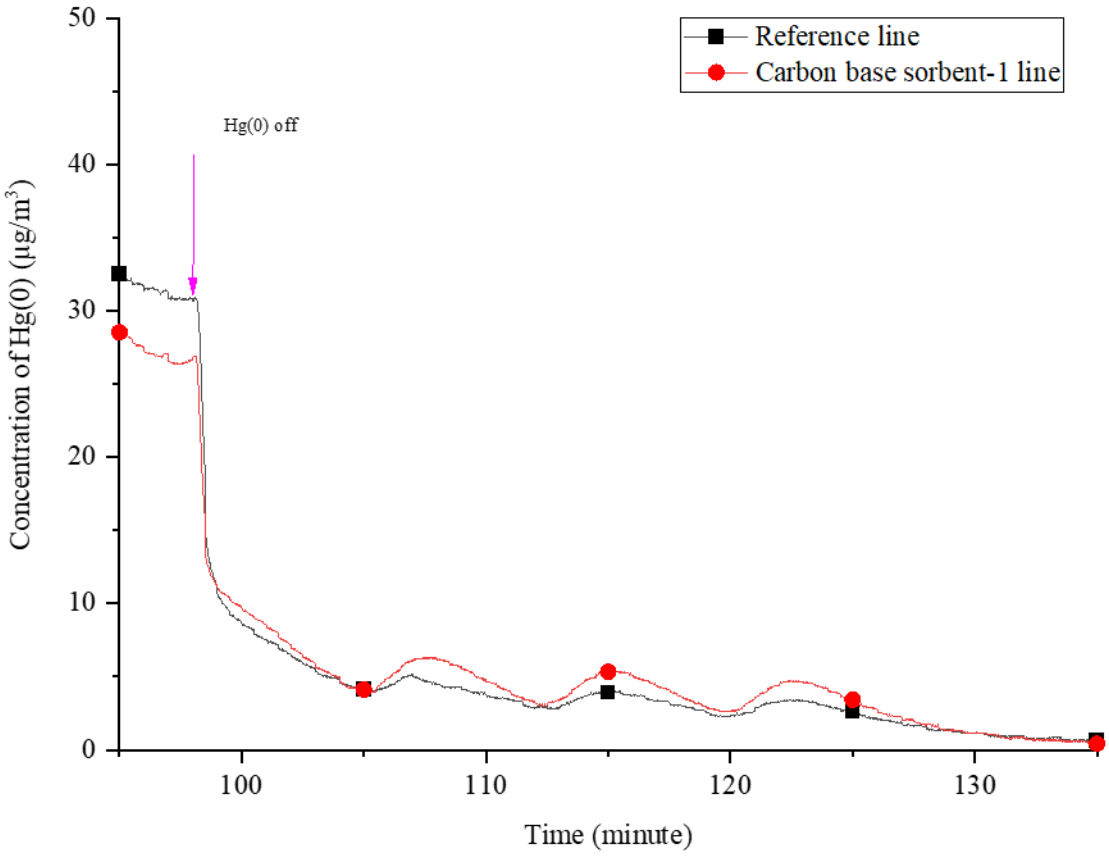

Figure 5.17. Hg(0) concentration measured on-line in reference and sorbent lines (C-1 sorbent in Hg(0) off stage)

5.3.4. Sulfur species influence on mercury capture

The sulfur species influence on Hg(0) capture in the simulated flue gas is already proofed by many researchers and their articles (Chen et al., 2014; Y. Xie et al., 2015; Z. He et al., 2020). During my research works, the only sources of sulfur species were from simulated flue gas and additional H_2S source. The simulated flue gas was generated from the laboratory-scale boiler. The main sulfur species in simulated flue gas was SO_2 – see Chapter 4.3. Small amounts of SO_3, H_2SO_3 and H_2SO_4 are also expected. The concentration of SO_2 in a simulated gas depends on the fuel and its flux. SO_3 is oxidized in some extent by the excess amount of O_2 in simulated flue gas, but SO_3 in flue gas is normally less than 5% of total amount of SO_2. Depending on the sorbent characteristics SO_2 may or may not compete with mercury for the sorbent active sites, decreasing or not the effectiveness of Hg(0) capture (table 5.11). SO_2 also may react with the sorbents surface structure components (metal oxides, such as CuO or Al_2O_3, have proven to be the best sorbents for SO_2 and Hg(0) capture (G. Li et al., 2015; Z. He et al., 2020)). SO_2 reacts with the surface oxygen of copper-based sorbents to form thermally stable copper sulfates (Y. Xie et al., 2015; Z. He et al., 2020), which inhibits Hg(0) removal efficiency. The assumed chemical reaction between SO_2 and sacrificial CuO is described by Equation (48)

$$CuO + SO_2 + 1/2O_2 \rightarrow CuSO_4 \quad (48)$$

Table 5.11 The effectiveness of Hg(0) capture [%] of specified sorbents in different experimental set-ups (VFGR and MPR) and at different stages

Sorbent	Hot air + Hg(0)	Simulated gas + Hg(0) + WFGD off	Simulated gas + Hg(0) + WFGD on
Carbon base sorbent-1	18	24	41
Carbon base sorbent-2	24	29	20
Carbon base sorbent-3	34	51	36
CuO (50 mg)	13.3	24.8	45.4
CuS (50 mg)	67.4	54.9	55.8

According to Zhou et al. (2015), SO_3 in the simulated flue gas has a favorable effect on mercury capture. Adsorbed SO_3 on the unburn carbon surface reacted with water vapor to produce H_2SO_4.

The adsorbed H_2SO_4 reacted with Hg^{2+} presented in the process gas to form $HgSO_4$. Yang et al. (2021) demonstrated the Hg(0) oxidation by SO_3 over the V_2O5/TiO_2 catalyst (the typical catalyst used in SCR systems). On the catalyst, both direct and indirect oxidation processes of Hg(0) were observed. In the direct method, SO_3 is converted to SO_4^{2-} before reacting with mercury to form $HgSO_4$. In the indirect process, oxygen is converting Hg(0) to HgO, which then reacted with SO_3 to form $HgSO_4$. These mechanisms may explain the Hg(0) capture efficiency increase, when the WFGD system was turned on (table 5.11). The small amount of SO_3 deposited on the sorbent surface and it influenced the activation site of sorbent.

The sulfur substances do not only influence the Hg(0) capture mechanism of sorbents, but they also influence the concentration of Hg(0) in flue gases. The table 5.12 shows the result how SO_2 and H_2S influence the concentration of Hg(0) in simulated flue gas. During those tests, the simulated flue gas generally did not contain the H_2S, so the H_2S was added, when it was needed. Since the WFGD system is capable to capture the soluble mercury forms from the simulated gas, the concentration of Hg(0) in the stream may decrease. It was proofed by Liu et al., 2019 and Li & Wang, 2021 who measured the results from the CFPPs. The WFGD slight influenced on Hg(0). Because the dissolved Hg^{2+} and Hg(0) in simulated flue gas generate Hg_2^{2+} on the surface of the limestone slurry layer which caused the Hg(0) decreased (Deng & Macherzynski, 2023). But when H_2S was added into simulated flue gas, the Hg(0) concentration was decreased rapidly (table 5.12).

Table 5.12 The mean Hg(0) concentrations [$\mu g/Nm^3$] at different experimental stages and impact of loaded H_2S (the VFGR reactor)

Test	Hot air + Hg(0)	Simulated gas + Hg(0) + no H_2S + WFGD off	Simulated gas + Hg(0) + no H_2S + WFGD on	Simulated gas + Hg(0) + H_2S + WFGD off	Simulated gas + Hg(0) + H_2S + WFGD on
1st	83.8	66.6	58.4	61.0	56.0
2nd	89.4	84.2	75.4	68.9	50.4
3rd	77.4	73.0	70.2	58.3	51.5
4th	87.3	92.8	88.1	69.2	60.4

So, H_2S gas does not only affect the concentration of Hg(0), but it also can influence the Hg(0) capture efficiency. For instance H_2S molecules influence the Hg(0) oxidation through the Langmuir–Hinshelwood or Eley–Rideal mechanisms. The lattice oxygen is the key to oxidize the

H_2S to form the sulfur radical onto the sorbent surface. When the Hg(0) deposits onto the sorbent, it reacts with the sulfides and forms mercury sulfides. The oxidation of Hg(0) via Langmuir–Hinshelwood mechanism is described by the following postulated Equations (49) to (52) (Z. Wang et al., 2018; Xing et al., 2022; Deng & Macherzynski, 2023):

$$H_2S_{(g)} \rightarrow H_2S_{(ads)} \quad (49)$$

$$H_2S_{(ads)} + O_\alpha \rightarrow S^{\cdot}_{(ads)} + H_2O \quad (50)$$

$$Hg(0)_{(g)} \rightarrow Hg_{(ads)} \quad (51)$$

$$S^{\cdot}_{(ads)} + Hg_{(ads)} \rightarrow HgS_{(ads)} \quad (52)$$

In case, when Hg(0) does not adsorb directly onto the sorbent to form the HgS, the Eley–Rideal mechanism may take place, as it is described by Equations (53) to (55) (Xue et al., 2015; X. Wu et al., 2021; Xing et al., 2022; An et al., 2023):

$$H_2S_{(g)} \rightarrow H_2S_{(ads)} \quad (53)$$

$$H_2S_{(ads)} + O_\alpha \rightarrow S^{\cdot}_{(ads)} + H_2O \quad (54)$$

$$S^{\cdot}_{(ads)} + Hg(0)_{(g)} \rightarrow HgS_{(ads)} \quad (55)$$

The influence of H_2S on Hg removal on sorbents in simulated gas, was studied and proofed by Wang et al. (2018), Wu et al. (2021) and Xing et al. (2022). Wang et al. (2018) report that H_2S enhanced the efficiency of Hg(0) removal over the MnO_2 sorbent. The effectiveness of Hg(0) capture increased from 82.3% to 90.5%, when temperature of the 400 ppm H_2S/N_2 mixture was increased from 80℃ to 160℃. On the other hand, the Hg(0) removal efficiency fall from 90% to 70% as the simulated gas temperature was furthermore increased from 160℃ to 200℃. This result was greater than the experiment conducted under pure N_2 conditions (maximum Hg(0) removal efficiency was 70% at 160℃). Wang et al. (2018) also reported that the Hg(0) removal efficiency increased from 85.9% to 96.9%, while the H_2S concentration in the simulated gas rose from 200 ppm to 800 ppm. Wu et al. (2021) and Xing et al. (2022) found that Fe_2O_3 or Fe_2O_3/TiO_2 mixture sorbents had a 95% of Hg(0) capture efficiency at temperatures between 100°C and 150°C, when H_2S was present in the simulated gas. This temperature range was also optimal for later H_2S removal with a Fe_2O_3/AC sorbent. H_2S served as the active site on the Fe_2O_3/AC sorbent, which

captured H_2S from the simulated gas. Then, it reacts with Hg(0) present in the simulated gas (J. Wang et al., 2022). Xing et al. (2022) found that other than H_2S gas components in the simulated gas, such as CO, H_2, and H_2O, inhibited the Hg(0) removal efficiency of Fe_2O_3/TiO_2 mixture sorbents at 150°C. However, the capture degree was still over 80% of Hg(0) (Xing et al., 2022).

H_2S is a pollutant gas present in flue gas (small amount) and coal-derived or biomass-derived syngas (high amount). But it may be a good reactant to capture Hg(0) from flue gas. Some research teams already studied H_2S and designed metal oxides or sulfides or carbon based metal oxide materials to remove Hg(0) and H_2S from process gas. And other teams studied surface reducing bacteria and tried to apply it in industries for producing H_2S. The produced H_2S reacts with Hg(0) to form HgS. These interesting works are also described details by Deng and Macherznski (2023). Those research team provide a new solution for Hg(0) capture technique in flue gas or syngas.

6. Expected applied fields of newly designed reactors

Construction of exemplary and research on the MPRs and MTLCRs fulfilled the goal of my studies. These two reactors, both promoted the Hg(0) capture efficiency by comparing the VFGR, when using the same mass of the same sorbent.

The MPR has a small dimension and a changeable, multiple pipe construction. The developed, extended version would be suitable to connect with the pipeline in the household before the stack or connect with household stove (Dziok et al., 2020; Jaworek et al., 2021). The empty hole inside the cylinder head can be use as the chamber to remove fly ash. The whole idea would be utilized to Hg(0) and PM emission controls in households in the village. This problem is presented in Chapters 1.3 and 1.4. There is no good solution to solve Hg(0) emission from scattered sources, especially in the developing countries. Also the sophisticated devices for PM removal which can be applied in the small-scale boilers are not affordable to this populations.

There is other application, where MPRs would be used to treat poison vapors: making of models and statues, such as characters from TV dramas, movies, games etc., and its painting. It is very popular in recent years. Some people chose the models and status making as a special hobby or profession. As well as some workshops also run the business to make profiles. However, the special paints are used to color models and statues, which contain toxic substances. Those toxic pollutants are usually vented out off houses or workshops through small individually ventilation

equipment. These small ventilators do not consist a pollutant treatment function. Installing pollution treatment equipment requires additional cost. Most of models and status makers consider that cost is an unnecessary and expensive price. Untreated toxic substances are released into the air and fall into the water or soil with rainfall, causing secondary pollution. And this is often overlooked. The MPR is made from the relatively cheap material—PTFE, which is easy to be cleaned and reused. Therefore, the price would be affordable by comparing with specialistic pollutant treatment equipment. The MPR installation is space-friendly. It can be installed at inlet or outlet of ventilator in a compact location. So, it is suitable for the model and statue makers who work at small room. After long time using, the coated PTFE pipes can be collected and recycled by the company which synthesized the sorbent inside the PTFE pipes or sale the MPRs.

The MTLCR is suitable for the small-scale institutions or industries which require the energy or especially heat from combustion of fossil fuels, and the sorbent system to capture pollutants from the flue gas. The MTLCRs may meet the requirement to capture the large amounts of Hg(0) from flue gas with the lower cost by comparing with other reactors. The PTFE material is easy to clean and maintenance. The MTLCR construction is changeable. Customers can design their own MTLCR construction based on their requirements. The MTLCR has the large number of possible sorbent beds, which offer the large contact area between any sorbent and mercury vapors. When the sorbent is spread onto the sorbent bed, even the its small amounts can obtain the large contact area. The large empty space between upside and downside sorbent beds reduces the velocity of flow and increases the contact time. Finally, the MTLCR promotes the Hg(0) capture efficiency of sorbent even the sorbent has the low Hg(0) capture efficiency. In Chapter 5.3.3, I presented that multiple layers of same sorbents or materials could not reach high Hg(0) capture efficiencies. A single MTLCR module offers up to eight sorbent beds within its construction, which may be filled with different kinds of sorbents or materials to archive much better Hg(0) capture efficiencies. The use of different sorbents combine together in one reactor, can significantly remove different kinds of pollutants from exhaust gas. The materials which would be applied in MTLCRs are any polymer sorbent catalysts like GORE™ (Ryfa et al., 2023), composite sorbents (Gorecki et al., 2022) or even liquefied materials. The MTLCR can be built from many modules to form an expanded absorber. It is possible to use up to 40 beds within one absorber (block) made of five modules). The expanded MTLCR may also offer more space for materials. According to the Equations (27) to (35), the velocity of gas inside the expanded MTLCR module may be regulated to control a

contact time. Several expanded MTLCR modules build a large-scale absorber. It can work for long time without exchanging materials. It reduces the maintenance time and costs. The concept of MTLCR modules could be changed when applied sorption materials are changed. For instance, I can increase the isolating plate width to enhance the contact time between materials in beds and gas, when the weak adsorption ability sorbent is applied (e.g. waste ash). Otherwise, I can use the highly reactive materials such as CuO or CuS, when there is only limited place for basic module of MTLCR.

At the current stage, I just proofed the idea that MPRs and MTLCRs could promote Hg(0) capture effectiveness from flue gas in the laboratory conditions. There are many issues have to be solved for a final version or product in further steps. For instance, I only tested the MPR which was made from PTFE. It is hard to predict the sorbent coating procedure along big PTFE pipes. The sorbent might have a tendency to peel off the internal surface of pipes. So, the process of seasoning the sorbents requires also some technical changes, because the removal of moisture from PFTE surface in laboratory conditions is time consuming. There are some other materials that may be also suitable to construct MPRs, such as titanium, stainless steel or alloy steel. Titanium is light and chemically resistant metal, not creating mercury amalgams, but is expensive. The electroplating process could be utilized to coat copper onto internal surface of metal tubes, followed by oxidation of copper. The size and number of tubes in MPRs shall be also consider in further steps. The size (diameter and length) affect a flow rate, gas velocity and contact area (Equations (17) to (19)) inside a single tube. If the MPR consist of 50 tubes, it will have a small flow rate, small gas velocity and large contact area, which promote better sorption efficiencies. But too many tubes in one MPR may be considered as waste of resources and it also requires a large space for installation. Some part of tubes may be not used during the gas ventilation process. And this possible design is hard to maintain and to exchange the coated tubes. Installation of MPRs at home or workshop shall be simple and easy as replacement of lamps. If installation or maintenance is too complex to the customer, it means that it requires additional service fee. The prototype of MPRs still need to be improved in context of its construction and coating efficiency.

The MTLCR can be also made from other materials like stainless steel or titanium. The stainless steel made MTLCR could transfer and maintain the heat more easily than the PTFE made MTLCR. Our PTFE MTLCRs required a long heating time before they reached the right temperature. Additionally, metal made MTLCRs could be produced via molds or lathe stamping techniques.

Theses processes can make the MTLCR module like multiple compartment dinner tray. This shape of module reduces weight and volume of MTLCRs. By contrast, the full construction of the PTFE made MTLCR is too heavy which is around 15 kg. It is hard to get the PTFE made MTLCR shape like dinner tray, because it requires additional processes to complete. PTFE has to be also considered as a material with a high coefficient of thermal expansion. When the PTFE material is under temperature over 120-150℃, the structure of PTFE may expand or change its shape. So, in addition, I used two layers of own-constructed metal clamps – Fig. 5.5, supporting the whole construction. That was the another reason causing the increased weight of whole module and reducing the heat transfer.

The MPRs and MTLCRs still require further structural and material development to become an applicable product. The idea is not only to utilize them in small-scale boilers or household exhausts treatment set-ups. They also can be applied at domestic or small institutions to treat other vapors form of heavy metals or volatile pollutants in exhaust gases. The size of MPRs and MTLCRs would be enlarged to fulfill this purpose. Therefore, the construction of MPRs and MTLCRs and materials used in each application shall be taken into consideration, when the installation placement is a crucial factor. Different kinds of structure and construction of modules may change the weight and cost of final version of MPRs and MTLCRs and the size of modules is usually connected with location of an installation.

7. Summary

The mercury pollution has attracted the society attention since the Minamata disaster in Japan. It could be tracked from the early twenty century, when the pollution was released from Noguchi's Chisso Company using Haber-Bosch process to make fertilizer. Mercury was a byproduct of this production and untreated was dumped into Minamata Bay (Kathryn Karasek, 2013). Till the mid-twenty century, over 3000 victims suffering from degeneration of the nervous system, have been recognized. It was called the Minamata disease which is caused by the toxic organomercury pollutants. After several decades, there were over 5000 victims around the world suffering the mercury caused neurological disease (Hamid, 2008).

According to the International Energy Agency, high-polluting energy sources derived from fossil fuels will be phased out by 2050, and clean energy and zero-emission sources will dominate the

energy supply. Before the date, the whole society still has a lot of efforts on removing Hg(0) from the different kinds of sources. Even though, 2050 is coming, the secondary pollution Hg(0) capture from the ocean or ground will be still tough issue to be solved. Therefore, study mercury and its species forms, its influence on ecosystems and its toxicity, are still an important work to be done in a field of human health and environmental protection.

7.1. Fossil fuel usages in China

Total coal consumption reached 404860 [10 Gg of SCE] in 2003, while total energy consumption increased from 197083 to 498314 [10 Gg of SCE] between 2003 and 2020. Mercury emissions have also increased by 70% within these 15 years. The Environment Protection Ministry of China has implemented regulations to limit emissions, but coal-dominated energy consumption remains a challenge. Although carbon emission peak and neutrality policies are expected to reduce role of coal in Chinese energy consumption structure, the coal domination will remain for a long period.

7.2. Mercury capture, its techniques and principles

Mercury capture techniques are available for industrial and domestic implementations, including fuel preparation, blending, physical or chemical treatment, and froth flotation. These techniques aim to reduce mercury content from fuel sources before fuel utilization, ensuring low cost and low pollutants emissions. However, these methods may cause water contamination after the fuel preparation process, making it difficult to remove organic bounded mercury.

Some conventional devices, such as APCDs, can reduce pollutants from exhaust gas, such as NOx, SO_2, and particulate matter. They are beneficial to mercury removal, but they can only reduce mercury concentration in flue gas to some extent. In conventional CFPPs, APCDs are implemented along the exhaust gas stream line, depending on fuel utilization and electricity generation capacity.

The dedicated treatment processes are also implemented to reduce mercury from wastewater or exhaust gases. These processes include ion exchange, membrane separation, activated sorbents, new material sorbents (MOFs, SPCs) as well as biotechnique treatment.

The principles of mercury capture are divided into physisorption and chemisorption. The chemisorption has four unique mechanisms, which could be used to explain the mercury capture

by selected sorbents and catalysts. The details of these four mechanisms were presented in Chapter 2.2.

7.3. The sulfur species influence on Hg(0) capture

The impact of sulfur species on the capture of Hg(0) in simulated flue gas has been extensively studied by researchers. SO_2 can compete with mercury to the sorbent active sites, decreasing the effectiveness of Hg(0) capture. It reacts with the surface structure of sorbents to inhibit Hg(0) removal efficiency (G. Li et al., 2015; Z. He et al., 2020). The influence of H_2S on Hg(0) removal on the metal oxides and metal oxide impregnated AC sorbents in simulated gas has been studied and proven by Wang et al. (2018), Z. Wang et al. (2018), X. Wu et al. (2021), and Xing et al. (2022). I have studied the sulfur species influence on Hg(0) capture and emission because the coal gasification processes are still important in the energy generation, and would dominate in the near future. Hg(0) and H_2S are the main pollutants in a syngas coming from coal gasification processes. Therefore, the development of methodologies or techniques for Hg(0) and H_2S removal from syngas is still advantageous and beneficial. The biotechnique or biotreatment is also popular in recent decades. Some research teams already studied using sulfate reduce bacteria to generate H_2S to reduce concentration of Hg(0) in gas systems. These advanced methodologies were described in Chapter 2.1.5 and in some details in (Deng & Macherzynski, 2023).

7.4. Mercury capture efficiency analyzing systems

The examples of mercury capture analyzing systems are described in details by (Macherzynski, 2018; Gorecki et al., 2022). On that basis I developed my own mercury capture efficiency analysis system. The system has some extensions, because I did not only measure mercury capture by selected sorbents, but also could determine the flue gas components such as CO_2, NO, SO_2, which giving the opportunity to measure differences in gas concentrations on both sides of absorbers (table 7.1). I also could determine the sulfur species influence on Hg(0) capture. The redesigned system can measure seven different gases: SO_2, NO, NO_2, O_2, CO, CO_2, H_2S, at four different points.

Table 7.1. Mean value of acidic gases after reference and sorbent reactor at WFGD on/off conditions				
Measurement position	WFGD conditions	SO_2 (mg/m^3)	NOx (mg/m^3)	CO_2 (%)
Reference reactor	off	1213	856	11.75
Sorbent reactor	off	1168	878	11.39
Reference reactor	on	15	968	9.47
Sorbent reactor	on	0	966	8.93

The system is primarily able to compare the removal of elemental mercury by different sorbents under the same conditions. Secondary it is helpful for simulations of the Hg(0) capture in different conditions which may occur in the power plants. A total flow rate of process gas can be regulated in an ideal range of 12—240 dm^3/h to obtain optimal air-fuel ratio—λ results, which is as close as possible to the flue gas in power plants. A flow rate is also inherently related to the contact time of tested sorbents with the process gas. These optimal λ results can be controlled by regulating the fuel loading, flow rate and fuel combustion temperature. A laboratory-scale WFGD system significantly reduces the concentration of SO_2 in simulated gas without meaningful removal of H_2S (table 7.2). O_2—SO_2—H_2S equilibrium can be regulated then. In this case, the SO_2 and H_2S influence on Hg(0) capture efficiency can be determined at different combinations of these two gases.

Table 7.2. Mean value of SO_2 and H_2S gases at WFGD on/off conditions		
WFGD conditions	SO_2 (mg/m^3)	H_2S (mg/m^3)
on	23	235
off	1175	292

Chapters 4.3 and 4.4 present additional results on key factors that were controlled during the experiment, such as the composition of the process gas and the concentration of Hg(0) in the limestone slurry. The stability of simulated flue gas composition - with or without Hg(0)/N_2 mixture – was carefully monitored in the redesigned set-up. The redesigned Hg(0) analysis system

produced the reliable and reproducible results regarding the Hg(0) capture efficiencies of various sorbents, and in different reactors.

7.5. Different kinds of absorbers applied

The experiments in my study were conducted with three kinds of reactors: the vertical flow gas reactor (VFGR), the self-designed multiple pipe reactor (MPR) and the self-designed multiple thin layer cubic reactor (MTLCR).

The VFGR is a typical fixed-bed type reactor to perform reliable sorbent quality tests. It was hard to improve the Hg(0) capture efficiency of some sorbents during experiments without increasing their mass in this reactor. Due to a short contact time and limited mixing of a process gas with sorbents inside the VFGR set-up, even increased mass of sorbents do not cause higher Hg(0) capture efficiencies (table 5.6). It may cause waste of sorbents without expected results.

The MPR and MTLCR set-ups have higher Hg(0) capture efficiencies than VFGR configuration, when using the same mass and sorbents (MPR vs. VFGR with CuO, CuS and MTLCR vs. VFGR with C-1, C-2, C-3). These two reactors provided longer contact time and larger contact area than the VFGR. According to the Equations (12) to (15), (17) to (20), (35) and (37), the contact time, contact area and the velocity of gases in each set-up were calculated and shown in table 7.3.

In the MPR set-up, the flow of simulated flue gas could be divided into maximum five sub-flows. The velocity of simulated flue gas in the 3-pipe MPR set-up (0.239 m/s) was much higher than in the VFGR set-up (0.028 m/s). However, the long coating section assured the Hg(0) capture efficiency increase even at high velocity. For the same amounts of Hg(0) passing through, the 3-pipe set-up provides three times bigger coating area and much longer contact time, which presumably promotes better oxidation of Hg(0). The sorbent cell area in VFGR was 5.31 cm^2 opposite to 13.19 cm^2 (3-CuO-coated pipes) as well as 18.84 cm^2 (3-CuS-coated pipes) in MPRs. The contact time in VFGR was 0.035 s opposite to 0.44 s (3-CuS-coated pipes) and 0.63 s (3-CuS-coated pipes) in MPRs.

In the MTLCR set-up, not only the contact area was much higher, but also the velocity of the gas passing along any sorbent bed was reduced to 0.018 m/s. In case of 2 g of any carbon base material inside the MTLCR set-up, there is one 28.27 cm^2 sorbent bed, and its contact time is 3.4 s. It is

quite opposite to data from the VFGR filled even with 6 g of any carbon base sorbent, which is characterized by smaller (15.93 cm^2) contact area, and shorter contact time of 1.17 s. In the two-sorbent bed MTLCR set-up (4g), the contact area doubles (56.54 cm^2) and contact time is 6.8 s. The full version of my MTLCR can offer 40 sorbent beds for selected sorbents to treat a simulated flue gas which contains the high concentration of Hg(0).

Table 7.3. Hg(0) capture efficiency, contact time and contact area in different reactors and systems.

Reactor	Sorbent	Number of beds or pipes applied	Velocity of gas passing through sorbents [m/s]	Contact area [cm^2]	Contact time [s]
VFGR	CuO	1	0.028	5.31	0.035
	CuS	1		5.31	0.035
	Carbon base sorbent	1		5.31	0.389
		2		10.62	0.778
		3		15.93	1.168
MPR	CuO	1	1.19	4.39	0.03
		3	0.239	13.19	0.44
	CuS	1	1.19	6.28	0.04
		3	0.239	18.84	0.63
MTLCR	Carbon base sorbent	1	0.018	28.27	3.40
		2		56.54	6.80

Based on data from tables 5.4, 5.6 and 7.3, I conclude that the contact area, contact time and the velocity of Hg(0) passing through sorbents of similar properties inside absorbers of different kinds, are the main, key factors influencing the Hg(0) capture efficiency. Using VFGRs, MPRs and MTLCRs, the series of sorbents with similar physical and chemical properties can be successfully tested (compared) towards Hg(0) and when adapted, towards other volatile substances. The use of three different absorbers let me to improve the series of tests by changing these three factors in a wide range. Both MPR and MTLCR designs are potentially useful. Both self-designed sorption reactors may have potential applications in larger constructions used to remove pollutants from different gases and vapors.

Reference

Altaf, A. R., Adewuyi, Y. G., Teng, H., Gang, L., & Abid, F. (2022). Elemental mercury (Hg0) removal from coal syngas using magnetic tea-biochar: Experimental and theoretical insights. *Journal of Environmental Sciences*, *122*, 150–161. https://doi.org/10.1016/J.JES.2021.09.033

Aquino, L. F. M. C. de, Ribeiro, R. de O. R., Simoes, J. S., Mano, S. B., Mársico, E. T., & Conte Junior, C. A. (2017). Mercury content in whey protein and potential risk for human health. *Journal of Food Composition and Analysis*, *59*, 141–144. https://doi.org/10.1016/J.JFCA.2017.02.014

Asadi, S., Pakizeh, M., & Chenar, M. P. (2011). *An investigation of reaction furnace temperatures and sulfur recovery*. *5*(3), 362–371. https://doi.org/10.1007/s11705-011-1106-z

Baran, P., Wdowin, M., Czarna, D., Żmuda, R., Kunecki, P., & Panek, R. (2017). Synthetic zeolites as potential sorbents of mercury from wastewater occurring during wet FGD processes of flue gas. *Journal of Cleaner Production*, *172*, 2636–2645. https://doi.org/10.1016/j.jclepro.2017.11.147

Behjati, M., Baghdadi, M., & Karbassi, A. (2018). Removal of mercury from contaminated saline wasters using dithiocarbamate functionalized-magnetic nanocomposite. *Journal of Environmental Management*, *213*, 66–78. https://doi.org/10.1016/J.JENVMAN.2018.02.052

Benhammou, A., Yaacoubi, A., Nibou, L., & Tanouti, B. (2005). Adsorption of metal ions onto Moroccan stevensite: kinetic and isotherm studies. *Journal of Colloid and Interface Science*, *282*(2), 320–326. https://doi.org/10.1016/J.JCIS.2004.08.168

Bernhoft, R. A. (2012). Mercury toxicity and treatment: A review of the literature. *Journal of Environmental and Public Health*, *2012*. https://doi.org/10.1155/2012/460508

Bessbousse, H., Rhlalou, T., Verchère, J.-F., & Lebrun, L. (2010). Mercury removal from wastewater using a poly(vinylalcohol)/poly(vinylimidazole) complexing membrane. *Chemical Engineering Journal*, *164*, 37–48. https://doi.org/10.1016/j.cej.2010.08.004

Bilandžija, N., Zgorelec, Ž., Pezo, L., Grubor, M., Velaga, A. G., & Krička, T. (2022). Solid biofuels properties of Miscanthus X giganteus cultivated on contaminated soil after phytoremediation process. *Journal of the Energy Institute*, *101*, 131–139. https://doi.org/10.1016/J.JOEI.2022.01.007

Bošnjakovic, M., & Sinaga, N. (2020). The Perspective of Large-Scale Production of Algae Biodiesel. *Applied Science*. https://doi.org/10.3390/app10228181

Bucatariu, F., Teodosiu, C., Morosanu, I., Fighir, D., Ciobanu, R., Petrila, L. M., & Mihai, M. (2021). An overview on composite sorbents based on polyelectrolytes used in advanced wastewater treatment. *Polymers*, *13*(22), 1–25. https://doi.org/10.3390/polym13223963

Budihardjo, M. A., Wibowo, Y. G., Ramadan, B. S., Serunting, M. A., Yohana, E., & Syafrudin. (2021). Mercury removal using modified activated carbon of peat soil and coal in simulated landfill leachate. *Environmental Technology and Innovation*, *24*, 102022. https://doi.org/10.1016/j.eti.2021.102022

Cai, J. H., & Jia, C. Q. (2010). Mercury Removal from Aqueous Solution Using Coke-Derived Sulfur-Impregnated Activated Carbons. *Industrial & Engineering Chemistry Research*, *49*(6), 2716–2721. https://doi.org/10.1021/ie901194r

Canil, D., Crockford, P. W., Rossin, R., & Telmer, K. (2015). Mercury in some arc crustal rocks and mantle peridotites and relevance to the moderately volatile element budget of the Earth. *Chemical Geology*, *396*, 134–142. https://doi.org/10.1016/j.chemgeo.2014.12.029

Cao, Y., Duan, Y., Kellie, S., Li, L., Xu, W., Riley, J. T., Pan, W. P., Chu, P., Mehta, A. K., & Carty, R. (2005). Impact of coal chlorine on mercury speciation and emission from a 100-MW utility boiler with cold-side electrostatic precipitators and low-NOx burners. *Energy and Fuels*, *19*(3), 842–854. https://doi.org/10.1021/ef034107u

Caravati, E. M., Erdman, A. R., Christianson, G., Nelson, L. S., Woolf, A. D., Booze, L. L., Cobaugh, D. J., Chyka, P. A., Scharman, E. J., Manoguerra, A. S., & Troutman, W. G. (2008). Elemental mercury exposure: An evidence-based consensus guideline for out-of-hospital management. *Clinical Toxicology*, *46*(1), 1–21. https://doi.org/10.1080/15563650701664731

CDC. (2013). *Understanding Thimerosal, Mercury, and Vaccine Safety*. 1–2. http://www.cdc.gov/vaccines/conversations

Chen, C., Liu, S., Gao, Y., & Liu, Y. (2014). Investigation on mercury reemission from limestone-gypsum wet flue gas desulfurization slurry. *The Scientific World Journal*, *2014*. https://doi.org/10.1155/2014/581724

Chen, S., & Wilson, D. B. (1997). Construction and characterization of Escherichia coli genetically engineered for bioremediation of Hg(2+)-contaminated environments. *Applied and Environmental Microbiology*, *63*(6), 2442–2445. https://doi.org/10.1128/aem.63.6.2442-2445.1997

Cheng, C. M., Chen, C. W., Zhu, J., Chen, C. W., Kuo, Y. W., Lin, T. H., Wen, S. H., Zeng, Y. S., Liu, J. C., & Pan, W. P. (2009). Measurement of vapor phase mercury emissions at coal-fired power plants using regular and speciating sorbent traps with in-stack and out-of-stack sampling methods. *Energy and Fuels*, *23*(10), 4831–4839. https://doi.org/10.1021/ef900294s

Clarkson, T. W., Magos, L., & Myers, G. J. (2003). The Toxicology of Mercury — Current Exposures and Clinical Manifestations. *New England Journal of Medicine*, *349*(18), 1731–1737. https://doi.org/10.1056/NEJMra022471

Coker, A. K. (2015). Industrial and Laboratory Reactors – Chemical Reaction Hazards and Process Integration of Reactors. In *Ludwig's Applied Process Design for Chemical and Petrochemical Plants*. https://doi.org/10.1016/b978-0-08-094242-1.00021-8

Cui, Z., Li, Z., Zhang, Y., Wang, X., Li, Q., Zhang, L., Feng, X., Li, X., Shang, L., & Yao, Z. (2019). Atmospheric Mercury Emissions from Residential Coal Combustion in Guizhou Province, Southwest China. *Energy and Fuels*, *33*(3), 1937–1943. https://doi.org/10.1021/ACS.ENERGYFUELS.8B03997/SUPPL_FILE/EF8B03997_SI_001.PDF

CSC (China State Council) (2022) The 14th five-year comprehensive work plan for energy conservation and emission reduction (in Chinese). http://www.gov.cn/zhengce/content/2022-01/24/content_5670202.htm. Accessed 22 Mar 2022

De Jesus, R. M., Dos Anjos, J. P., Torres, E. A., Da Rocha, G. O., & De Andrade, J. B. (2020). *Fine and Coarse Particle-Bound Mercury in (Bio)fuels and Biodiesel/ Diesel Exhaust under Real World Circumstances*. https://doi.org/10.1021/acs.energyfuels.0c01639

De Simone, F., Artaxo, P., Bencardino, M., Cinnirella, S., Carbone, F., D'amore, F., Dommergue, A., Feng, X. Bin, Gencarelli, C. N., Hedgecock, I. M., Landis, M. S., Sprovieri, F., Suzuki, N., Wängberg, I., &

Pirrone, N. (2017). Particulate-phase mercury emissions from biomass burning and impact on resulting deposition: a modelling assessment EPA Public Access. *Atmos Chem Phys*, *17*, 1881–1899. https://doi.org/10.5194/acp-17-1881-2017

Dean, J. (2009). Estimation of Mercury Bioaccumulation Potential from Wastewater Treatment Plants in Receiving Waters: Phase 1. *Water Intelligence Online*, *8*. https://doi.org/10.2166/9781780403601

Deng, X., & Wilson, D. B. (2001). Bioaccumulation of mercury from wastewater by genetically engineered Escherichia coli. *Appl Microbiol Biotechnol*, *56*(1–2), 276–279. https://doi.org/10.1007/s002530100620

Deng, Y., & Macherzyński, M. (2023). Mercury capture in process gases and its mechanisms in different industries: theoretical and practical aspects, including the influence of sulfur compounds on mercury removal. *Chemical and Process Engineering: New Frontiers*, *44*(No 1), e5–e5. https://doi.org/10.24425/cpe.2022.142294

Dong, L., Wang, H., Huang, Y., Chen, H., Cheng, H., Liu, L., Xu, L., Zha, J., Yu, M., Wang, S., & Duan, Y. (2021). Elemental mercury removal from coal-fired flue gas using recyclable magnetic Mn-Fe based attapulgite sorbent. *Chemical Engineering Journal*, *407*, 127182. https://doi.org/10.1016/J.CEJ.2020.127182

Dórea, J. G., Bezerra, V. L. V. A., Fajon, V., & Horvat, M. (2011). Speciation of methyl- and ethyl-mercury in hair of breastfed infants acutely exposed to thimerosal-containing vaccines. *Clinica Chimica Acta*, *412*(17–18), 1563–1566. https://doi.org/10.1016/J.CCA.2011.05.003

Dranga, B. A., Lazar, L., & Koeser, H. (2012). Oxidation catalysts for elemental mercury in flue gases - A review. *Catalysts*, *2*(1), 139–170. https://doi.org/10.3390/catal2010139

Du, W., Yin, L., Zhuo, Y., Xu, Q., Zhang, L., & Chen, C. (2014). Catalytic oxidation and adsorption of elemental mercury over CuCl 2-impregnated sorbents. *Industrial and Engineering Chemistry Research*, *53*(2), 582–591. https://doi.org/10.1021/ie4016073

Dujardin, M. C., Cazé, C., & Vroman, I. (2000). Ion-exchange resins bearing thiol groups to remove mercury.: Part 1: synthesis and use of polymers prepared from thioester supported resin. *Reactive and Functional Polymers*, *43*(1–2), 123–132. https://doi.org/10.1016/S1381-5148(99)00011-5

Dziok, T., Kołodziejska, E. K., & Kołodziejska, E. L. (2020). *Mercury content in woody biomass and its removal in the torrefaction process*. 0–1.

Dziok, T., & Penkała, K. (2020). The possibility of reducing emissions from households by using coal briquettes. *Polityka Energetyczna*, *23*(3), 55–70. https://doi.org/10.33223/EPJ/126438

Dziok, T., & Strugała, A. (2017). Preliminary assessment of the possibility of mercury removal from hard coal with the use of air concentrating tables. *Gospodarka Surowcami Mineralnymi / Mineral Resources Management*, *33*(4), 125–142. https://doi.org/10.1515/gospo-2017-0043

Environment Protection Ministry of China, 2016, Guideline on Best Available Technologies of Pollution Prevention and Control for Thermal Power Plant, HJ2301—2016, from http:// www.mep.gov.cn/gkml/hbb/bgth/201610/W020161009327656386426.pdf

Eldin.Elhag, D., Osman, H. O., & Dahab, A. A. (2015). Investigation of mercury content in cosmetic products by using direct mercury analyzer. *American Journal of PharmTech Research*, *5*(June), 205–212.

Ewers, B. W., Crampton, A. S., Biener, M. M., & Friend, C. M. (2017). Thermally activated formation of reactive lattice oxygen in titania on nanoporous gold. *Journal of Physical Chemistry C*, *121*(39), 21405–21410. https://doi.org/10.1021/acs.jpcc.7b06316

Farkhondeh, T., Afshari, R., Mehrpour, O., & Samarghandian, S. (2019). *Mercury and Atherosclerosis: Cell Biology, Pathophysiology, and Epidemiological Studies*. https://doi.org/10.1007/s12011-019-01899-w

Feingold, B. J., Berky, A., Hsu-Kim, H., Rojas Jurado, E., & Pan, W. K. (2020). Population-based dietary exposure to mercury through fish consumption in the Southern Peruvian Amazon. *Environmental Research*, *183*, 108720. https://doi.org/10.1016/J.ENVRES.2019.108720

Ferreira, C. A., Ni, D., Rosenkrans, Z. T., & Cai, W. (2018). Scavenging of reactive oxygen and nitrogen species with nanomaterials. In *Nano Research* (Vol. 11, Issue 10, pp. 4955–4984). https://doi.org/10.1007/s12274-018-2092-y

Finkelman, R. B. (1993). Trace and Minor Elements in Coal. In *Nature* (Vol. 11). https://doi.org/10.1007/978-1-4615-2890-6_28

Fitzgerald, F., & Vandal, G. M. (1991). *(No Title)*.

FAO. 2018. The State of World Fisheries and Aquaculture 2018 - Meeting the sustainable development goals. Rome.

Fu, Z., Zhang, S., Li, X., Shao, J., Wang, K., & Chen, H. (2015). MSW oxy-enriched incineration technology applied in China: Combustion temperature, flue gas loss and economic considerations. *Waste Management*, *38*(1), 149–156. https://doi.org/10.1016/J.WASMAN.2014.12.026

Gallego, S., Benavides, M., & Tomaro, M. (2002). Involvement of an antioxidant defence system in the adaptive response to heavy metal ions in Helianthus annuus L. cells. *Plant Growth Regulation*, *36*(3), 267–273. https://doi.org/10.1023/A:1016536319908

Garnier, R., Fuster, J. M., Conso, F., Dautzenberg, B., Sors, C., & Fournier, E. (1981). Acute mercury vapour poisoning (author's transl). *Toxicological European research. Recherche europeenne en toxicologie*, *3*(2), 77–86. http://europepmc.org/abstract/MED/7245189

Ghodbane, I., & Hamdaoui, O. (2008). Removal of mercury(II) from aqueous media using eucalyptus bark: Kinetic and equilibrium studies. *Journal of Hazardous Materials*, *160*(2–3), 301–309. https://doi.org/10.1016/J.JHAZMAT.2008.02.116

Gingerich, D. B., Zhao, Y., & Mauter, M. S. (2019). Environmentally significant shifts in trace element emissions from coal plants complying with the 1990 Clean Air Act Amendments. *Energy Policy*, *132*, 1206–1215. https://doi.org/10.1016/J.ENPOL.2019.07.003

Glass, G. E., Sorensen, J. A., Schmidt, K. W., Rapp, G. R., Yap, D., & Fraser, D. (1991). Mercury deposition and sources for the upper great lakes region. *Water Air & Soil Pollution* , *56*, 235–249.

Gliozzo, E. (2021). Pigments — Mercury-based red (cinnabar-vermilion) and white (calomel) and their degradation products. *Archaeological and Anthropological Sciences*, *13*(11). https://doi.org/10.1007/s12520-021-01402-4

Gode, F., & Pehlivan, E. (2006). Removal of chromium(III) from aqueous solutions using Lewatit S 100: The effect of pH, time, metal concentration and temperature. *Journal of Hazardous Materials*, *136*(2), 330–337. https://doi.org/10.1016/J.JHAZMAT.2005.12.021

Górecki, J., Łoś, A., Macherzynski, M., Gołaś, J., Burmistrz, P., & Borovec, K. (2016). A portable, continuous system for mercury speciation in flue gas and process gases. *Fuel Processing Technology*, *154*, 44–51. https://doi.org/10.1016/j.fuproc.2016.08.005

Gorecki, J., Macherzynski, M., Chmielowiec, J., Borovec, K., Wałeka, M., Deng, Y., Sarbinowski, J., & Pasciak, G. (2022). *The Methods and Stands for Testing Fixed Sorbent and Sorbent Polymer Composite Materials for the Removal of Mercury from Flue Gases*. https://doi.org/10.3390/en15238891

Green-Ruiz, C. (2006). Mercury(II) removal from aqueous solutions by nonviable Bacillus sp. from a tropical estuary. *Bioresource Technology*, *97*(15), 1907–1911. https://doi.org/10.1016/J.BIORTECH.2005.08.014

Gungor, O., Ozkaya, A. K., Kirik, S., Dalkiran, T., Gungor, G., Isikay, S., Davutoglu, M., & Dilber, C. (2019). Acute Mercury Poisoning in a Group of School Children. *PEDIATRIC EMERGENCY CARE*, *35*(10), 696–699. https://doi.org/10.1097/PEC.0000000000001011

Guo, P., Guo, X., & Zheng, C. (2010). Roles of γ-Fe 2 O 3 in fly ash for mercury removal: Results of density functional theory study. *Applied Surface Science*, *256*(23), 6991–6996. https://doi.org/10.1016/j.apsusc.2010.05.013

Gupta, S., Kershaw, S. V, Rogach S Gupta, A. L., Kershaw, S. V, & Rogach, A. L. (2013). 25th Anniversary Article: Ion Exchange in Colloidal Nanocrystals. *Advance Materials*, *25*(48), 6923–6944. https://doi.org/10.1002/adma.201302400

GDP (current US$). World Bank Open Data. (n.d.). https://data.worldbank.org/indicator/NY.GDP.MKTP.CD

Global Sulphur Dioxide (so_2) emissions by world region. Our World in Data. (n.d.). https://ourworldindata.org/grapher/so-emissions-by-world-region-in-million-tonnes

Habashi, F. (2013). *Mercury, Physical and Chemical Properties BT - Encyclopedia of Metalloproteins* (R. H. Kretsinger, V. N. Uversky, & E. A. Permyakov, Eds.; pp. 1375–1377). Springer New York. https://doi.org/10.1007/978-1-4614-1533-6_307

Hamann, C. R., Boonchai, W., Wen, L., Sakanashi, E. N., Chu, C. Y., Hamann, K., Hamann, C. P., Sinniah, K., & Hamann, D. (2014). Spectrometric analysis of mercury content in 549 skin-lightening products: Is mercury toxicity a hidden global health hazard? *Journal of the American Academy of Dermatology*, *70*(2), 281-287.e3. https://doi.org/10.1016/J.JAAD.2013.09.050

Hamid, M. (2008). Comments on "In Vitro and in Vivo Estrogenicity of UV Screens." *Otology & Neurotology*, *29*(7), 1045. https://doi.org/10.1097/mao.0b013e31818658d5

He, F., Wang, W., Moon, J.-W., Howe, J., Pierce, E., & Liang, L. (2012). Rapid Removal of Hg(II) from Aqueous Solutions Using Thiol-Functionalized Zn-Doped Biomagnetite Particles. *ACS Applied Materials & Interfaces*, *4*, 4373–4379. https://doi.org/10.1021/am301031g

He, J., Yee, K.-K., Xu, Z., Zeller, M., Hunter, A. D., Chui, S. S.-Y., & Che, C.-M. (2011). Thioether side chains improve the stability, fluorescence, and metal uptake of a metal-organic framework. *Chemistry of Materials*, *23*(11), 2940–2947. https://doi.org/10.1021/cm200557e

He, K., Mi, Z., Chen, L., Coffman, M., & Liang, S. (2021). Critical transmission sectors in embodied atmospheric mercury emission network in China. *Journal of Industrial Ecology*, *25*, 1644–1656. https://doi.org/10.1111/jiec.13172

He, Z., Xie, Y., Wang, Y., Xu, J., & Hu, J. (2020). Removal of Mercury from Coal-Fired Flue Gas and Its Sulfur Tolerance Characteristics by Mn, Ce Modified γ -Al2O3Catalyst. *Journal of Chemistry*, *2020*. https://doi.org/10.1155/2020/8702745

Hernández, S., Islam, Md. S., Thompson, S., Kearschner, M., Hatakeyama, E., Malekzadeh, N., Hoelen, T., & Bhattacharyya, D. (2019). Thiol-Functionalized Membranes for Mercury Capture from Water. *Industrial & Engineering Chemistry Research*. https://doi.org/10.1021/acs.iecr.9b03761

Hisham, M. W. M., & Benson, S. W. (1995). Thermochemistry of the deacon process. *Journal of Physical Chemistry*, *99*(16), 6194–6198. https://doi.org/10.1021/j100016a065

Hua, K., Xu, X., Luo, Z., Fang, D., Bao, R., & Yi, J. (2019). Effective Removal of Mercury Ions in Aqueous Solutions: A Review. *Current Nanoscience*, *16*(3), 363–375. https://doi.org/10.2174/1573413715666190112110659

Huo, Q., Wang, Y., Chen, H., Han, L., Wang, J., Bao, W., Chang, L., & Xie, K. (2019). ZnS/AC sorbent derived from the high sulfur petroleum coke for mercury removal. *Fuel Processing Technology*, *191*(December 2018), 36–43. https://doi.org/10.1016/j.fuproc.2019.03.025

Hurley, J. P., Watras, C. J., & Bloom, N. S. (1991). Mercury cycling in a northern wisconsin seepage lake: The role of particulate matter in vertical transport. *Water Air & Soil Pollution*, *56*, 543–551.

Iannazzo, D., Pistone, A., Ziccarelli, I., Espro, C., Galvagno, S., Giofré, S. V, Romeo, R., Cicero, N., Bua, G. D., Lanza, G., Legnani, L., & Chiacchio, M. A. (2017). Removal of heavy metal ions from wastewaters using dendrimer-functionalized multi-walled carbon nanotubes. *Environ Sci Pollut Res Int*, *24*(17), 14735–14747. https://doi.org/10.1007/s11356-017-9086-2

Ie, I. R., Chen, W. C., Yuan, C. S., Hung, C. H., Lin, Y. C., Tsai, H. H., & Jen, Y. S. (2012). Enhancing the adsorption of vapor-phase mercury chloride with an innovative composite sulfur-impregnated activated carbon. *Journal of Hazardous Materials*, *217–218*, 43–50. https://doi.org/10.1016/j.jhazmat.2012.02.035

International Energy Agency. (2000). *International Energy Agency (IEA) World Energy Outlook 2000*. *179*(4073), 549–550.

International Energy Agency. (2022). International Energy Agency (IEA) World Energy Outlook 2022. *Https://Www.Iea.Org/Reports/World-Energy-Outlook-2022/Executive-Summary*, 524. https://www.iea.org/reports/world-energy-outlook-2022

James, B. S., Shetty, R. S., Kamath, A., & Shetty, A. (2020). Household cooking fuel use and its health effects among rural women in southern India-A cross-sectional study. *PLoS ONE*, *15*(4). https://doi.org/10.1371/journal.pone.0231757

Jaworek, A., Sobczyk, A. T., Marchewicz, A., Krupa, A., & Czech, T. (2021). Particulate matter emission control from small residential boilers after biomass combustion. A review. *Renewable and Sustainable Energy Reviews*, *137*(January 2020), 110446. https://doi.org/10.1016/j.rser.2020.110446

Jian, L. I., Zhong, H. A. N., Qi, Y. A. N., Shou, G. E., Wei, Y., Lei, C. H. E., & Sheng, W. U. (2020). *Analytical methods for the determination of mercury species in natural gas condensate*. *48*(12).

Jiang, X., & Wang, F. (2019). *Mercury emissions in China: a general review*. *1*, 127–132. https://doi.org/10.1007/s42768-019-00012-0

Johnson-Arbor, K., Tefera, E., & Farrell, J. (2021). *Characteristics and treatment of elemental mercury intoxication: A case series*. https://doi.org/10.1002/hsr2.293

Kathryn Karasek. (2013). Environmental disaster in Japan. *Historical Perspectives: Santa Clara University Undergraduate Journal of History, Series II*, *18*, 92–103. http://ieeexplore.ieee.org/document/5876207/

Khan, F., Momtaz, S., & Abdollahi, M. (2019). The relationship between mercury exposure and epigenetic alterations regarding human health, risk assessment and diagnostic strategies. *Journal of Trace Elements in Medicine and Biology*, *52*(November 2018), 37–47. https://doi.org/10.1016/j.jtemb.2018.11.006

Kho, F., Koppel, D. J., von Hellfeld, R., Hastings, A., Gissi, F., Cresswell, T., & Higgins, S. (2022). Current understanding of the ecological risk of mercury from subsea oil and gas infrastructure to marine ecosystems. *Journal of Hazardous Materials*, *438*(June), 129348. https://doi.org/10.1016/j.jhazmat.2022.129348

Kobielska, P. A., Howarth, A. J., Farha, O. K., & Nayak, S. (2018). Metal–organic frameworks for heavy metal removal from water. *Coordination Chemistry Reviews*, *358*, 92–107. https://doi.org/10.1016/j.ccr.2017.12.010

Kochel, A., Cieplinska, A., & Szymanek, A. (2012). Limestone in flue gas desulphurization in oxygen-enriched atmospheres - Part I: The effect of CO2 on limestone calcination. *Chemical and Process Engineering - Inzynieria Chemiczna i Procesowa*, *33*(2), 255–262. https://doi.org/10.2478/v10176-012-0023-0

Kopyść, E., Pyrzyńska, K., Garboś, S., & Bulska, E. (2000). Determination of mercury by cold-vapor atomic absorption spectrometry with preconcentration on a gold-trap. *Analytical Sciences*, *16*(12), 1309–1312. https://doi.org/10.2116/analsci.16.1309

Li, B., & Wang, H. (2021). Effect of flue gas purification facilities of coal-fired power plant on mercury emission. *Energy Reports*, *7*, 190–196. https://doi.org/10.1016/j.egyr.2021.01.094

Li, G., Shen, B., Li, Y., Zhao, B., Wang, F., He, C., Wang, Y., & Zhang, M. (2015). Removal of element mercury by medicine residue derived biochars in presence of various gas compositions. *Journal of Hazardous Materials*, *298*, 162–169. https://doi.org/10.1016/J.JHAZMAT.2015.05.031

Li, Y., Liu, M., Tang, Y., Jia, Y., Wang, Q., Ma, Q., Hong, J., Zuo, J., & Yuan, X. (2022). Life cycle impact of winter heating in rural China from the perspective of environment, economy, and user experience. *Energy Conversion and Management*, *269*, 116156. https://doi.org/10.1016/J.ENCONMAN.2022.116156

Liang, P., Feng, X., Zhang, C., Zhang, J., Cao, Y., You, Q., Leung, A. O. W., Wong, M. H., & Wu, S. C. (2015). Human exposure to mercury in a compact fluorescent lamp manufacturing area: By food (rice and fish) consumption and occupational exposure. *Environmental Pollution*, *198*, 126–132. https://doi.org/10.1016/j.envpol.2014.12.036

Lin, F., Wang, Z., Zhang, Z., He, Y., Zhu, Y., Shao, J., Yuan, D., Chen, G., & Cen, K. (2020). Flue gas treatment with ozone oxidation: An overview on NOx, organic pollutants, and mercury. *Chemical Engineering Journal*, *382*, 123030. https://doi.org/10.1016/J.CEJ.2019.123030

Lin, S., Al-Shawabkeh, A., Matsuda, H., Hasatani, M., & Horio, M. (1995). H2S Reactions with Limestone and Calcined Limestone. *Journal of Chemical Engineering of Japan*, *28*(6), 708–714. https://doi.org/10.1252/jcej.28.708

Lindberg, S. E., Turner, R. R., Meyers, T. P., Taylor, G. E., & Schroeder, W. H. (1991). *ATMOSPHERIC CONCENTRATIONS AND DEPOSITION OF Hg TO A DECIDUOUS FOREST ATWALKER BRANCH WATERSHED, TENNESSEE, USA*.

Ling, L., Fan, M., Wang, B., & Zhang, R. (2015). Application of computational chemistry in understanding the mechanisms of mercury removal technologies: A review. *Energy and Environmental Science*, *8*(11), 3109–3133. https://doi.org/10.1039/c5ee02255j

Littlepage, T. (2013). *Mercury in Crude Oils*. 1–5.

Liu, Q. (2013). Mercury concentration in natural gas and its distribution in the Tarim Basin. *Science China: Earth Sciences*, *56*(8), 1371–1379. https://doi.org/10.1007/s11430-013-4609-2

Liu, S., Chen, J., Cao, Y., Yang, H., Chen, C., & Jia, W. (2019). Distribution of mercury in the combustion products from coal-fired power plants in Guizhou, southwest China. *Journal of the Air & Waste Management Association*, *69*(2), 234–245. https://doi.org/10.1080/10962247.2018.1535461

Liu, T., Che, J.-X., Hu, Y.-Z., Dong, X.-W., Liu, X.-Y., & Che, C.-M. (2014). Alkenyl/Thiol-Derived Metal–Organic Frameworks (MOFs) by Means of Postsynthetic Modification for Effective Mercury Adsorption. *Chemistry—A European Journal*, *20*(43), 14090–14095. https://doi.org/10.1002/chem.201403382

Liu, W., Vidić, R. D., & Brown, T. D. (1998). Optimization of sulfur impregnation protocol for fixed-bed application of activated carbon-based sorbents for gas-phase mercury removal. *Environmental Science and Technology*, *32*(4), 531–538. https://doi.org/10.1021/es970630+

Liu, W., Xu, H., Liao, Y., Quan, Z., Li, S., Zhao, S., Qu, Z., & Yan, N. (2019). Recyclable CuS sorbent with large mercury adsorption capacity in the presence of SO2 from non-ferrous metal smelting flue gas. *Fuel*, *235*(July 2018), 847–854. https://doi.org/10.1016/j.fuel.2018.08.062

Lowell, S., Shields, J. E., Thomas, M. A., & Thommes, M. (2004). *Characterization of Porous Solids and Powders: Surface Area, Pore Size and Density*.

Luo, Z., Duan, Y., Huang, T., Liu, S., Huang, Y., Dong, L., Ren, S., Tao, J., & Gu, X. (2019). Emission and Migration Characteristics of Mercury in a 0.3 MWth CFB Boiler with Ammonium Bromide-Modified Rice Husk Char Injection into Flue [Research-article]. *Energy & Fuels*, *33*(8), 7578–7586. https://doi.org/10.1021/acs.energyfuels.9b01440

Macherzyński, M. (2018). *Redukcja emisji rtęci do środowiska - wybrane problemy w świetle badań laboratoryjnych i przemysłowych*. Wydawnictwa AGH.

Maiti, D., Ansari, I., Rather, M. A., & Deepa, A. (2019). Comprehensive review on wastewater discharged from the coal-related industries – characteristics and treatment strategies. *Water Science and Technology*, *79*(11), 2023–2035. https://doi.org/10.2166/wst.2019.195

Masoomi, I., Kamata, H., Yukimura, A., Ohtsubo, K., Schmid, M. O., & Scheffknecht, G. (2020). Investigation on the behavior of mercury across the flue gas treatment of coal combustion power plants using a lab-scale firing system. *Fuel Processing Technology*, *201*(January), 1–8. https://doi.org/10.1016/j.fuproc.2020.106340

Menger-Krug, E., Niederste-Hollenberg, J., Hillenbrand, T., & Hiessl, H. (2012). *Integration of Microalgae Systems at Municipal Wastewater Treatment Plants: Implications for Energy and Emission Balances*. https://doi.org/10.1021/es301967y

Mojammal, A. H. M., Back, S. K., Seo, Y. C., & Kim, J. H. (2019). Mass balance and behavior of mercury in oil refinery facilities. *Atmospheric Pollution Research*, *10*(1), 145–151. https://doi.org/10.1016/J.APR.2018.07.002

Morita, H., Tanaka, H., & Shimomura, S. (1995). Atomic fluorescence spectrometry of mercury: principles and developments. *Spectrochimica Acta Part B: Atomic Spectroscopy*, *50*(1), 69–84. https://doi.org/10.1016/0584-8547(94)00116-D

Mukherjee, A. B., Zevenhoven, R., Bhattacharya, P., Sajwan, K. S., & Kikuchi, R. (2008). Mercury flow via coal and coal utilization by-products: A global perspective. *Resources, Conservation and Recycling*, *52*(4), 571–591. https://doi.org/10.1016/j.resconrec.2007.09.002

Nanusha, M. Y., Carlier, J. D., Carvalho, G. I., Costa, M. C., & Paiva, A. P. (2019). Separation and recovery of Pd and Fe as nanosized metal sulphides by combining solvent extraction with biological strategies based on the use of sulphate-reducing bacteria. *Separation and Purification Technology*, *212*(November 2018), 747–756. https://doi.org/10.1016/j.seppur.2018.11.062

National Bureau of Statistics of China. (2023). The total energy and kinds of energy consumption 2003-2020 in China. https://data.stats.gov.cn/english/easyquery.htm?cn=C01

O'Connor, D., Peng, T., Li, G., Wang, S., Duan, L., Mulder, J., Cornelissen, G., Cheng, Z., Yang, S., & Hou, D. (2018). Sulfur-modified rice husk biochar: A green method for the remediation of mercury contaminated soil. *Science of the Total Environment*, *621*, 819–826. https://doi.org/10.1016/j.scitotenv.2017.11.213

Osipova, N. A., Tkacheva, E. v., Arbuzov, S. I., Yazikov, E. G., & Matveenko, I. A. (2019). Mercury in Coals and Soils from Coal-Mining Regions. *Solid Fuel Chemistry*, *53*(6), 411–417. https://doi.org/10.3103/S036152191907005X

Ozuah, P. O. (2000). Mercury poisoning. *Current Problems in Pediatrics*, *30*(3), 91–99. https://doi.org/10.1067/MPS.2000.104054

Park, S. H., Araki, S., Nakata, A., Kim, Y. H., Park, J. A., Tanigawa, T., Yokoyama, K., & Sato, H. (2000). Effects of occupational metallic mercury vapour exposure on suppressor-inducer (CD4+CD45RA+) T lymphocytes and CD57+CD16+ natural killer cells. *International Archives of Occupational and Environmental Health*, *73*(8), 537–542. https://doi.org/10.1007/s004200000173

Pasinszki, T., Krebsz, M., Chand, D., Kótai, L., Homonnay, Z., Sajó, I. E., & Váczi, T. (2020). Carbon microspheres decorated with iron sulfide nanoparticles for mercury(II) removal from water. *Journal of Materials Science*, *55*(4), 1425–1435. https://doi.org/10.1007/s10853-019-04032-3

Pirrone, N., Cinnirella, S., Feng, X., Finkelman, R. B., Friedli, H. R., Leaner, J., Mason, R., Mukherjee, A. B., Stracher, G. B., Streets, D. G., & Telmer, K. (2010). Global mercury emissions to the atmosphere from anthropogenic and natural sources. *Atmospheric Chemistry and Physics*, *10*(13), 5951–5964. https://doi.org/10.5194/acp-10-5951-2010

Presto, A. A., & Granite, E. J. (2008). Noble metal catalysts for mercury oxidation in utility flue gas. *Platinum Metals Review*, *52*(3), 144–154. https://doi.org/10.1595/147106708X319256

Prins, R. (2018). Eley–Rideal, the Other Mechanism. *Topics in Catalysis*, *61*(9–11), 714–721. https://doi.org/10.1007/s11244-018-0948-8

Qu, Z., Yan, L., Li, L., Xu, J., Liu, M., Li, Z., & Yan, N. (2014). *Ultraeffective ZnS Nanocrystals Sorbent for Mercury(II) Removal Based on Size-Dependent Cation Exchange*. https://doi.org/10.1021/am504896w

Raj, D., Chowdhury, A., & Maiti, S. K. (2017). Ecological risk assessment of mercury and other heavy metals in soils of coal mining area: A case study from the eastern part of a Jharia coal field, India. *Human and Ecological Risk Assessment*, *23*(4), 767–787. https://doi.org/10.1080/10807039.2016.1278519

Ravindra, K., Kaur-Sidhu, M., Mor, S., & John, S. (2019). Trend in household energy consumption pattern in India: A case study on the influence of socio-cultural factors for the choice of clean fuel use. *Journal of Cleaner Production*, *213*, 1024–1034. https://doi.org/10.1016/J.JCLEPRO.2018.12.092

Ray, C., Sarkar, S., Dutta, S., Roy, A., Sahoo, R., Negishi, Y., & Pal, T. (2015). Evolution of tubular copper sulfide nanostructures from copper(i)–metal organic precursor: a superior platform for the removal of Hg(ii) and Pb(ii) ions. *RSC Advances*, *5*(16), 12446–12453. https://doi.org/10.1039/C4RA09999K

Risk, R. P. A., & Limited, P. A. (2002). *Risks to health and the environment related to the use of mercury products*.

Roshan, S. A., & Mofidi, A. (2014). Comparison of Fixed and Fluidized Beds Adsorber with Economic , Engineering , and Environmental approach. *International Journal of Occupational Hygiene*, 165–174.

Ryfa, A., Żmuda, R., Mandrela, S., Białecki, R., Adamczyk, W., Nowak, M., Lelek, Ł., Bandoła, D., Pichura, M., Płonka, J., & Wdowin, M. (2023). Experimental and numerical investigation of mercury removal from flue gas by sorbent polymer composite. *Fuel*, *333*(June 2022). https://doi.org/10.1016/j.fuel.2022.126470

S. Mark Wilhelm, Lian Liang, Deborah Cussen, & David A. Kirchgessner. (2007). *Research Mercury in Crude Oil Processed in the United States (2004)*. https://doi.org/10.1021/es062742j

Saad, M. G., Dosoky, N. S., Zoromba, M. S., & Shafik, H. M. (2019). *Algal Biofuels: Current Status and Key Challenges*. https://doi.org/10.3390/en12101920

Safari, F., Akramian, M., Salehi-Arjmand, H., & Khadivi, A. (2019). Physiological and molecular mechanisms underlying salicylic acid-mitigated mercury toxicity in lemon balm (Melissa officinalis L.). *Ecotoxicology and Environmental Safety*, *183*, 109542. https://doi.org/10.1016/J.ECOENV.2019.109542

Sahoo, G., Sharma, A., & Chandra Dash, A. (2022). Biomass from trees for bioenergy and biofuels – A briefing paper. *Materials Today: Proceedings*, *65*, 461–467. https://doi.org/10.1016/J.MATPR.2022.02.639

Shen, H., Luo, Z., Xiong, R., Liu, X., Zhang, L., Li, Y., Du, W., Chen, Y., Cheng, H., Shen, G., & Tao, S. (2021). A critical review of pollutant emission factors from fuel combustion in home stoves. *Environment International*, *157*, 106841. https://doi.org/10.1016/J.ENVINT.2021.106841

Shi, J., Chen, Y., Xu, L., Hong, Y., Li, M., Fan, X., Yin, L., Chen, Y., Yang, C., Chen, G., Liu, T., Ji, X., & Chen, J. (2022). Measurement report: Atmospheric mercury in a coastal city of Southeast China – inter-annual variations and influencing factors. *Atmospheric Chemistry and Physics*, *22*(17), 11187–11202. https://doi.org/10.5194/acp-22-11187-2022

Shin, Y., Fryxell, G., Um, W., Parker, K., Mattigod, S., & Skaggs, R. (2007). Sulfur-Functionalized Mesoporous Carbon. *Advanced Functional Materials*, *17*, 2897–2901. https://doi.org/10.1002/adfm.200601230

Smith, A. M., & Nie, S. (2011). Bright and Compact Alloyed Quantum Dots with Broadly Tunable Near-Infrared Absorption and Fluorescence Spectra through Mercury Cation Exchange. *AGH UNIV OF SCIENCE AND TECHNOLOGY*, *133*, 15. https://doi.org/10.1021/ja108482a

Steijns, M., Derks, F., Verloop, A., & Mars, P. (1976). The mechanism of the catalytic oxidation of hydrogen sulfide. II. Kinetics and mechanism of hydrogen sulfide oxidation catalyzed by sulfur. *Journal of Catalysis*, *42*(1), 87–95. https://doi.org/10.1016/0021-9517(76)90094-4

Su, Y., Liu, X., Teng, Y., & Zhang, K. (2021). Mercury speciation in various coals based on sequential chemical extraction and thermal analysis methods. *Energies*, *14*(9), 1–20. https://doi.org/10.3390/en14092361

Sun, D. T., Peng, L., Reeder, W. S., Mohamad Moosavi, S., Tiana, D., Britt, D. K., Oveisi, E., & Queen, W. L. (2018). *Rapid, Selective Heavy Metal Removal from Water by a Metal− Organic Framework/Polydopamine Composite*. https://doi.org/10.1021/acscentsci.7b00605

Swain, E. B., Jakus, P. M., Rice, G., Lupi, F., Maxson, P. A., Pacyna, J. M., Penn, A., Spiegel, S. J., & Veiga, M. M. (2007). Socioeconomic consequences of mercury use and pollution. *Ambio*, *36*(1), 45–61. https://doi.org/10.1579/0044-7447(2007)36[45:SCOMUA]2.0.CO;2

Tang, Y., Wang, S., Wu, Q., Liu, K., Wang, L., Li, S., Gao, W., Zhang, L., Zheng, H., Li, Z., & Hao, J. (2018). Recent decrease trend of atmospheric mercury concentrations in East China: the influence of anthropogenic emissions. *Atmospheric Chemistry and Physics*, *18*(11), 8279–8291. https://doi.org/10.5194/acp-18-8279-2018

Tauanov, Z., Tsakiridis, P. E., Mikhalovsky, S. v., & Inglezakis, V. J. (2018). Synthetic coal fly ash-derived zeolites doped with silver nanoparticles for mercury (II) removal from water. *Journal of Environmental Management*, *224*(July), 164–171. https://doi.org/10.1016/j.jenvman.2018.07.049

Tchinda, A., Ngameni, E., Kenfack, I., & Walcarius, A. (2009). One-Step Preparation of Thiol-Functionalized Porous Clay Heterostructures: Application to Hg(II) Binding and Characterization of Mass Transport Issues. *Chemistry of Materials - CHEM MATER*, *21*. https://doi.org/10.1021/cm8024022

Thommes, M., & Cychosz, K. A. (2014). Physical adsorption characterization of nanoporous materials: progress and challenges. *Adsorption*, *20*, 233–250. https://doi.org/10.1007/s10450-014-9606-z

Tong, Y., Wang, K., Gao, J., Yue, T., Zuo, P., Wang, C., Tong, L., Zhang, X., Zhang, Y., Liang, Q., & Liu, J. (2022). Mercury distribution and emission reduction potentials of Chinese coal-fired industrial boilers. *Air Quality, Atmosphere & Health*, *15*, 967–978. https://doi.org/10.1007/s11869-022-01183-2

Trovarelli, A., De Leitenburg, C., Boaro, M., & Dolcetti, G. (1999). The utilization of ceria in industrial catalysis. *Catalysis Today*, *50*(2), 353–367. https://doi.org/10.1016/S0920-5861(98)00515-X

Tsai, W.-T., Tsai, C.-H., & Shen, Y.-H. (2023). Environmental policy and legal framework for controlling mercury emissions from stationary sources: a case study in Taiwan. *Journal of Material Cycles and Waste Management* . https://doi.org/10.1007/s10163-023-01665-0

UNEP. (2018). Global mercury assessment 2018. *Global Mercury Assessment 2018: Sources, Emissions, Releases and Environmental Transport*, *November*, 1–60. https://doi.org/10.1016/S0300-483X(03)00203-8

Urgun-Demirtas, M., Benda, P. L., Gillenwater, P. S., Negri, M. C., Xiong, H., & Snyder, S. W. (2012). Achieving very low mercury levels in refinery wastewater by membrane filtration. *Journal of Hazardous Materials*, *215–216*, 98–107. https://doi.org/10.1016/j.jhazmat.2012.02.040

Vimercati, L., Santarelli, L., Pesola, G., Drago, I., Lasorsa, G., Valentino, M., Vacca, A., & Soleo, L. (2001). Monocyte-macrophage system and polymorphonuclear leukocytes in workers exposed to low levels of metallic mercury. *Science of The Total Environment*, *270*(1–3), 157–163. https://doi.org/10.1016/S0048-9697(00)00780-4

WHO – World Health Organization: World health statistics 2010. WHO Library Cataloguing-in-Publication Data. ISBN: 978 92 4 156398 7.

Wang, J., Deng, B., Wang, X., & Zheng, J. (2009). Adsorption of Aqueous Hg(II) by Sulfur-Impregnated Activated Carbon. *Environmental Engineering Science - ENVIRON ENG SCI*, *26*, 1693–1699. https://doi.org/10.1089/ees.2008.0418

Wang, J., Fang, Y., Wang, H., Bai, G., Qin, W., & Zhang, J. (2022). Simultaneous Removal of Hg0 and H_2S over a Regenerable Fe2 O3/AC Catalyst. *Atmosphere*, *13*(3). https://doi.org/10.3390/atmos13030425

Wang, J., Wang, X., Zhang, P., An, J., Cao, B., Geng, Y., Luo, T., Wang, L., & Pan, K. (2016). Thiol-functionalized electrospun polyacrylonitrile nanofibrous membrane for highly efficient removal of mercury ions. *Chemical Engineering Research and Design*, *113*, 1–8. https://doi.org/10.1016/j.cherd.2016.07.007

Wang, S., & Peng, Y. (2010). Natural zeolites as effective adsorbents in water and wastewater treatment. *Chemical Engineering Journal*, *156*(1), 11–24. https://doi.org/10.1016/J.CEJ.2009.10.029

Wang, Z., Liu, J., Yang, Y., Miao, S., & Shen, F. (2018). Effect of the Mechanism of H2S on Elemental Mercury Removal Using the MnO2 Sorbent during Coal Gasification. *Energy and Fuels*, *32*(4), 4453–4460. https://doi.org/10.1021/acs.energyfuels.7b03092

Wang, Z., Liu, J., Yang, Y., Yu, Y., Yan, X., & Zhang, Z. (2020). AMn2O4 (A=Cu, Ni and Zn) sorbents coupling high adsorption and regeneration performance for elemental mercury removal from syngas. *Journal of Hazardous Materials*, *388*, 121738. https://doi.org/10.1016/J.JHAZMAT.2019.121738

Walawska, B., Szymanek, A., Pajdak, A., & Nowak, M. (2014). Flue gas desulfurization by mechanically and thermally activated sodium bicarbonate. *Polish Journal of Chemical Technology*, *16*(3), 56–62. https://doi.org/10.2478/pjct-2014-0051

Wdowin, M., Macherzynski, M., Panek, R., Górecki, J., & Franus, W. (2015). Investigation of the sorption of mercury vapour from exhaust gas by an Ag-X zeolite. *Clay Minerals*, *50*(1), 31–40. https://doi.org/10.1180/claymin.2015.050.1.04

Wdowin, M., Macherzynski, M., Panek, R., Wałęka, M., & Górecki, J. (2020). Analysis of selected mineral and waste sorbents for the capture of elemental mercury from exhaust gases. *Mineralogia*, *51*(1), 17–35. https://doi.org/10.2478/mipo-2020-0003

Wierzchowski, K., Chećko, J., & Pyka, I. (2017). Variability of Mercury Content in Coal Matter From Coal Seams of The Upper Silesia Coal Basin. *Archives of Mining Sciences*, *62*(4), 843–856. https://doi.org/10.1515/amsc-2017-0058

Wu, X., Duan, Y., Meng, J., Geng, X., Shen, A., & Hu, J. (2021). Experimental Study on the Mercury Removal of a H2S-Modified Fe2O3Adsorbent. *Industrial and Engineering Chemistry Research*, *60*(48), 17429–17438. https://doi.org/10.1021/acs.iecr.1c01998

Wu, Z., Ye, H., Shan, Y., Chen, B., & Li, J. (2020). A city-level inventory for atmospheric mercury emissions from coal combustion in China. *Atmospheric Environment*, *223*, 117245. https://doi.org/10.1016/J.ATMOSENV.2019.117245

Xing, X., Zhang, X., Tang, J., Cui, L., & Dong, Y. (2022). Removal of gaseous elemental mercury from simulated syngas over Fe2O3/TiO2 sorbents. *Fuel*, *311*(December 2021), 122614. https://doi.org/10.1016/j.fuel.2021.122614

Xiong, C., Chen, X., & Liu, X. (2012). Synthesis, characterization and application of ethylenediamine functionalized chelating resin for copper preconcentration in tea samples. *Chemical Engineering Journal*, *203*, 115–122. https://doi.org/10.1016/j.cej.2012.06.131

Xu, W., Adewuyi, Y. G., Liu, Y., & Wang, Y. (2018). Removal of elemental mercury from flue gas using CuO x and CeO 2 modified rice straw chars enhanced by ultrasound. *Fuel Processing Technology*, *170*(July 2017), 21–31. https://doi.org/10.1016/j.fuproc.2017.10.017

Yan, Q., Han, Z., & Wang, S. (2017a). Geochemical Characteristics of Mercury in Oil and Gas. *IOP Conference Series: Earth and Environmental Science*, *63*(1). https://doi.org/10.1088/1755-1315/63/1/012024

Yan, Q., Han, Z., & Wang, S. (2017b). Geochemical Characteristics of Mercury in Oil and Gas. *IOP Conference Series: Earth and Environmental Science*, *63*, 012024. https://doi.org/10.1088/1755-1315/63/1/012024

Yang, J., Li, Q., Zhu, W., Qu, W., Li, M., Xu, Z., Yang, Z., Liu, H., & Li, H. (2021). Recyclable chalcopyrite sorbent for mercury removal from coal combustion flue gas. *Fuel*, *290*(January), 120049. https://doi.org/10.1016/j.fuel.2020.120049

Yang, J., Zhao, Y., Guo, X., Li, H., Zhang, J., & Zheng, C. (2018). Removal of elemental mercury from flue gas by recyclable CuCl2 modified magnetospheres from fly ash. Part 4. Performance of sorbent injection in an entrained flow reactor system. *Fuel*, *220*(January), 403–411. https://doi.org/10.1016/j.fuel.2018.01.132

Yang, W., Li, Y., Shi, S., Chen, H., Shan, Y., & Liu, Y. (2019). Mercury removal from flue gas by magnetic iron-copper oxide modified porous char derived from biomass materials. *Fuel*, *256*, 115977. https://doi.org/10.1016/J.FUEL.2019.115977

Yee, K.-K., Reimer, N., Liu, J., Cheng, S.-Y., Yiu, S.-M., Weber, J., Stock, N., & Xu, Z. (2013). Effective Mercury Sorption by Thiol-Laced Metal−Organic Frameworks: in Strong Acid and the Vapor Phase. *J. Am. Chem. Soc*, *135*, 17. https://doi.org/10.1021/ja400212k

Yoo, J. S., Rong, X., Liu, Y., & Kolpak, A. M. (2018). Role of Lattice Oxygen Participation in Understanding Trends in the Oxygen Evolution Reaction on Perovskites [Research-article]. *ACS Catalysis*, *8*(5), 4628–4636. https://doi.org/10.1021/acscatal.8b00612

Zhang, L., Wang, S., Wu, Q., Wang, F., Lin, C. J., Zhang, L., Hui, M., Yang, M., Su, H., & Hao, J. (2016). Mercury transformation and speciation in flue gases from anthropogenic emission sources: A critical

review. *Atmospheric Chemistry and Physics*, *16*(4), 2417–2433. https://doi.org/10.5194/acp-16-2417-2016

Zhang, Q., Mei, J., Sun, P., Zhao, H., Guo, Y., & Yang, S. (2020). Mechanism of Elemental Mercury Oxidation over Copper-Based Oxide Catalysts: Kinetics and Transient Reaction Studies. *Industrial and Engineering Chemistry Research*, *59*(1), 61–70. https://doi.org/10.1021/acs.iecr.9b04806

Zhang, W., Lu, Z., Xu, Y., Wang, C., Gu, Y., Xu, H., & Streets, D. G. (2017). Black carbon emissions from biomass and coal in rural China. *Atmospheric Environment*. https://doi.org/10.1016/j.atmosenv.2017.12.029

Zhao, S., Sun, C., Zhang, Y., Jiao, T., Zhang, W., Liang, P., & Zhang, H. (2019). Determination of mercury occurrence and thermal stability in high ash bituminous coal based on sink-float and sequential chemical extraction method. *Fuel*, *253*(January), 571–579. https://doi.org/10.1016/j.fuel.2019.05.054

Zhou, J., Du, B., Shang, L., Wang, Z., Cui, H., Fan, X., & Zhou, J. (2020). Mercury fluxes, budgets, and pools in forest ecosystems of China: A review. *Critical Reviews in Environmental Science and Technology*, *50*(14), 1411–1450. https://doi.org/10.1080/10643389.2019.1661176

Zhou, Q., Duan, Y. F., Zhao, S. L., Zhu, C., She, M., Zhang, J., & Wang, S. Q. (2015). Modeling and experimental studies of in-duct mercury capture by activated carbon injection in an entrained flow reactor. *Fuel Processing Technology*, *140*, 304–311. https://doi.org/10.1016/j.fuproc.2015.08.018

Zhou, Y., Yang, J., Dong, L., Gao, T., Li, Z., Ji, Y., Zhao, Y., Pan, S., Zhang, J., & Zheng, C. (2020). Removal of elemental mercury from flue gas by recyclable CuCl2 modified magnetospheres from fly ash: Part 5. Industrial scale studies at a 50 MWth coal-fired power plant. *Fuel*, *266*, 117052. https://doi.org/10.1016/J.FUEL.2020.117052